

Dynamics and Control Functional Division Report

Jon Chrone
Kevin Daugherty
Jeremy Davis
Kevin Earle
Josh Ellis
Mark Grigg
Bhalvinder Gulati
Becky Maiorano
Ellen McDorman
Josh Michener

November 18, 2004

Contents

List of Figures	v
List of Tables	vi
List of Abbreviations	vii
List of Symbols	ix
1 Introduction	1
1.1 Astrodynamics	1
1.1.1 Orbit Types	1
1.1.2 Orbit Trade Studies	2
1.1.3 The Δv Budget	2
1.1.4 Orbit Determination & Maintenance	2
1.2 Attitude Determination and Control System	3
1.2.1 Requirements	3
1.2.2 Modes	4
1.2.3 Disturbance Torques	4
1.2.4 Control Approaches	5
1.2.5 Algorithms	6
1.3 Propulsion	7
1.3.1 Propulsion System Alternatives	7
1.3.2 Mission Phase Requirements	9
1.3.3 Performance Considerations	9
1.4 Interactions Between Dynamics and Control Subdivisions	9
1.4.1 Astrodynamics and ADCS	9
1.4.2 Astrodynamics and Propulsion	10
1.4.3 ADCS and Propulsion	10
1.5 Interaction with Other Functional Divisions	10
1.5.1 Structures and Launch Vehicles	10
1.5.2 Power, Thermal, and Environments	11
1.5.3 Communications, Command and Data Handling	12
1.6 Conclusion	12

2	Modelling and Analysis	13
2.1	Astrodynamics	13
2.1.1	Equations of Motion	13
2.1.2	Orbit Geometry	15
2.1.3	Mission Analysis	20
2.1.4	Orbit Maneuvers	25
2.1.5	Launch Windows	32
2.1.6	Orbit Perturbations	32
2.1.7	Orbit Maintenance and Stationkeeping	35
2.1.8	Guidance and Navigation Subsystem	36
2.2	Attitude Determination and Control Systems	36
2.2.1	Requirements	36
2.2.2	Control Modes	37
2.2.3	Sensors	39
2.2.4	Disturbance Torques	45
2.2.5	Control Approaches	48
2.2.6	Algorithms	52
2.3	Propulsion	63
2.3.1	Specific Impulse and the Rocket Equation	64
2.3.2	Chemical Rockets	65
2.3.3	Cold Gas Propulsion	71
2.3.4	Electric Propulsion	72
2.3.5	Thermal Propulsion	74
2.3.6	Propellant-less Propulsion	76
2.3.7	Conclusion	78
2.4	Analysis Tools	78
2.4.1	Satellite Tool Kit	79
2.4.2	WinOrbit	79
2.4.3	Spacecraft Control Toolbox	79
2.5	Interactions with Other Functional Divisions	79
2.5.1	Astrodynamics and S&LV	80
2.5.2	Astrodynamics and PT&E	80
2.5.3	Astrodynamics and CC&DH	80
2.5.4	ADCS and S&LV	81
2.5.5	ADCS and PT&E	81
2.5.6	ADCS and CC&DH	81
2.5.7	Propulsion and S&LV	81
2.5.8	Propulsion and PT&E	82
2.5.9	Propulsion and CC&DH	82
2.6	Interactions Among D&C Subdivisions	82
2.6.1	Astrodynamics and ADCS	83
2.6.2	Astrodynamics and Propulsion	83

2.6.3	ADCS and Propulsion	83
2.7	Conclusion	84
3	Examples	85
3.1	Orbit Examples	85
3.1.1	Hohmann Transfer from Earth to Mars	85
3.1.2	Type I Direct Earth-Mars Transfer	90
3.2	ADCS Examples	92
3.2.1	Torques	93
3.2.2	Algorithms	94
3.2.3	Control Approaches	95
3.3	Propulsion Examples	97
3.3.1	Selection of an Upper-Stage Rocket and Sizing of Propellant Tanks for a Mission to Mars	97
3.3.2	Low Earth Orbit to Geosynchronous Orbit Transfer	100
3.3.3	Earth to Venus Transfer	101
3.4	Conclusion	102
4	Summary and Conclusions	103
4.1	Astrodynamics	103
4.1.1	Conclusions	104
4.1.2	Recommendations	105
4.2	ADCS	106
4.2.1	Conclusions	107
4.2.2	Recommendations	108
4.3	Propulsion	109
4.3.1	Conclusions	110
4.3.2	Recommendations	111
4.4	Conclusion	112
A	Astronomical Data	115
B	Useful Tables	116

List of Figures

2.1	Geometry of an elliptical orbit	16
2.2	Geometry of a parabolic orbit	18
2.3	Geometry of a hyperbolic orbit	19
2.4	The (3-1-3) Euler angle description of the orbit plane	21
2.5	Illustration of a Hohmann transfer orbit	26
2.6	Illustration of an orbit plane change maneuver	27
2.7	Departure orbit to reach outer planet	28
2.8	Departure orbit to reach inner planet	28
2.9	Arrival orbit to the inner planet Venus	29
2.10	Arrival orbit to the outer planet Mars	30
2.11	Solar Sail Pitch Angle.	31
2.12	Schematic of an Ideal Rocket.	66
2.13	Schematic of a Typical Hydrazine Rocket.	69
2.14	Schematic of a Typical Solid Rocket	70
2.15	Solid Rocket Grain Designs with Their Thrust Time Histories.	71
2.16	Schematic of a Typical Hybrid Rocket.	71
2.17	Nuclear Electric Propulsion Vehicle Concept	73
2.18	Nuclear Thermal Propulsion Vehicle Concept	75
2.19	Solar Orbit Transfer Vehicle.	76
2.20	Physical Solar Sail.	77
2.21	Magnetic Solar Sail.	77
3.1	Hohmann transfer from Earth to Mars	86
3.2	Nonminimum energy transfer orbit from Earth to Mars	90
3.3	TISSUE Spacecraft	93
3.4	Propellant mass ratio versus specific impulse for a Mars mission with a Δv of 6.5 km/s.	98
3.5	Solar Sail Time of Flights from Earth to Venus.	102
A.1	Planetary Symbols	115

List of Tables

2.1	ADCS Sensors ¹⁵	45
2.2	Attitude Control Methods and Their Capabilities (adapted from Ref. 11) . .	50
3.1	Mass Ratios for Different Thrusters.	101
A.1	Astronomical Data	115
B.1	Various Companies's Thrusters	116
B.2	Examples of Available Monopropellant Hydrazine Rockets.	116
B.3	Examples of Available Bipropellant Rockets.	117
B.4	Examples of Available Solid Rockets.	118
B.5	Examples of Hybrid Rockets Currently Available or in Development.	119
B.6	Available Earth, Magnetic, Star, and Sun Sensors	120

List of Abbreviations

ADCS	Attitude Determination and Control System
AGI	Analytical Graphics, Inc.
AOS	Acquisition of signal
AU	Astronomical unit
BOL	Beginning of life
CAD	Computer-aided design
CC&DH	Communications, Command and Data Handling
Cg	Center of gravity
CMG	Control moment gyro
D&C	Dynamics and Control
EOL	End of life
EP	Electric propulsion
GEO	Geostationary orbit
HET	Hall effect thruster
IT	Ion Thruster
JD	Julian Date
LEO	Low Earth orbit
LOS	Loss of signal
LST	Local Sidereal Time
MMH	Monomethyl hydrazine
NERVA	Nuclear Engines for Rocket Vehicle Application
NTP	Nuclear Thermal Propulsion
PD	Plus derivative
PPT	Pulsed Plasma Thruster
PT&E	Power, Thermal, and Environment
QUEST	Quaternion estimation
RFP	Request for Proposal
RG	Rate gyro
RIG	Rate integrated gyro
RLG	Ring laser gyro
RW	Reaction wheel
S&LV	Structures and Launch Vehicle
SMAD	<i>Space Mission Analysis and Design</i>

SRP	Solar radiation pressure
SSP	Subsatellite point
STK	Satellite Tool Kit
TLE	Two-line element set
TOF	Time of flight

List of Symbols

Roman

A_e	Cross-sectional area Rocket exit area
A_f	Cross sectional area of front of spacecraft
A_t	Rocket nozzle throat area
A_s	Surface area of spacecraft
A_{sail}	Solar sail area
a	Semimajor axis
a_D	Acceleration due to drag
a_r	Acceleration due to solar radiation
a_x	Acceleration due to SRP in x -direction
a_y	Acceleration due to SRP in y -direction
B	Magnetic field strength Q-method and QUEST parameter
b	Semiminor axis
C	Direction cosine matrix
C_D	Dimensionless drag coefficient
C_d	Drag coefficient
C_F	Thrust coefficient
$C_{i,j}$	Inverse Euler rotation matrix components
$C_{p,b}$	Specific heat of block material
$C_{p,b}$	Specific heat of propellant
c	Speed of light
c^*	Characteristic velocity
c_{pa}	Center of aerodynamic pressure
c_{ps}	Center of solar pressure
cg	Center of gravity
D	Drag force Magnetic dipole Parabolic anomaly Residual dipole

d	Thruster duty cycle
	Shortest distance between hyperbolic approach asymptote
d_a	Shortest distance between hyperbolic approach asymptote
d_m	Miss distance
\hat{d}	Unit dipole direction
E	Eccentric anomaly
	Energy
e	Eccentricity
	East unit vector in topological frame
\hat{e}	Principal vector
F	Force
	Solar flux
	Thrust
F_b	Body force
F_g	Gravitational force
F_{Other}	Combination of other forces
F_s	Solar constant
F_{Total}	Total force
\mathcal{F}_s	Sun sensor frame
f	True anomaly
G	Universal gravitational constant
g	Acceleration due to gravity at surface of the Earth
H	Altitude
	Hyperbolic anomaly
\mathbf{H}	Angular momentum vector
H_0	Earth's magnetic field constant
H_i	Component of angular momentum
h	Angular momentum
	Altitude
h_0	Atmospheric scale height
\mathbf{I}	Identity matrix
I	Moment of inertia
I_α	Current output of sun sensor
I_0	Initial current
I_j	Modified Bessel functions for $j = 1, 2, 3$
I_{sp}	Specific impulse
$I_{sp,max}$	Maximum specific impulse
I_α	Current output
i	Angle of incidence
	Inclination angle
$\hat{\mathbf{i}}$	Cartesian unit vector in x -direction

J_n	Dimensionless geopotential coefficients
j	Current
$\hat{\mathbf{j}}$	Cartesian unit vector in y -direction
K	Impulse ratio constant
\mathbf{K}	Q-method matrix
K_p	Position gain
K_r	Rate gain
$\hat{\mathbf{k}}$	Cartesian unit vector in z -direction
k_R	Inertia ratio
k_Y	Inertia ratio
L	Electrode spacing
	Geocentric Latitude
	Lagrangian function
	Latitude
	Moment arm length
	Torque
L_s	Sub-satellite longitude
\mathcal{L}	Lagrangian function
l	Longitude
M	Euler rotation matrix
	Magnetic moment of Earth
	Mass of orbited body
	Mean anomaly
M_0	Initial mean anomaly
M_{Sun}	Mean anomaly of Sun
M_w	Molecular weight
m	Mass
	Particle mass
	Spacecraft mass
m_b	Burnout mass
m_{block}	Mass of block
m_f	Final mass of spacecraft after a thrusting period
m_h	Mass of fuel
m_i	Mass of particle
\mathbf{m}_i^*	Magnetic field vector
m_j	Mass of particle
m_L	Payload mass
m_0	Spacecraft initial mass
m_{OX}	Oxidizer mass
m_p	Propellant mass
m_r	Mass of rocket

m_s	Spacecraft structural mass
m_{sc}	Spacecraft mass
\dot{m}	Mass flow rate
N	Inertial frame
	Vector to ascending node
n	Mean angular motion of satellite
	North unit vector in topological frame
	Number of revolutions
\hat{n}	Second unit vector in topological frame
P	Perifocal frame
	Orbital period
	Power
P_∞	Ambient pressure
P_0	Stagnation pressure
P_b	Beam power
P_c	Combustion chamber pressure
P_e	Pressure at rocket exit
P_i	Input power
P_n	Legendre polynomials
\mathbf{p}	Rodrigues parameter principal rotation vector
p	Semilatus rectum
Q_R	Heat supplied to propellant during combustion
\mathbf{q}	Euler parameters attitude vector
q	Particle charge
	Reflectance factor
q_i	Rodrigues parameters
R	Mixture ratio
	Orbit radius
	Planet radius
	Spacecraft mass ratio
\mathbf{R}^{bi}	Triad rotation matrix
R_E	Radius of the Earth
R_g	Gas constant
\mathbf{R}_i	Position vector of particle
R_m	Mars equatorial radius
R_\oplus	Radius of Earth
r	Inner radius of tank
	Position / radial distance
r_1	Initial position
r_2	Final position
r_3	Periapsis radius of the hyperbolic approach orbit

\hat{r}	Direction vector of spacecraft
r_a	Apoapsis radius
\mathbf{r}_c	Position vector from center of mass
r_{eq}	Equatorial radius
r_H	Radius of hydrogen tank
\mathbf{r}_i	Position vector from the origin to body i
\mathbf{r}_{ij}	Position vector from body i to body j
r_m	Mars orbital radius
r_O	Radius of oxygen tank
r_p	Periapsis radius
\mathbf{r}_p	Ground station position vector relative to center of Earth
\mathbf{r}_s	Satellite position vector relative to center of Earth
r_{SOI}	Radius of sphere of influence
\mathbf{S}	Q-method and QUEST parameter
$\hat{\mathbf{s}}$	Sun direction vector
r_{si}	Radius of sphere of influence
s	Distance from center of mass to thrust application point
$\mathbf{s}_i^T \{\hat{\mathbf{i}}\}$	Sun direction vector
$\mathbf{s}_b^T \{\hat{\mathbf{b}}\}$	Sun direction vector
\mathbf{s}_s	Sun direction vector
\mathbf{s}_s^*	Non-unit Sun direction vector
T	Magnitude of kinetic energy
	Thrust
	Topological frame
\mathbf{T}	Vector thrust
T_0	Stagnation temperature
T_a	Aerodynamic torque
\mathbf{T}_b	Body reference matrix
T_c	Control torque
T_D	Disturbance torque
	Peak disturbance torque
T_g	Gravity gradient torque
\mathbf{T}_i	Inertia reference matrix
T_{int}	Separatrix kinetic energy
T_m	Magnetic torque
T_{max}	Maximum kinetic energy
	Maximum temperature
T_{min}	Minimum kinetic energy
	Minimum temperature
T_{RW}	Torque of a reaction wheel
T_{sp}	Solar radiation torque

T_{thrust}	Thruster torque
T_{UT}	Period in universal time
t	Time
	Time since epoch
t_0	Initial time
t_{AOS}	Acquisition of signal time
t_b	Burn time
\mathbf{t}_b	Normalized reference body vector
\mathbf{t}_i	Normalized reference inertial vector
t_{LOS}	Loss of signal time
u	Up unit vector in topological frame
V	Potential energy
	Volume
V_0	Velocity of satellite immediately after launch
V_a	Potential difference
V_{eq}	Velocity of Earth's rotation at equator
V_L	Inertial velocity of launch site
v	Velocity
v_0	Initial velocity
v_1	Initial velocity
v_2	Final velocity
	Arrival velocity
v_3	Departure velocity
v_4	Heliocentric velocity as spacecraft exits sphere of influence on fly-by
$v_{\theta 1}$	Initial tangent velocity
$v_{\theta 2}$	Final tangent velocity
v_a	Velocity to apoapsis
\mathbf{v}_b	Normalized measured body vector
v_c	Circular velocity
v_e	Propellant exit velocity
	Velocity of Earth
v_{eq}	Equivalent velocity
v_{esc}	Escape velocity
v_{ex}	Propellant exhaust velocity
v_g	Ground track velocity
v_i	Combined velocity of v_y and v_z
\mathbf{v}_i	Normalized measured inertial vector
\mathbf{v}_{kb}	Q-method body measurement vector
\mathbf{v}_{ki}	Q-method inertial measurement vector
v_m	Velocity of Mars
v_p	Velocity to periapsis

v_{planet}	Velocity of planet
v_{sail}	Logarithmic velocity of sail
v_{sp}	Spiral velocity
v_{total}	Total velocity
v_y	Velocity in y -direction
v_z	Velocity in z -direction
W	Work
x	Cartesian coordinate
y	Cartesian coordinate
Z	Q-method and QUEST parameter
z	Cartesian coordinate

Greek

α	Angle between orbital plane and Moon's orbit
	Azimuth angle
	Euler rotation angle - first
	Solar pitch angle
	Specific mass
	Sun incidence angle
α_0	Sun incidence angle tilted
α_1	Sun incidence angle of first photocell
α_2	Sun incidence angle of second photocell
α_m	Unit dipole parameter
β	Euler rotation angle - second
	Launch azimuth
	Sail lightness factor
	Solar lightness factor
β	Euler vector
β_0	Euler parameter - first
β_1	Euler parameter - second
β_2	Euler parameter - third
β_3	Euler parameter - fourth
β_i	Inertial launch azimuth
γ	Angle between orbital and ecliptic plane
	Correction to account for velocity contribution caused by Earth's rotation
	Euler rotation angle - third

	Payload ratio
	Sidereal time
	Specific heat ratio
δ	Angle in equatorial plane from nearest node to longitude of launch site
	Latitude
δ_s	Sub-satellite latitude
ϵ	Elevation angle
	Structural coefficient
ϵ_0	Permittivity of free space
η	Efficiency
θ	Euler angle
	Slew angle
	Maximum z-axis deviation from vertical
θ_ϵ	Allowable attitude error
θ_1	Euler rotation angle - first
θ_2	Euler rotation angle - second
θ_3	Euler rotation angle - third
θ_a	Allowable motion / pointing accuracy
θ_{g0}	Greenwich sidereal time at epoch
θ_i	Angle between Mars' relative velocity vector and orbital path
θ'_m	Coelevation of dipole
λ	Eigenvalue of \mathbf{K} matrix in Q-method
$\lambda_{ecliptic}$	Ecliptic longitude of Sun
λ_{MSun}	Mean longitude of Sun
λ_{opt}	Largest eigenvalue of \mathbf{K} matrix in QUEST method
μ	Gravitational coefficient
μ_\odot	Gravitational coefficient of Sun
μ_e	Gravitational coefficient of Earth
μ_m	Gravitational coefficient of Mars
μ_{planet}	Gravitational coefficient of planet
ν	Relative velocity in the planet-centric frame
ν_0	Initial relative velocity
$\nu_{0,Hohmann}$	Initial Hohmann relative velocity
ν_1	Relative velocity at edge of sphere
ν_2	Relative arrival velocity of target planet
ν_3	Relative departure velocity of target planet
ν_c	Relative velocity of Earth
ν_{cm}	Burn necessary to circularize orbit around Mars
ρ	Atmospheric density
	Fuel density
ρ	Satellite position vector relative to ground station

ρ_0	Density at initial latitude
ρ_p	Atmospheric density at perigee
Σ	Principal axis angle constant
σ	Modified Rodrigues principal rotation vector
σ	Q-method and QUEST parameter
	Sail loading factor
	Standard deviation
σ_2	Heading angle
σ_4	Angle between heliocentric exit velocity and Mars' orbital path
σ_{crit}	Critical solar sail loading factor
σ_{cyl}	Allowable stress of cylindrical tank walls
σ_i	Modified Rodrigues parameters
σ_{sc}	Spacecraft sail loading factor
σ_{sph}	Allowable stress of spherical tank walls
Φ	Principal axis rotation angle
	Half turn angle
	Hyperbolic asymptote angle
ϕ	Euler angle
	Flight path angle
	Gravitational potential function
	Spiral angle
ϕ_2	Angle between heliocentric and Mars relative velocity vectors
ϕ'_m	East longitude of dipole
ϕ_{opt}	Optimum spiral angle
φ_2	Heading angle
ψ	Euler angle
Ω	Angle of right ascension of ascending node
	Momentum wheel's relative angular velocity
Ω_{Moon}	Angle of right ascension of ascending node of the Moon
Ω_{Sun}	Angle of right ascension of ascending node of the Sun
ω	Argument of periapsis
	Angular velocity
ω_i	Component of angular velocity vector
ω_{Moon}	Argument of periapsis of the Moon
ω_n	Bandwidth
ω_s	Angular velocity of satellite
ω_{Sun}	Argument of periapsis of the Sun
ω_{\oplus}	Rotation rate of the Earth

Planetary Symbols

Planetary symbols A.1 can be found with Astronomical data in Appendix A.

Notation

The symbol x is used here as generic example, any symbol may be used in place of x . Notation may be combined, for example $\dot{\mathbf{x}}$ is the inertial derivative of the x vector

\mathbf{x}	vector
x	scalar magnitude \mathbf{x}
$\hat{\mathbf{x}}$	unit vector \mathbf{x}
x_i	x for body i
$[X]$	matrix \mathbf{x}
\dot{x}	first derivative of x
\ddot{x}	second derivative of x
Δx	change in x
dx or $d(x)$	derivative of x
$\frac{dy}{dx}$ or $\frac{d(y)}{d(x)}$	derivative of y with respect to x
$\frac{d^2y}{dx^2}$ or $\frac{d^2(y)}{d(x^2)}$	second derivative of y with respect to x

Chapter 1

Introduction

Astrodynamics, Attitude Determination and Control System (ADCS), and Propulsion are the subdivisions that make up the Dynamics and Control (D&C) Functional Division. The three subdivisions are primarily responsible for determining and controlling the location and orientation of the spacecraft throughout the mission. Therefore, the subdivisions must design the spacecraft's orbit, insert the spacecraft into that orbit, and control the spacecraft's orientation in the orbit. The three subdivisions must work together to accomplish these objectives, due to the overlapping responsibilities. In this chapter, the responsibilities of the three subdivisions are briefly outlined and the interactions between each subdivision and all other subdivisions are discussed. Later chapters provide an in depth discussion of each subsystem as well as examples of how the subsystems interact.

1.1 Astrodynamics

The Astrodynamics Subdivision is responsible for three aspects of a space mission: orbit selection, mission analysis, and guidance and navigation. The subdivision must determine what the mission entails and how to best accomplish the mission while maximizing efficiency and simplicity. In this section the various orbit types are discussed followed by an introduction to the idea of orbit trade studies. The development of the Δv budget is also discussed, as is orbit determination and maintenance.

1.1.1 Orbit Types

There are two fundamental categories of orbits: closed and open.¹¹ In a closed orbit the orbiting body completes periodic circuits around the attracting mass. An open orbit is one in which the orbiting body continues past the attracting mass and does not return. The energy of the orbit determines whether the orbit is open or closed.¹⁵ There are two basic varieties of closed orbits, elliptical and circular, and two basic varieties of open orbits, hyperbolic and parabolic. The majority of satellites are in elliptical orbits. Hyperbolic orbits are used for missions requiring a spacecraft to escape the influence of an attracting mass.

Another method of orbit classification is based upon the function of the orbit. There are two types of operational orbits that are characterized by the primary purpose of the spacecraft: space-referenced and Earth-referenced. A spacecraft that is orbiting Earth and whose primary purpose deals with Earth is referred to as being in an Earth-referenced orbit. If the principle characteristic of an orbit is that it is somewhere in space and not orbiting a specific celestial body, the orbit is called space-referenced. An example of such an orbit is an orbit around a Lagrange point.¹¹

Orbit-related mission requirements must be defined for each mission segment. Such requirements include coverage, sensitivity, environment and survivability, launch capability, ground communications, and orbit lifetime. For example, the first step in finding the appropriate orbit for an Earth-referenced mission is to determine if a specialized orbit applies, such as a geosynchronous, Sun-synchronous, Molniya, or Frozen orbit. Each of these specialized orbits should be examined individually to determine if its characteristics meet the mission requirements at a reasonable cost. Spacecraft do not need to be in specialized orbits, but these orbits are in common use because of their valuable characteristics.¹¹

1.1.2 Orbit Trade Studies

Various orbit design trade studies, all of which are dependant upon the mission requirements, are necessary for a successful space mission. The purpose of these trade studies is to establish the best orbit by taking into account each of the mission requirements. Orbit parameters such as altitude and inclination are given a range of possible values. Each orbit is then evaluated with respect to how it affects the specified requirements. This evaluation weighs the advantages and disadvantages of each orbit and establishes all possible alternate orbits. From these possible orbits further analysis of cost or performance is performed until a single orbit is selected.¹¹

1.1.3 The Δv Budget

Another responsibility of the Astrodynamics Subdivision is to develop a Δv budget. This budget is mainly constrained by the amount of fuel that the spacecraft can carry or produce.¹¹ The Δv budget is used to make any form of velocity change, from changing orbit shapes or inclinations to making various adjustments to maintain the desired orbit. The best Δv budget is the smallest possible that can accomplish the mission with a sufficient margin to allow for any additional adjustments that may be needed.

1.1.4 Orbit Determination & Maintenance

Orbit determination relies strongly on the function of the spacecraft and the limits of the payload.¹¹ For example, if the spacecraft is to observe specific regions of the Earth and cannot be in a high altitude orbit due to the payload's maximum resolution abilities, then

the orbit is constrained to a LEO, and the inclination angle must be one such that the satellite passes over the designated areas.

Effects such as perturbations alter the orbit in often undesirable ways, and the orbit must be corrected in order to complete the mission. Orbit maintenance requires determining how the orbit has deviated from the desired orbit and communicating with the ADCS subdivision to make the necessary corrections.

As outlined in this section, the Astrodynamics Subdivision selects the orbit for a given mission, performs necessary mission analysis, and conducts all guidance and navigation. However, the Astrodynamics Subdivision does not make sure the spacecraft is in a correct or stable attitude, or provide the forces needed to change the orbit and stabilize the spacecraft. These duties fall to the ADCS and Propulsion Subdivisions, which are discussed in the next two sections.

1.2 Attitude Determination and Control System

The purpose of the Attitude Determination and Control System (ADCS) is to stabilize the satellite and place it in a desired attitude. Achieving these tasks requires various sensors to determine the attitude, as well as actuators to maintain the attitude. The sensors and actuators are selected based on the required attitude accuracy.

1.2.1 Requirements

The attitude determination and control system must fulfill certain requirements in order for a spacecraft to meet mission objectives. These requirements are determined by operational constraints and design criteria. First, attitude control must be maintained. The accuracy of the vehicle's attitude must be controlled with respect to a direction commanded by the ground station, while the range of motion is limited by the control performance of the spacecraft. Attitude control has several other requirements, such as jitter and drift, which must be kept at a minimum to prevent errors in sensor data and to prevent the spacecraft from drifting off course. Secondly, attitude determination should have a small enough error to properly maintain a mission-dependent orientation with respect to a reference point. The spacecraft must keep this desired orientation for purposes such as communication and proper data acquisition. Two other sub-requirements can be implemented in the control system. The first sub-requirement is keeping ground communication, which is essential for maintaining correct orbit positions. Maintaining ground communication also necessitates certain roll and pitch attitude constraints. The second sub-requirement is that the ADCS must support the scientific mission. A probe is required to collect valid data for the spacecraft. This probe should not point in a direction where the data would be corrupted, such as in the wake of the spacecraft. All of these requirements are closely related to the control modes of the spacecraft.¹¹

1.2.2 Modes

Defining the control modes requires analyzing the mission profile and mission objectives. Each mode corresponds to a different action or condition of the ADCS. Orbit insertion, normal, slew, and safe are the four major modes. The orbital insertion mode occurs directly after the spacecraft detaches from the launch vehicle. The spacecraft can either have no control, simple spin stabilization, or full control. The normal mode occurs between thrusting maneuvers, and the requirements for this mode drive the ADCS design. The slew mode is used to reorient the spacecraft as required. Safe mode (also known as stand-by mode) is used when a major malfunction occurs, such as a thruster or a booster malfunction. Energy consumption is reduced and the spacecraft is oriented to ensure that the power requirement is fulfilled. All rates are measured and stored for possible downlink to the ground station.¹¹

1.2.3 Disturbance Torques

When designing a spacecraft, the disturbance torques from the spacecraft's surrounding environment must be considered. The four major types of external disturbance torques are solar radiation, gravity gradients, magnetic fields, and aerodynamic. Factors such as the orbit altitude, mass properties, spacecraft geometry, and spacecraft orientation affect the magnitude of each disturbance torque and therefore which type of torque is dominant.¹¹ Once the expected disturbance torque is known, the ADCS actuators, the sizes of the actuators, and the angular momentum storage capacity may be determined.

Solar radiation torques are caused by light particles exerting pressure on the surface of the spacecraft. The amount of pressure exerted depends on the surface's reflectivity. The solar radiation torque is also influenced by the surface area of the spacecraft and the location of the center of mass.¹¹ For Earth-oriented vehicles, solar radiation pressure produces a cyclic torque. For Sun-oriented vehicles and platforms separate from the vehicles, solar radiation pressure produces a constant torque that accumulates and requires active control.

Gravity gradient torques are caused by differences in the gravitational forces on portions of the spacecraft due to the distances between the center of the Earth and that portion of the spacecraft. Applying Newton's Law of Universal Gravitation, the portion of the spacecraft closer to Earth experiences a larger gravitational pull than the portion of the spacecraft further away. The difference in gravitational forces results in a tendency for the spacecraft to rotate so that it is aligned along its long axis, the axis of minimum inertia. Therefore, the gravity gradient torque depends on the orbit altitude and the spacecraft inertias. For Earth-oriented vehicles, the gravity gradient results in a constant torque. For inertially oriented vehicles, the gravity gradient torque is cyclic.¹¹

Magnetic field torques are caused when the spacecraft's internal magnetic field attempts to align with the Earth's magnetic field. The spacecraft's internal magnetic field is created by the magnetism of its structural materials and the electrical currents within its instrumentation. The magnetic torque is also influenced by factors like magnetic flux density, eddy currents, orbit inclination, and the orbit altitude.¹⁶ The magnetic field results in a cyclic torque, regardless of vehicle orientation.¹¹

Aerodynamic torques are caused by interactions between the atmosphere and the spacecraft. The aerodynamic torque increases as the density of the atmosphere increases; therefore, orbit altitude is an influential factor in the amount of aerodynamic torque experienced by a spacecraft. Since the aerodynamic torques are similar to those encountered by airplanes, the shape of the spacecraft and its center of gravity also affect the aerodynamic torque. The aerodynamic torque is constant for Earth-oriented vehicles but variable for inertially oriented vehicles.¹¹

Internal torques also impact the spacecraft and can be incorporated into the design. For instance, it is possible to compensate for known disturbance torques due to fuel sloshing or rotating machinery within the vehicle. Misalignments in the thrusters that cause disturbance torques can be corrected within a closed-loop control system.¹¹ Other types of internal torques that should be considered include movement of antennas and instruments, deployment of booms and other appendages, and movement of solar panels.

1.2.4 Control Approaches

There are three general categories of spacecraft attitude control techniques: passive stabilization, spin control, and three-axis control. Each of these techniques encompasses several possible methods for stabilizing and controlling a spacecraft in orbit.¹¹

The first attitude control technique is the passive stabilization technique. Gravity-gradient stabilization, where gravity induced torques counteract other external torques, is a common method under this category. Because this method allows for rotation about the nadir axis, it is often used in combination with a momentum wheel oriented perpendicular to the nadir and velocity directions. Another passive stabilization technique involves the use of permanent magnets to force a particular orientation with respect to Earth's magnetic field. These methods are attractive because they require little energy to maintain and are simple in nature.¹¹

The second attitude control technique is the spin control technique, which stabilizes a spacecraft through gyroscopic stability. When a spacecraft is spun about a given axis, it resists changes to the orientation of that axis due to its conservation of angular momentum.¹¹ Spacecraft spun about the maximum moment of inertia axis remain stable despite energy dissipation, whereas spacecraft spun about the other two axes become unstable as energy is lost.¹⁵ These stability conditions result in disk-shaped spinners that are constrained in size by the launch vehicle diameter. Dual-spin spacecraft, on the other hand, can remain stable when spinning about any inertial axis, thus allowing for longer, thinner spacecraft. Dual-spin spacecraft have two portions that rotate at different speeds, often with one section held steady with respect to the Earth or the Sun. However, the added complexity of the joint between the two rotating sections poses a significant drawback over the simple spinner. One disadvantage of both simple-spin and dual-spin spacecraft is that they require considerable energy to change the orientation of the angular momentum vector.¹¹

In discussing the performance of spin-controlled spacecraft, defining the terms precession, wobble, and nutation is important. Precession refers to the realignment of the angular

momentum vector due to external torques on the spacecraft. Wobble is caused by the difference between the intended spin axis of the body and the actual angular momentum axis, which occurs when the angular momentum axis is aligned with a principal axis of inertia rather than a body reference axis. Nutation is the motion resulting from the misalignment of the angular momentum vector and the principal axis of inertia. All three of these motions are used to describe the overall behavior of the spacecraft.¹¹

The third attitude control technique is the three-axis control technique, typically involving a combination of thrusters, magnets, momentum and reaction wheels, and control moment gyros (CMGs).¹¹ Thrusters can be used exclusively for shorter duration missions where high torques are required, but are typically used with magnets to augment a reaction wheel or CMG system. Although more maneuverable and more easily controlled than spacecraft utilizing the first two control techniques, three-axis controlled spacecraft are also more expensive and complex.

Reaction wheels work through varying the speed of the wheel in response to external torques such that the original angular momentum of the spacecraft is maintained. These wheels are limited by the bearings and motors to a certain saturation speed, such that when that speed is approached, thrusters and/or magnets must be used to dissipate the excess momentum and reduce their speed.¹⁵ This action of “bleeding off” momentum is known as desaturation, momentum unloading, or momentum dumping.¹¹

Control moment gyros work similarly to spin-stabilized spacecraft in utilizing the torques caused by rotating a spinning disk, and offer greater torque capability than reaction wheels. However, CMGs are also subject to gimbal lock, in which case the desired torque can not be created. Oftentimes both reaction wheels and CMGs are utilized in sets of four: three located on orthogonal axes, and the fourth as a back-up.¹⁵

Yet another three-axis control method is known as a momentum bias system. In a momentum bias system, there is a variable speed wheel oriented along the pitch axis, providing stabilization similar to a spinning spacecraft. A momentum bias system is similar to a reaction wheel, but it can also provide pitch control by varying the speed of the wheel.¹¹

1.2.5 Algorithms

Applying linear theory to describe the dynamics of the attitude control system enables a preliminary analysis of the system’s performance. As the system develops, its model requires additional linear and nonlinear equations. For example, feedback loops enhance the performance of the system, but also increase the complexity of the system.

Different types of attitude control systems necessitate different parameters and algorithms to analyze the system’s performance. For instance, a system for three-axis stabilization relies on the position gain and bandwidth, whereas a system for spin stabilization relies on the nutation frequency as the key parameter. The position gain is the control torque resulting from a unit attitude error and the bandwidth is the frequency at which control authority begins to diminish. The level of accuracy required also affects the algorithms used; different methods of averaging and smoothing of data input from the feedback sources impact the

accuracy of the control system. Even choices as simple as the coordinate frame impact the rotations necessary, as the different methods of describing a spacecraft's orientation have different singularities.¹¹

The ADCS Subdivision is responsible for determining the requirements of the mission in terms of attitude accuracy and the methods used to maintain the attitude. Considerations such as the control modes, disturbance torques, control mechanisms, and the algorithms utilized to determine the controls were all introduced. However, attitude corrections are not possible without a means of providing thrust. The Propulsion Subdivision, which is discussed in the next section, determines the fuel necessary to control the spacecraft's attitude, and also provides the means by which the spacecraft enters into and changes its orbit.

1.3 Propulsion

The purpose of a spacecraft's in-space propulsion system is two-fold. First, it serves as a means to transfer payloads from one orbit to another, as well as to place the spacecraft on trajectories for interplanetary or interstellar missions. Second, it provides thrust that is needed for attitude control and orbit corrections. Both of these functions are vital to the performance and operation of any spacecraft, making propulsion system design one of the most important aspects of spacecraft design. When determining what propulsion system is used for a given mission, several issues must be considered. These issues include, but are not limited to: what types of propulsion systems are currently available or will be available at the time of launch, what mission phases have different propulsion requirements, and how a change in the desired performance of the spacecraft affects the design of the propulsion system. These questions are the most important questions that must be addressed in the propulsion system design process, and are discussed in a brief and broad manner in this section.

1.3.1 Propulsion System Alternatives

The in-space propulsion systems currently available or in development operate using a wide range of propulsion methods. The available systems also have a wide range of performance capabilities, and can thus be used as a spacecraft's primary means of propulsion as well as for orbit maintenance, maneuvering, and attitude control purposes. The following discussion describes some of the more popular and promising systems.

The most widely used propulsion system is the chemical rocket, of which there are two types: the solid rocket and the liquid rocket. In a solid rocket, a solid propellant core is ignited and the resulting combustion gases are accelerated through a nozzle to create thrust. Liquid rockets, on the other hand, use the combustion products of a liquid propellant to create thrust. Both monopropellant and bipropellant liquid rockets are used at the present time. The range of thrust provided by solid and liquid rockets is on the order of 5 to 5,000,000 N. Hybrid rockets that use both solid and liquid propellants also exist, but can only provide thrust up to about 3,500,000 N. Due to their broad thrust range, chemical

rockets are versatile, and are used for main propulsion, orbit maintenance, maneuvering, and attitude control.¹¹

The most basic propulsion system currently available is the cold gas system, which uses an inert gas stored at a high pressure as propellant. To create thrust, the gas is simply accelerated through a nozzle. The thrust created through this process ranges from about 0.05 to 200 N, which is small when compared to other propulsion systems. Because of this small thrust, cold gas systems are mostly used for attitude control. Also, cold gas systems are reliable and cheap, but they are the heaviest systems available with respect to their performance capabilities.¹¹

Electrical propulsion systems are currently in operation or are in the development stages. Three main classifications of electric propulsion exist: electrostatic, electrothermal, and electromagnetic.⁷ In electrostatic propulsion, the propellant is composed of discrete charged particles that are accelerated by electrostatic forces. The ion engine falls under this category of electrical propulsion. Electrothermal propulsion utilizes either an electrical arc discharge (arcjet) or electrical heating through walls (resistojet) to heat up the propellant. Once the propellant is heated, thrust is created by accelerating it through a nozzle. In electromagnetic propulsion, a stream of an electrically conducting fluid is accelerated using electromagnetic and pressure forces.⁷ The thrust created by any of these electrical propulsion systems is relatively small, however, being on the same level as cold gas systems. For this reason, electrical propulsion has many applications in attitude control. On the other hand, the propellant mass needed in an electrical propulsion system is often small when compared to other propulsion systems, meaning that electrical propulsion systems can operate for longer periods of time. If mission duration is not a vital concern, electrical propulsion can be used to accelerate a payload to a high speed over a long period of time.

Various types of propulsion systems that utilize solar sails are presently in development. One type of proposed solar sail uses the momentum of solar particles to propel a payload. As the solar particles impact the sail, their momentum is transferred to the sail, which then accelerates the payload to a tremendous speed. Another proposed way to use sails in space is to use a large laser on the Earth or other celestial body to beam energy to the sail. Such a system would be needed for missions to the outer reaches of the solar system, as the momentum that can be extracted from solar particles is inversely proportional to distance from the Sun.

One final issue to consider is that if there is no constraint on the launch date of a given mission, there are a number of advanced propulsion systems that can also be considered. For example, if an interstellar mission is being considered for a hundred or so years in the future, it is perfectly acceptable to consider propulsion systems that rely on nuclear fusion or even antimatter to provide power. As long the mission launch date is not until sometime in the future, almost any conceivable propulsion system is possible.

1.3.2 Mission Phase Requirements

The different propulsion requirements for the various phases of a space mission must be considered during the design or selection of a propulsion system. The required performance of the propulsion system is not the same during different phases of the mission, so the effects of each separate mission phase on the system performance must be analyzed in conjunction with more general performance of the entire mission. For example, the total mass of propellant available over the entire mission may be constrained, so the amount of propellant needed for the initial orbit insertion, any transfer orbits, and all anticipated control maneuvers must be determined and fit to this constraint. Determining the requirements for each mission phase also assists in the determination of which mission phases are the most expensive (or inexpensive) in terms of both materials and cost, or how propellant can be diverted from one mission phase to another.

1.3.3 Performance Considerations

The effects of changing the desired performance of a spacecraft must also be considered when determining what type of propulsion system is used. Changing the desired specific impulse, Δv budget, time of flight, spacecraft mass, pointing requirements, or any other performance parameter has an influence on what propulsion system must be used. If larger Δv 's are desired, a system that produces the most thrust may be selected. On the other hand, if a higher specific impulse is needed and the time of flight is not important, a low-thrust electrical propulsion system may be used. Whatever the case may be, the propulsion system will have to be altered several times during the design process in order to account for changes in the desired performance of the spacecraft.

1.4 Interactions Between Dynamics and Control Subdivisions

Each of the three D&C subdivisions has an impact on the other two subdivisions. These interactions must be properly understood and modelled in order to arrive at an optimal spacecraft design, and are discussed in this section.

1.4.1 Astrodynamics and ADCS

The Astrodynamics and Attitude Determination and Control System Subdivisions must work closely together. The orbit has an effect on the types of torques experienced by the spacecraft. The inclination of the orbit has an effect on the selection and accuracy of the sensors. Attitude determination is crucial when changing orbit types. The attitude of the spacecraft affects which sensors are used to determine the current location of the spacecraft. For example, a sun sensor pointing towards the Earth cannot be used effectively. The orbit

insertion type affects what type of insertion mode is used, and therefore the stability of the spacecraft.

1.4.2 Astrodynamics and Propulsion

The Propulsion and Astrodynamics Subdivisions communicate to develop the propellant budget. The Astrodynamics Subdivision determines the mission's orbits and transfers, which are then translated into a Δv budget. The Propulsion Subdivision then determines the required propellant to meet the Δv budget. Further, the two groups must work together to determine whether a low-thrust or high-thrust propulsions system must be used.

1.4.3 ADCS and Propulsion

The most important interaction between the ADCS and the Propulsion Subdivisions is the location of the thrusters. Appropriately placed thrusters provide the torques necessary to control the spacecraft. The Propulsion Subdivision develops a propellant budget based upon the estimated amount of attitude correction that must be performed. To reduce the propellant needed for ADCS actions, different types of actuators, including control moment gyros and momentum wheels, can be used in place of thrusters to create the torques required to change the spacecrafts attitude.

1.5 Interaction with Other Functional Divisions

Communication between the different functional divisions is necessary to create an optimized final design, as the decisions made in the design of the three D&C subsystems impact the designs of the other three functional divisions. Furthermore, those functional divisions must provide the three D&C subdivisions with information so that the D&C subsystems can be designed.

1.5.1 Structures and Launch Vehicles

The S&LV Functional Division is responsible for sizing the spacecraft's primary structural members, identifying the requirements for mechanisms and deployables, and selecting the launch vehicle. These responsibilities are directly related to several of the D&C responsibilities, such as determining the propellant budget, selecting the location of certain ADCS components, and designing the orbits to be used. As a result, cooperation is needed to ensure that correct and up-to-date information is communicated between the two groups.

The performance capabilities of the selected launch vehicle and the mass of the spacecraft are driving factors in starting the orbit design process. Assuming no constraints, the Astrodynamics Subdivision defines the desired Earth or interplanetary trajectory. The Launch Vehicle Subdivision then provides a vehicle that can meet the trajectory requirement and has the capability to accommodate the mass of the spacecraft, with a sufficient mass margin.

However, constraints do exist, such as the limited number of launch vehicles and the maximum mass that can be launched into space on a given launch vehicle. In addition, a Request For Proposal (RFP) may add constraints that further limit the maximum possible mass, or even specify a specific launch vehicle. Under such circumstances, the two subdivisions must devise a solution that meets both the mission's needs in terms of mass and the orbit design's requirements for trajectory insertion.

Interaction is also needed between the Structures, ADCS, and Propulsion Subdivisions, particularly in the areas of mass and location of components. The masses of the D&C subsystems must be communicated to the S&LV Function Division so that an overall spacecraft mass can be determined. In addition, the ADCS Subdivision must work with the Structures Subdivision to determine the spacecraft's moments of inertia, which affects the design of the control system. The locations of certain Propulsion and ADCS subsystem components, such as thrusters, engines, and magnetic torque rods, must also be determined in cooperation with the Structures subsystem. The forces and moments exerted by such components affect the structural integrity of the spacecraft. Also, the components' locations drive the performance of the ADCS and Propulsion systems and, in the case of thrusters and engines, the propellant mass required by the Propulsion system.

Further communication is also required between the Propulsion and Structures Subdivisions. For instance, propulsion systems require propellant tanks that are primary structural elements of the spacecraft and must be designed by the Structures Subdivision. Other propulsion systems, such as solar thermal or solar sails, may require the use of deployables in order to be effective.

1.5.2 Power, Thermal, and Environments

The PT&E Functional Division is responsible for creating the power budget, developing the thermal requirements of the spacecraft, and modelling the effect of the space environment on the spacecraft and its components. These responsibilities require information that can be provided by the D&C Functional Division, with small cooperation needed between the ADCS and Power subsystems to establish the spacecraft's operating orientation.

The Power Subdivision works closely with the Astrodynamics and ADCS Subdivisions, focusing on the location and the orientation of the spacecraft. The size of a spacecraft's batteries and solar arrays are driven by its beginning-of-life (BOL) and end-of-life (EOL) power requirements, which are primarily calculated as a function of solar cell degradation and the spacecraft's distance from the sun. If solar arrays are used, the Astrodynamics Subdivision provides the Power Subdivision with the spacecraft's distance from the Sun throughout its orbit, particularly at the spacecraft's BOL and EOL. Furthermore, the mission lifetime must be taken into account in the orbit design, as shorter mission lifetimes reduce the prolonged effect of solar cell degradation. The ADCS and Power Subdivisions also cooperate to ensure that the spacecraft's operating orientation allows enough power to be obtained and to verify that the pointing requirements of the arrays are met. Both the ADCS and Propulsion Subdivisions also provide the Power Subdivision with subsystem power requirements.

The Thermal Subdivision uses the thermal requirements of the Propulsion and ADCS subsystem components to create a thermal model. This model is utilized to ensure the safety of the subsystem components. In addition, the Thermal Subdivision obtains the location and orientation of the spacecraft from the Astrodynamics and ADCS Subdivisions to take into account radiation effects.

The Environment Subdivision works with D&C Subdivisions to establish a model of the surrounding environment, so that its effects on the spacecraft components can be determined. The spacecraft's location and orientation must be provided by the Astrodynamics and ADCS Subdivisions so that a model of the exterior environment can be determined. Furthermore, the Environment Subdivision cooperates with the Propulsion Subdivision to ensure the propellant exhaust gases are not harmful to the spacecraft.

1.5.3 Communications, Command and Data Handling

The Communication Subdivision of the Communications, Command and Data Handling (CC&DH) Functional Division works closely with the Astrodynamics and ADCS Subdivision of the D&C Functional Division to define the spacecraft pointing requirements and to obtain the location of the spacecraft throughout its orbit. Depending on the mission profile and the payload, the communications system may be the driving factor in the determination of pointing requirements. The ADCS and Communication Subdivisions must work together to determine if the communications system has this impact. The Communication Subdivision also works with the Astrodynamics Subdivision to determine the location of the spacecraft relative to Earth or communication satellites. This information is needed to perform link margin analysis, as one of the major inputs to such analysis is distance between the communicating objects. As a minimum link margin must be met, the distances may drive the power required by the Communication subsystem and the antenna selection.

1.6 Conclusion

Chapter 1 gives a brief overview of the three subdivisions that make up the D&C Functional Division: Astrodynamics, Attitude Determination and Control System, and Propulsion. The Astrodynamics Subdivision is responsible for orbit types, orbit trade studies, Δv budget, and orbit determination and maintenance. The ADCS Subdivision determines the stability requirements for a given mission and the mechanisms utilized to maintain the appropriate attitude. The Propulsion Subdivision selects the propulsion system and develops a propellant mass budget. These three subdivisions must exchange information amongst each other, as well as with other functional divisions, in order to develop an optimal design. A brief discussion of these interactions was presented in this chapter, and a more detailed discussion is provided in the next chapter. Chapter 2 also provides an in-depth analysis of the D&C subsystems. Examples of these interactions and analyses will be provided in Chapter 3.

Chapter 2

Modelling and Analysis

This chapter outlines the analysis needed for modelling each of the D&C subdivisions. Subsystems within the astrodynamics, attitude determination and control, and propulsion subdivisions are analyzed using various modelling tools. Equations, charts, and tables are gathered for each physical subsystem a spacecraft uses. The interactions among the subdivisions and the other functional divisions are addressed.

2.1 Astrodynamics

Different orbit shapes, planes, and constraints must first be considered to model and analyze the desired mission geometry and the guidance and navigation system. The equations of motion for N-body or two-body systems must be utilized to complete the orbit determination process.

2.1.1 Equations of Motion

Kepler, originally working with Brahe, developed what are now known as Kepler's three laws:

First Law The orbit of each planet is an ellipse, with the sun at a focus.

Second Law The line joining the planet to the sun sweeps out equal areas in equal times.

Third Law The square of the period of a planet is proportional to the cube of its mean distance to the sun.¹

Some years later, Newton published a book called *Principia* which contained the now famous Newton's Laws of Motion:

First Law Every body continues in its state of rest or of uniform motion in a straight line unless it is compelled to change that state by forces impressed upon it.

Second Law The rate of change of momentum is proportional to the force impressed and is in the same direction as that force.

Third Law To every action there is always opposed an equal reaction.¹

Newton's second law can be written mathematically as:

$$\sum \mathbf{F} = m\ddot{\mathbf{r}} \quad (2.1)$$

where \mathbf{F} is the force, m is the mass of the object, and $\ddot{\mathbf{r}}$ is the acceleration of the object. For orbiting bodies, Newton's second law is the sum of the gravitational forces resulting in Newton's Law of Gravitation, which can be written as:

$$\mathbf{F}_g = -\frac{GMm}{r^3}\mathbf{r} \quad (2.2)$$

where bmF_g is the gravitational force on the object, G is the universal gravitational constant ($G = 6.67 \times 10^{-11}\text{m}^3/\text{s}^2$), M is the mass of the orbited body, and \mathbf{r} is the vector from the central body to the object.

The gravitational coefficient (μ) is a constant for each body. The value of μ for various celestial bodies can be found in Appendix A, and is defined as:

$$\mu \equiv GM \quad (2.3)$$

The N-Body Problem

The total force of gravity on any body is the sum of each of the gravitational force vectors from all the other bodies in the system, therefore:

$$\mathbf{F}_g = -Gm_i \sum_{j=1}^n \frac{m_j}{r_{ji}^3} \mathbf{r}_{ji} \quad j \neq i \quad (2.4)$$

Other external forces (\mathbf{F}_{Other}) factor into the total force (\mathbf{F}_{Total}) equation giving:

$$\mathbf{F}_{Total} = \mathbf{F}_g + \mathbf{F}_{Other} \quad (2.5)$$

The most general form of the equations of motion for an N-body system can be written as:

$$\ddot{\mathbf{r}}_i = \frac{\mathbf{F}_{Total}}{m_i} - \dot{\mathbf{r}}_i \frac{\dot{m}_i}{m_i} \quad (2.6)$$

Examples of external forces represented by \mathbf{F}_{Other} include drag, thrust, solar pressure, or the J_2 effect. These effects, known as perturbing forces, are further described in Section 2.1.6. When the forces from all sources are analyzed, the gravitational force from the central body typically dominates, and is essentially equal to the net force, under most circumstances. As a result, the other forces can be assumed to be negligible, leading to the simpler two-body analysis of the problem.

Two-Body Problem

When perturbing forces are neglected, the general equation of motion in Eq. 2.6 simplifies to:

$$\ddot{\mathbf{r}} + \frac{\mu}{r^3}\mathbf{r} = 0 \quad (2.7)$$

The orbits described by this equation are conic sections, having a constant energy (E) and angular momentum vector (\mathbf{h}) that can be expressed as:

$$E = \frac{v^2}{2} - \frac{\mu}{r} \quad (2.8)$$

$$\mathbf{h} = \mathbf{r} \times \mathbf{v} \quad (2.9)$$

where \mathbf{v} is the velocity of the object. Equation 2.9 can be rewritten as

$$h = rv \cos \phi \quad (2.10)$$

where ϕ is the angle between a line drawn perpendicular to the position and velocity vectors.

2.1.2 Orbit Geometry

In a two-body problem, all orbits are conic sections, and can thus be described by the same set of variables. Figure 2.1 shows a sample elliptical orbit and the terminology used in describing an orbit. The size and shape of an orbit can be described by the lengths of the semimajor axis (a) and the semiminor axis (b). The eccentricity (e) of an orbit is a parameter describing the shape of an orbit in terms of the relationship between the semimajor and semiminor axes. The semilatus rectum (p) is the perpendicular distance between the semimajor axis and the orbit. The true anomaly angle (f) is the angle between the semimajor axis and the position vector of the orbiting craft as measured from the focus of the orbit.

Some equations describing the position of the satellite relative to the massive body are true for all orbits. Orbits fall under three main shapes as described in Chapter 1: elliptical, parabolic, and hyperbolic.

The following equation holds true to define the semilatus rectum for all orbits *except* parabolic, because $a = \infty$ and $e = 1$ for parabolic orbits.

$$p = a(1 - e^2) \quad (2.11)$$

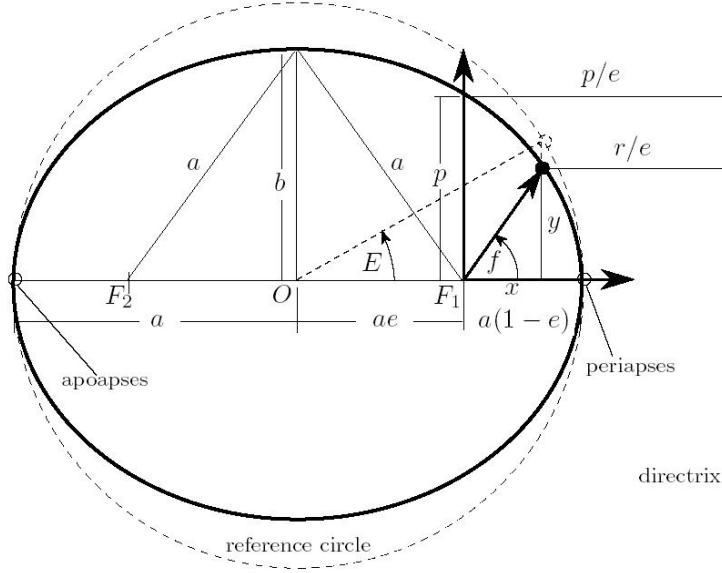


Figure 2.1: Geometry of an elliptical orbit¹⁵

For a parabolic orbit, p is defined as:

$$p = 2r_p \quad (2.12)$$

where r_p is the radius at periapsis. The radial distance from the central body to the satellite can be related to the true anomaly by:

$$r = \frac{p}{1 + e \cos f} \quad (2.13)$$

Although the true anomaly has a convenient direct geometric interpretation, it is not always mathematically convenient to express the spacecraft location through this angle. Instead, the mean anomaly (M) is typically used in describing the location of a spacecraft in an orbit. Although the mean anomaly has no convenient geometric definition, it does vary linearly with time according to the equation:

$$M = M_0 + n(t - t_0) \quad (2.14)$$

where M_0 is the mean anomaly at time t_0 , and n is the mean angular motion of the satellite, which is related to the gravitational coefficient and the semi-major axis of the orbit.

For all conic sections the eccentricity vector (\mathbf{e}) can be defined as

$$\mathbf{e} = \frac{\mathbf{v} \times \mathbf{h}}{\mu} - \frac{\mathbf{r}}{r} \quad (2.15)$$

Since the velocity vector is perpendicular to the position vector at periapsis and apoapsis, the angular momentum magnitude from Eq. 2.10 can be written as:

$$h = r_p v_p = r_a v_a \quad (2.16)$$

and the energy of an orbit being defined as in Eq. 2.8. These equations hold for all orbits, and now it is beneficial to look at each orbit shape individually, starting with elliptic orbits.

Elliptic Orbits

A sample elliptic orbit is illustrated in Fig. 2.1, with the central body located at focus F_1 . For the special case when the ellipse is a circle, $a = b$ and the two focal points coincide at the same location. The eccentricity of an ellipse can vary from $0 \leq e < 1$ and is defined as:

$$e = \frac{\sqrt{a^2 - b^2}}{a} \quad (2.17)$$

The radial distance to the point can be related to the cartesian x and y coordinates through:

$$x = r \cos f \quad (2.18a)$$

$$y = r \sin f \quad (2.18b)$$

For elliptical orbits the distance to the periapsis, the point of closest approach to the primary focus, and the apoapsis, the furthest point on the orbit from the focus, can be expressed as:

$$r_p = \frac{p}{1 + e} = a(1 - e) \quad (2.19a)$$

$$r_a = \frac{p}{1 - e} = a(1 + e) \quad (2.19b)$$

In addition to the true anomaly, the eccentric anomaly (E) is often used to define the location of the craft in orbit. Imagine the ellipse being “stretched” along the semiminor axis into the shape of a perfect reference circle. The angular position of the new orbit location relative to the ellipse center is the eccentric anomaly shown in Fig. 2.1.¹⁵ The radius and true anomaly are related to the eccentric anomaly by:

$$r = a(1 - e \cos E) \quad (2.20)$$

$$\tan \frac{f}{2} = \sqrt{\frac{1 + e}{1 - e}} \tan \frac{E}{2} \quad (2.21)$$

The mean anomaly of an elliptic orbit relates to the eccentric anomaly in the following equation:

$$M = E - e \sin E \quad (2.22)$$

The mean angular motion (n) in an elliptic orbit is defined as

$$n = \sqrt{\frac{\mu}{a^3}} \quad (2.23)$$

The period of the orbit (P) is defined as

$$P = \frac{2\pi}{\sqrt{\mu}} a^{3/2} \quad (2.24)$$

which fits Kepler's third law since $P^2 \propto a^3$

For the special case of an elliptical orbit where $e=0$, a circular orbit is formed. For this case, the radius remains constant with $r = a$ so the required velocity for the orbit is

$$v_c = \sqrt{\frac{\mu}{r}} \quad (2.25)$$

Parabolic Orbits

The parabolic orbit has an eccentricity of zero, with a sample parabolic orbit being shown in Fig. 2.2. A satellite in a parabolic orbit will continue to, and stop at, "infinity." The energy

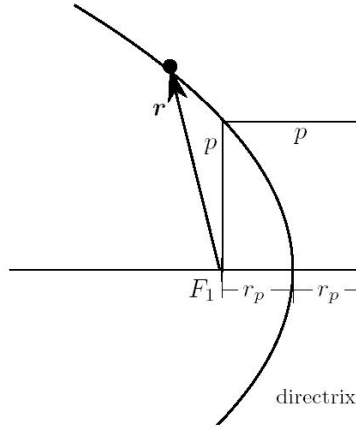


Figure 2.2: Geometry of a parabolic orbit¹⁵

of a parabolic orbit is defined to be zero, so:

$$E = \frac{v_{esc}^2}{2} - \frac{\mu}{r} = 0 \quad (2.26)$$

where v_{esc} is the escape velocity of the central body.

Like the elliptic orbit, another angle, the parabolic anomaly (D), is used occasionally in place of the true anomaly. The two are related by:

$$\tan \frac{f}{2} = D \sqrt{2r_p} \quad (2.27)$$

The mean anomaly of a parabolic orbit is defined as:

$$M = \frac{r_p D}{2} + \frac{D^3}{6} \quad (2.28)$$

and the mean angular motion is defined as:

$$n = \sqrt{\mu} \quad (2.29)$$

The velocity of a satellite at any point in the parabolic orbit is often referred to as the escape velocity, since an object with this velocity will eventually “escape” the influence of the massive body about which it is orbiting and go to “infinity.” This velocity is determined from the energy equation:

$$v_{esc} = \sqrt{\frac{2\mu}{r}} \quad (2.30)$$

If the satellite has a higher velocity than the escape velocity, then the energy of the orbit will be positive, and the resulting shape will be hyperbolic.

Hyperbolic Orbits

The semimajor axis for a hyperbola is commonly represented by a negative quantity as shown in Fig. 2.3. This conversion allows many parameters for a hyperbolic orbit to be similar algebraically to the elliptic ones.¹⁵ The semiminor axis for a hyperbolic orbit can be expressed as:

$$b = a\sqrt{e^2 - 1} \quad (2.31)$$

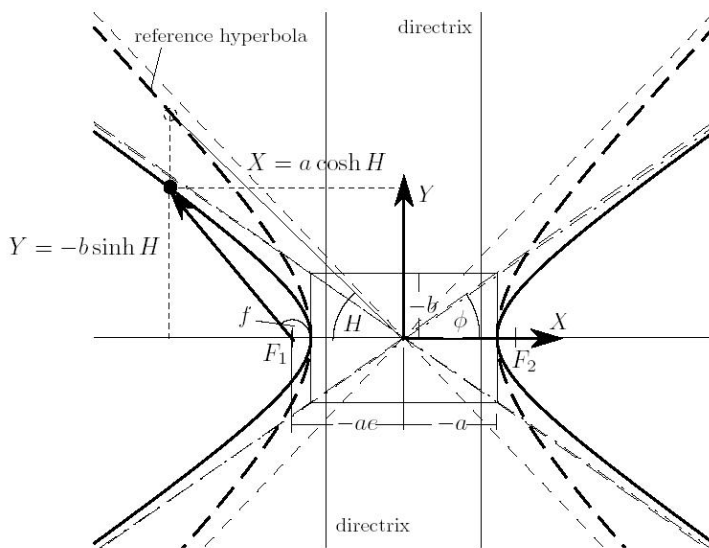


Figure 2.3: Geometry of a hyperbolic orbit¹⁵

Again, its more convenient to express the location within the orbit through another anomaly angle. For hyperbolas the hyperbolic anomaly (H) is used. The reference hyperbola

has an eccentricity of $e = \sqrt{2}$, which corresponds to having an asymptotic slope of 45 deg, leading to the definition:

$$r = a(1 - e \cosh H) \quad (2.32)$$

where the hyperbolic anomaly can be related to the true anomaly through:

$$\tan \frac{f}{2} = \sqrt{\frac{e+1}{e-1}} \tanh \frac{H}{2} \quad (2.33)$$

The mean anomaly of a hyperbolic orbit is defined as:

$$M = e \sinh H - H \quad (2.34)$$

and the mean angular motion is defined as:

$$n = \sqrt{\frac{\mu}{(-a)^3}} \quad (2.35)$$

Orbit Plane Orientation & Orbit Elements

The above analysis allows the determination of the geometry and motion of a satellite within the orbital plane. The orbit plane is defined relative to the equatorial plane of the central body. Figure 2.4 shows an example of an orbit plane and its alignment relative to the Equatorial Ecliptic Plane. Typically, orbit plane orientations are described using 3-1-3 Euler angles. A 3-1-3 Euler angle description means that first the plane rotates through an angle about the 3-axis of the body-fixed reference frame, then about the new 1-axis, then finally about the new 3-axis. In Fig. 2.4 the first rotation of the orbit plane is the longitude of the ascending node (Ω), the second is the inclination angle (i), and the third is the argument of periapses (ω).

Since the orbital size and shape can be defined accurately given two constants, a and e , the orientation of this orbit can be defined with three constants, i , Ω , and ω , and the spacecraft's location within the orbit can be defined through the mean anomaly, M , the location and motion of the satellite can be described with six variables. This commonly used set is given as:

$$\{a, e, i, \Omega, \omega, M\}$$

These six orbit variables are called the *orbit elements*.¹⁵

2.1.3 Mission Analysis

Ground Tracks

A ground track or ground trace is a plot showing the path of the subsatellite point (SSP) on the surface of the Earth. For circular orbits, the SSP marks out a sinusoidal pattern

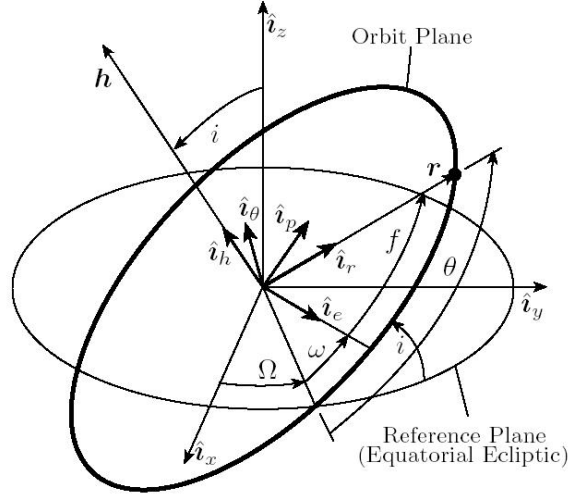


Figure 2.4: The (3-1-3) Euler angle description of the orbit plane¹⁵

as it moves around the Earth due to the rotation of the Earth. For a circular orbit with inclination i , subsatellite latitude, δ_s , and subsatellite longitude, L_s :

$$\sin \delta_s = \sin i \sin \omega_s t \quad (2.36)$$

$$\tan L_s \omega = \cos i \tan \omega_s t \quad (2.37)$$

where t is the time starting when the SSP last crossed the equator moving north, ω is the rotational velocity of the body about its axis ($\omega_{\oplus} = 0.00417807$ deg/sec), and ω_s is the angular velocity of the satellite. For a circular orbit, the satellite's angular velocity is related to the orbit period by:

$$\omega_s = 2\pi/P \quad (2.38)$$

There is a maximum value of ω_s corresponding to an orbit with orbital radius equal to that of the orbited body. The velocity of the ground track, v_g , is given by:

$$v_g = \frac{2\pi R}{P} \quad (2.39)$$

where R is the equatorial radius of the orbited body. Imposing the same restriction on the period yields a maximum ground track velocity.¹¹

Tracking

For satellite tracking it is convenient to define the topological frame, $T : \{\hat{e}, \hat{n}, \hat{u}\}$. The frame is positioned on the surface of the Earth such that the first unit direction (\hat{e}) points East, the second unit direction (\hat{n}) points North, and the third unit direction (\hat{u}) points

up. Starting in an inertial Earth centered frame, the position (${}^N\mathbf{r}_p$) of a ground station as function of time is given by

$${}^N\mathbf{r}_p = \begin{pmatrix} \cos \delta \cos \gamma(t) \\ \cos \delta \sin \gamma(t) \\ \sin \delta \end{pmatrix} \quad (2.40)$$

where δ is the latitude of the ground station and $\gamma(t)$ is the local sidereal time of the ground station.

The position vector of the satellite relative to the ground station ($\boldsymbol{\rho}$) is defined by:

$${}^N\boldsymbol{\rho} = {}^N\mathbf{r}_s - {}^N\mathbf{r}_p \quad (2.41)$$

where ${}^N\mathbf{r}_s$ is the position of the satellite relative to the center of the Earth. The position vector can be transformed to the topological frame using a rotation matrix ($[TN]$) defined by:

$$[TN] = \begin{bmatrix} -\sin \gamma & \cos \gamma & 0 \\ \cos \gamma & \sin \gamma \sin \delta & \cos \delta \\ \cos \gamma \cos \delta & \sin \gamma \cos \delta & \sin \delta \end{bmatrix} \quad (2.42)$$

$${}^T\boldsymbol{\rho} = [TN]{}^N\boldsymbol{\rho} \quad (2.43)$$

where the leading superscripts T and N denote the topological inertial frames respectively. The components of $\boldsymbol{\rho}$ in the topological frame (ρ_e, ρ_n, ρ_u) are given by:

$${}^T\boldsymbol{\rho} = \begin{pmatrix} \rho_e \\ \rho_n \\ \rho_u \end{pmatrix} \quad (2.44)$$

$$\rho_e = \rho \cos \epsilon \sin \alpha \quad (2.45a)$$

$$\rho_n = \rho \cos \epsilon \cos \alpha \quad (2.45b)$$

$$\rho_u = \rho \sin \epsilon \quad (2.45c)$$

where α is the azimuth angle, and ϵ is the elevation angle. The azimuth angle is defined as the angle that $\boldsymbol{\rho}$ makes with North, and elevation angle is defined as the angle $\boldsymbol{\rho}$ makes from the horizon. The azimuth and elevation angles can be found by

$$\alpha = \tan^{-1} \rho_e / \rho_n \quad (2.46)$$

$$\epsilon = \sin^{-1} \rho_u / \rho \quad (2.47)$$

A positive elevation angle corresponds to a satellite position above the horizon, meaning it is visible from the ground station.¹⁴

Orbit Determination

Given the position and velocity vectors for a satellite it is possible to determine the corresponding orbital elements for that satellite. The accuracy of this process is limited by the degree to which the position and velocity vectors are known, as well as the forces acting on the satellite. The vector to the ascending node (\mathbf{N}):

$$\mathbf{N} = \hat{\mathbf{k}} \times \hat{\mathbf{h}} \quad (2.48)$$

$$\hat{\mathbf{N}} = \mathbf{N}/N \quad (2.49)$$

using a unit vector normal to the equatorial plane ($\hat{\mathbf{z}}$). The eccentricity vector is defined in Eq. 2.15 and has magnitude equal to the eccentricity of the orbit. To find the semimajor axis Eq. 2.8 is used. The semilatus rectum can be found by:

$$p = |\mathbf{h}^2|/\mu \quad (2.50)$$

Using these equations the eccentricity, inclination, right ascension of the ascending node, argument of perigee, and true anomaly, can be found by:

$$e = |\mathbf{e}| \quad (2.51)$$

$$\cos i = h_z/|\mathbf{h}| \quad (2.52)$$

$$\tan \Omega = N_y/N_x \quad (2.53)$$

$$\cos \omega = \hat{\mathbf{e}} \cdot \hat{\mathbf{N}} \quad (2.54)$$

$$\cos f = \hat{\mathbf{r}} \cdot \hat{\mathbf{e}} \quad (2.55)$$

The inverse process, finding the position and velocity vectors given the orbital elements, can also be done. This process takes the orbital elements at a given initial time, propagates those elements to a future time, and then translates those elements into inertial position and velocity vectors. The only orbit element that changes with time is the mean anomaly angle. Converting the mean anomaly to true anomaly is a two-step process. The mean anomaly is first converted to an eccentric, parabolic, or hyperbolic anomaly, depending on the orbit shape, and is then converted into the true anomaly.

Using the perifocal frame simplifies the calculation of the position and velocity vectors. The perifocal frame is a right-handed coordinate system with the first unit direction lying in the orbit plane pointing towards periapses, the second unit direction also lying in the orbit plane, and the third unit direction perpendicular to the orbit plane pointing in the direction of the angular momentum vector. The position coordinates in the perifocal frame can be found as:

$$r_1 = p \left(\frac{\cos f}{1 + e \cos f} \right) \quad (2.56a)$$

$$r_2 = p \left(\frac{\sin f}{1 + e \cos f} \right) \quad (2.56b)$$

and the velocity components are given by:

$$v_1 = \sqrt{\frac{\mu}{p}} \sin f \tag{2.57a}$$

$$v_2 = \sqrt{\frac{\mu}{p}} (e + \cos f) \tag{2.57b}$$

Moving these position and velocity vectors from the perifocal frame to an inertial frame requires a coordinate transformation using the rotation matrix

$$[NP] = \begin{bmatrix} \cos \Omega \sin \omega - \sin \Omega \sin \omega \cos i & -\cos \Omega \sin \omega - \sin \Omega \cos \omega \cos i & \sin \Omega \sin i \\ \sin \Omega \cos \omega + \cos \Omega \sin \omega \cos i & -\sin \Omega \sin \omega + \cos \Omega \cos \omega \cos i & -\cos \Omega \sin i \\ \sin \omega \sin i & \cos \omega \sin i & \cos i \end{bmatrix} \tag{2.58}$$

The position and velocity vectors are given by

$${}^N \mathbf{r} = [NP]^P \mathbf{r} \tag{2.59}$$

$${}^N \mathbf{v} = [NP]^P \mathbf{v} \tag{2.60}$$

where the leading superscript N denotes the inertial frame, and the leading superscript P denotes the perifocal frame.¹⁷

Two Line Element Sets

Two line element sets are an easy way to convey all the information necessary to determine the position of a satellite. They provide a standard format for all satellites orbiting the Earth. Two line element sets (TLE) are sometimes given with three lines of data. An example TLE from a weather satellite is

```
NOAA 12
1 21263U 91032A 04280.43027275 .00000130 00000-0 73626-4 0 7634
2 21263 98.6801 267.0670 0013728 87.6314 272.6437 14.25415614696090
```

Line zero of the TLE is the name of the satellite. Lines one and two contain all the data in the following format:⁹

```
aaaaaaaaaaaaaaaaaaaaaaaaaaaa
1 nnnnnu nnnnnlll nnnnn.nnnnnnnn .nnnnnnnnn nnnnnn-n nnnnnnn-n n nnnnn
2 nnnnn nnnnnnnn nnnnnnnn nnnnnnn nnnnnnnn nnnnnnnn nnnnnnnnnnnnnnnnn
```

Line 1

Column	Description
01	Line Number
03-07	Satellite ID
08	Classification
10-17	International Designator
19-20	Epoch year
21-23	Epoch day
24-32	Epoch time (in fraction of day)
34-43	1st time derivative of mean motion
45-52	2nd time derivative of mean motion
54-61	BSTAR drag term
63	Ephemeris type
65-68	Element type
69	Mod-10 Checksum

Line 2

Column	Description
01	Line Number
03-07	Satellite ID
09-16	Inclination (in degrees)
18-25	Right Ascension of Ascending Node (in degrees)
27-33	Eccentricity (assumed decimal)
35-42	Argument of perigee (in degrees)
44-51	Mean Anomaly (in degrees)
53-63	Mean motion (in revolutions per day)
64-68	Revolution number at epoch
69	Mod-10 Checksum

2.1.4 Orbit Maneuvers

Most missions require orbit maneuvering upon reaching an initial parking orbit. From this orbit, the mission may require continuous orbit maintenance, jumping to a higher altitude, changing orbital planes, leaving orbit or a combination of all four. The requirements of the mission and the capital available to meet these requirements affect all aspects of orbital maneuvering decisions. For most cases, minimum fuel consumption is the driving constraint. Therefore, this section addresses the most commonly used orbit maneuvering techniques designed to minimize fuel consumption. Also, various situations requiring large consumptions of fuel is addressed.

Coplanar Orbit Transfers

The most common in-plane orbit transfer for minimizing energy, thus minimizing fuel usage, is termed the Hohmann transfer orbit. The Hohmann is an elliptical orbit used to transfer

from one circular orbit to another circular orbit. This transfer orbit has its periapsis tangent to the inner orbit and its apopapsis tangent to the outer orbit. One can transfer from either an inner orbit or an outer orbit.

Figure 2.5 can be viewed for better understanding. At periapses (P_1) a burn is performed obtaining velocity v_1 in addition to the initial velocity $v_{\theta 1}$ starting the transfer orbit. At apoapses (P_2), a second burn is performed, obtaining velocity v_2 in addition to the tangent velocity $v_{\theta 2}$ to obtain a new circular orbit. The Hohmann transfer can be thought of as a two-burn transfer. The following equations show how to obtain the required Δv for the orbit transfer:

$$\Delta v_{total} = \Delta v_1 + \Delta v_2 \tag{2.61a}$$

$$= \sqrt{\mu} \left[\left| \left(\frac{2}{r_1} - \frac{1}{a_t} \right)^{1/2} - \left(\frac{1}{r_1} \right)^{1/2} \right| + \left| \left(\frac{2}{r_2} - \frac{1}{a_t} \right)^{1/2} - \left(\frac{1}{r_2} \right)^{1/2} \right| \right] \tag{2.61b}$$

where Δv_{total} is the total change in velocity, and a_t is the semimajor axis of the transfer orbit.¹¹

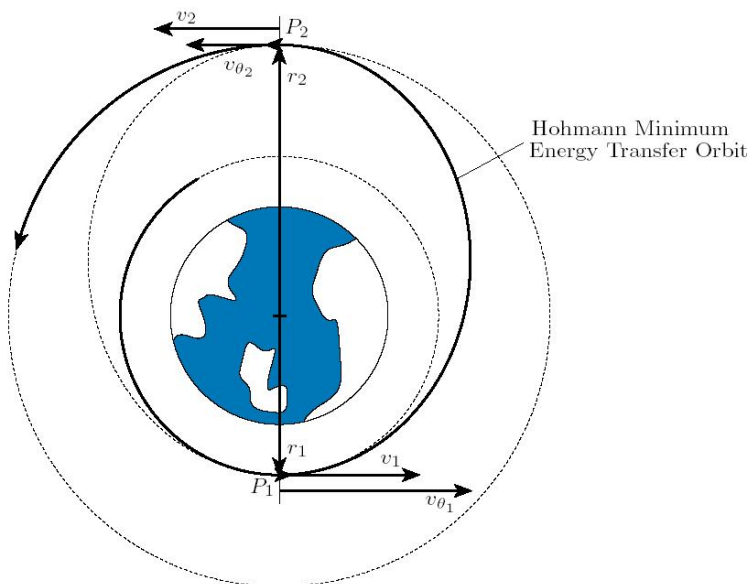


Figure 2.5: Illustration of a Hohmann transfer orbit¹⁵

Orbit Plane Changes

Orbit plane changes consist of two types: simple and combined. A simple plane change only requires a Δv component perpendicular to the initial velocity of the current orbit. This plane change does not alter the size of the orbit, only its orientation. A combined plane change incorporates both an altitude adjustment and a plane adjustment in order to reduce the Δv

required versus executing separate maneuvers. However, in certain orbit arrangements, a combined plane change requires more Δv than separate orbit maneuvers. The required Δv for just a plane change, which is shown in Fig. 2.6, is:

$$\Delta v = 2v_1 \sin(\Delta i/2) \quad (2.62)$$

The required Δv for a plane change combined with a Hohmann transfer between two circular orbits is:

$$\Delta v = \sqrt{v_1^2 + v_2^2 - 2v_1v_2 \cos(\Delta i)} \quad (2.63)$$

where v_1 is the velocity of the inner orbit and v_2 is the velocity of the outer orbit.¹¹

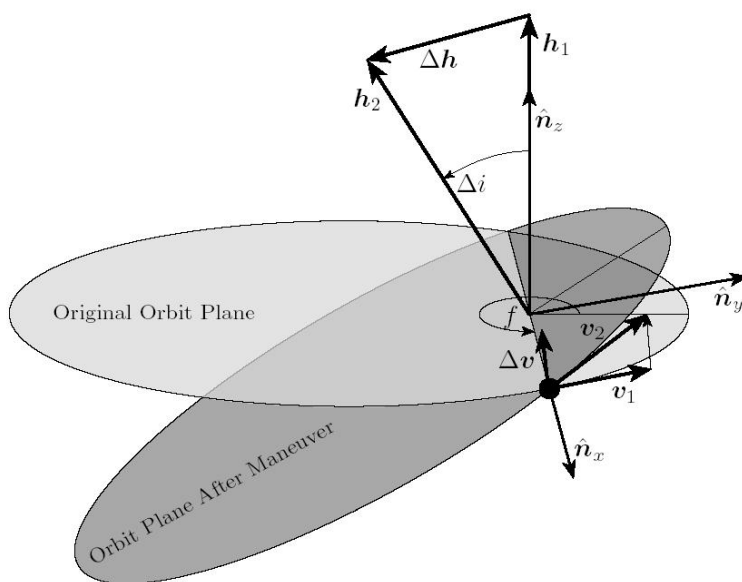


Figure 2.6: Illustration of an orbit plane change maneuver¹⁵

Patched Conic Sections

Orbital maneuvers such as transfers, velocity changes, and plane adjustments can be performed through the interactions with planets or other massive objects in space. These interactions occur by a process called a planetary fly-by. The general concepts and equations required to perform a fly-by will be discussed in this section.

Every body in space has a sphere of influence. This concept is based on the gravitational influence of a body relative to the gravitational influence of its central body. The radius of this sphere (r_{SOI}) is defined by:

$$r_{SOI} = \left(\frac{m}{M}\right)^{2/5} r_{12} \quad (2.64)$$

where m is the mass of the body, M is the mass of its central body, and r_{12} is the orbital radius of the body. The mass of the central body is assumed to be much greater than the mass of the body, $M \gg m$. An example would be the Sun, the central body, and the Earth, the body.

To escape the sphere of influence a hyperbolic orbit is used, with a burn being required to place the spacecraft in this orbit, as shown in Figure 2.7. The $\Delta\nu$ for the maneuver is:

$$\Delta\nu = \nu_0 - \nu_c = \sqrt{2\nu_c^2 + \nu_1^2} - \nu_c \quad (2.65)$$

where ν_c is the orbit velocity of the spacecraft and ν_1 is the velocity at the sphere's edge. The velocities used are planetary relative velocities (nu). The computations leading to the arrival of the final equation can be found in Schaub.¹⁵

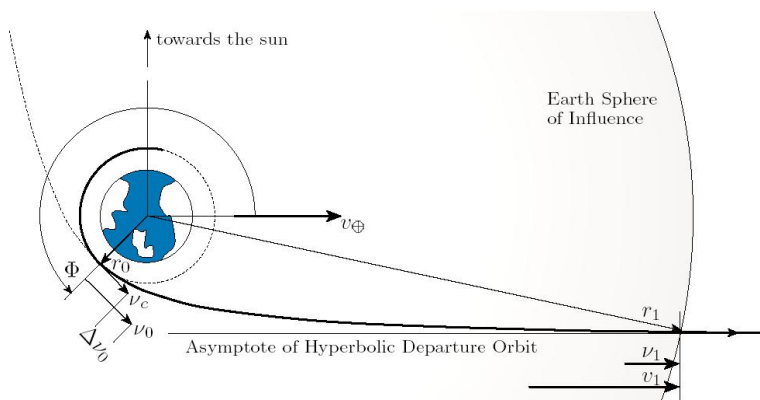


Figure 2.7: Departure orbit to reach outer planet¹⁵

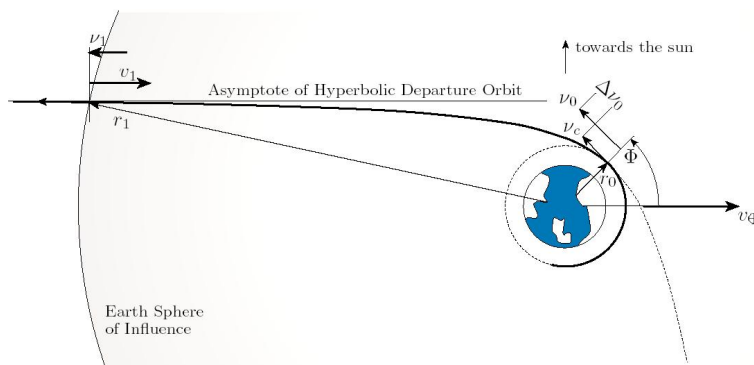


Figure 2.8: Departure orbit to reach inner planet¹⁵

The target planet may either be an inner or outer planet. The concept is the same with modified arrival equations for calculation purposes. Upon arriving at the target, there are two orbit possibilities: parabolic or hyperbolic. If original target alignments were done accurately,

then the craft can perform a planetary fly-by in a continued hyperbolic or parabolic orbit, thus gaining or reducing energy or changing direction. The angle between the velocity vectors of the spacecraft and the target planet when the craft enters that planet's sphere of influence is termed the heading angle (σ_2) and can be calculated by:

$$\sigma_2 = \cos^{-1} \left(\frac{h}{r_{SOI} v_2} \right) \quad (2.66)$$

where h is the magnitude of the angular momentum, r_{SOI} is the radius of the planet's sphere of influence, and v_2 is the arrival velocity. If an elliptical orbit is required, another burn will be required. The following equations govern this burn:

$$\nu_3 = \sqrt{2 \frac{\mu}{r_3} + v_2^2} \quad (2.67a)$$

$$\Delta \nu_3 = \nu_c - \nu_3 \quad (2.67b)$$

$$\nu_c = \sqrt{\frac{\mu}{r_3}} \quad (2.67c)$$

where r_3 is the periapsis of the hyperbolic arrival orbit, ν_3 is the target planet's relative departure velocity, ν_c is the target orbit's planetary relative velocity, and $\Delta \nu_0$ is the required burn to keep the craft in an elliptical orbit around the target planet. Figures 2.9 and 2.10 are illustrations of arrival to inner and outer planets.

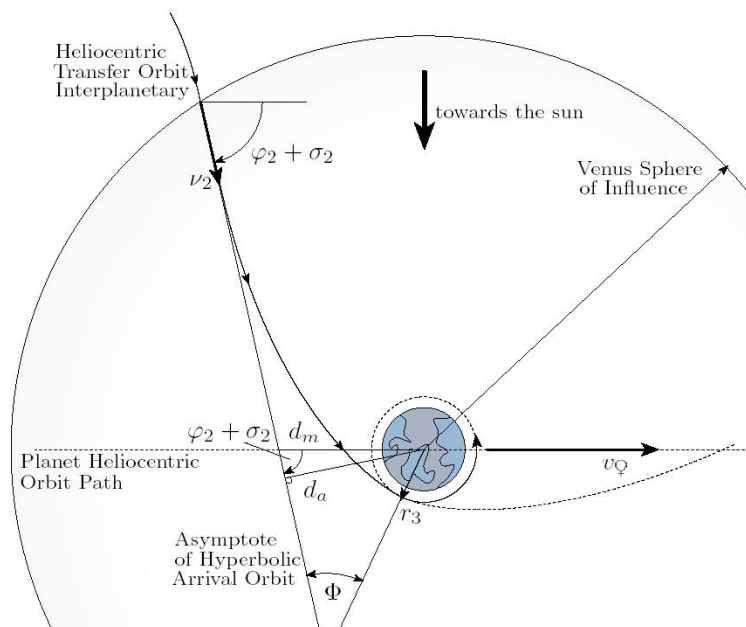


Figure 2.9: Arrival orbit to the inner planet Venus¹⁵

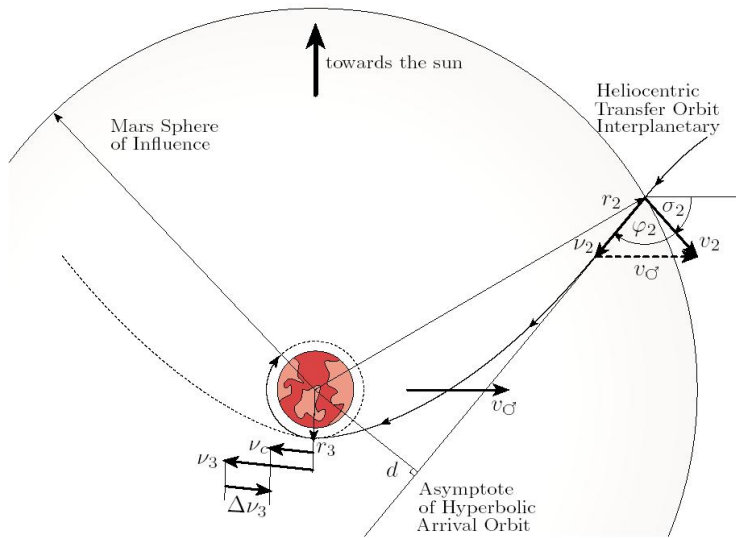


Figure 2.10: Arrival orbit to the outer planet Mars¹⁵

Low Thrust Trajectories

Low thrust propulsion systems, such as thermal or electric systems, have a higher specific impulses (I_{sp}) than high thrust propulsion systems and therefore require less propellant for a given Δv . However, orbit maneuvers utilizing low thrust propulsion systems can not be based on the assumption that changes in velocity occur instantaneously. Instead, a constant acceleration is applied throughout the orbit, often with varying magnitude and direction of the thrust vector. The type of trajectory that results requires more Δv than conventional high thrust trajectories but, with the higher I_{sp} s associated with many low thrust propulsion systems, still often uses less propellant than conventional propulsion types.

Simple modelling of the Δv required for a low thrust, spiral trajectory (Δv_{spr}) can be accomplished assuming a constant thrust both in magnitude and direction and can be found using the following equation:

$$\Delta v_{spr} = \sqrt{\mu} \left(\frac{1}{\sqrt{r_1}} - \frac{1}{\sqrt{r_2}} \right) \quad (2.68)$$

where r_1 is the initial radius and r_2 is the final radius. In designing low-thrust trajectories, however, it is often more efficient from the perspective of reducing the wet mass of the spacecraft to vary the thrust vector throughout the orbit. This analysis can be accomplished through the use of a variety of numerical techniques, which can be used to either propagate the orbit according to a defined thrust vector profile or optimize the orbit given a set of constraints and a cost function.

Solar Sail Trajectories

Solar sail orbits are low thrust orbits, but have some unique properties under certain circumstances that bear further discussion. The two distinct properties of a solar sails that significantly impact its orbit are its sail lightness factor (β), which will be discussed further in Section 2.3.6, and the sail's orientation, defined by its pitch angle (α) in the two dimensional case. The pitch angle is the angle between the vector normal to the sail and the x-axis, as can be seen in Figure 2.11. As shown in this figure, the x-axis is aligned with the solar radiation pressure, extending radially from the sun.

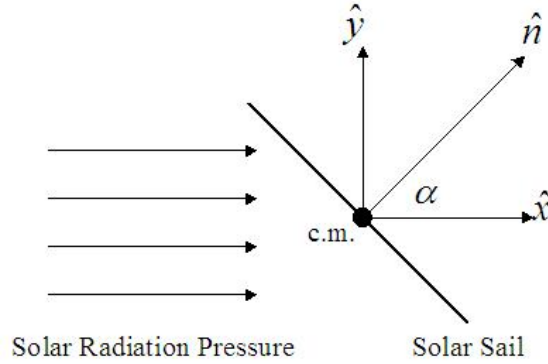


Figure 2.11: Solar Sail Pitch Angle, α .

If a constant pitch angle is assumed and the sail's trajectory has a certain initial flight path angle, a heliocentric solar sail's trajectory will be logarithmic. This flight path angle, or spiral angle, is related to the constant pitch angle by the following equation:

$$\frac{\sin \phi \cos \phi}{2 - \sin \phi^2} = \frac{\beta \cos^2 \alpha \sin \alpha}{1 - \beta \cos \alpha^3} \quad (2.69)$$

where ϕ is the spiral angle. If the trajectory is logarithmic, several properties of the orbit, such as velocity, true anomaly, and time-of-flight, can be determined. The velocity of the sail with a logarithmic trajectory at a given orbital radius is:

$$v_{sail} = \sqrt{\frac{\mu}{r}} \sqrt{1 - \beta \cos \phi^2 (\cos \phi - \sin \phi \tan \phi)} \quad (2.70)$$

where r is the solar radius of the spacecraft. The true anomaly can be calculated using:

$$f = \frac{\log \frac{r_2}{r_1}}{\tan \phi} \quad (2.71)$$

The time required to get from one point to another in a logarithmic trajectory is:

$$TOF_{sail} = \frac{1}{3} \left(r_2^{\frac{3}{2}} - r_1^{\frac{3}{2}} \right) \sqrt{\frac{1 - \beta \cos \phi^3}{\beta^2 \mu \cos \phi^4 \sin \phi^2}} \quad (2.72)$$

These equations, while describing logarithmic trajectories, are principally dependant on the selected solar sail's pitch angle, which can be optimized. Since solar sails require no propellant, optimizing the trajectories typically requires minimizing the time required to make the transfer. The optimum pitch angle that minimizes the transfer time is related to the sail lightness factor by the following equation:

$$\beta = \left(\frac{2}{\cos \phi_{opt}} \right) \left(\frac{1 - 2 \tan \phi_{opt}^2}{2 - \tan \phi_{opt}^2} \right) \quad (2.73)$$

Whereas logarithmic trajectories are the only stable solar sail orbits with a fixed pitch angle, solar sails need significant hyperbolic excess velocities to achieve the orbit's required initial spiral angle. In addition, such an orbit fails to make use of one advantage of low thrust propulsion: the ability to make changes in the orbit throughout the entire transfer, continually modifying the trajectory to meet the needs of the mission. As a result, to maximize the potential of the technology, numerical optimization techniques should be performed using the pitch angle as a variable. For these numerical techniques the acceleration due to solar radiation pressure is:

$$a_x = \frac{2F \cos \phi^2}{c\sigma} \cos \phi \quad (2.74)$$

$$a_y = \frac{2F \cos \phi^2}{c\sigma} \sin \phi \quad (2.75)$$

where F is the solar flux, c is the speed of light, and σ is the sail loading factor.¹²

2.1.5 Launch Windows

A launch window is a period of time through which a spacecraft can be launched into its objective orbit. This window is affected by the latitude and longitude of the launch site, as well as the inclination and right ascension of the ascending node of the objective orbit. For a launch window to exist, the launch site must pass through the orbital plane. This requirement places restrictions on the orbital inclinations possible from a given launch latitude (L) whereby either one, two, or no launch windows exist.

2.1.6 Orbit Perturbations

Keplerian orbits provide analytical approximations for true orbits. However, Kepler's laws do not take into account the other forces described in Eq. 2.5 and are based on the use of point masses. Consequently, Kepler's laws do not describe real orbits exactly, but do provide good approximations of the orbits.

Orbit perturbations are deviations of a real orbit from a reference Keplerian orbit and are usually classified according to the perturbations effect on the Keplerian orbit elements. The classifications are third body interactions, non-gravitational forces, and non-spherical mass distributions. This section covers the cause of these perturbations, their modification of classic Keplerian orbits, and various formulas that are used to approximate them.¹⁷

Nonspherical Mass Distribution

The Earth is typically modelled as a perfect sphere when it is an ellipsoid. The rotation of the Earth causes mass to be forced to the equator, thus slightly flattening the polar regions. This oblateness results in the equatorial radii being greater than the polar radii. The increased mass around the equator creates an added gravitational effect on satellites that depends on latitude and longitude. The acceleration of a spacecraft can be found by taking the gradient of the gravitational potential function, ϕ . One form of the geopotential function is:

$$\phi = (\mu_{\oplus}/r) \left(1 - \sum_{i=1}^{\infty} J_n \left(\frac{R_{\oplus}}{r} \right)^n P_n \sin L \right) \quad (2.76)$$

where R_{\oplus} is Earth's equatorial radius, P_n are Legendre polynomials, L is geocentric latitude, and J_n are the dimensionless geopotential coefficients where the first three values are:¹⁷

$$\begin{aligned} J_2 &= 0.00108263 \\ J_3 &= -0.00000254 \\ J_4 &= -0.00000161 \end{aligned}$$

The potential created by the nonspherical Earth affects all of the orbital elements causing orbit precession rates, and is termed the J_2 effect. On average, the values of the semimajor axis, eccentricity, and inclination will not vary. However, the dominant effects occur in the ascending node, argument of perigee, and mean anomaly. The average rates are as follows:¹⁵

$$\frac{d\alpha}{dt} = 0 \quad (2.77a)$$

$$\frac{de}{dt} = 0 \quad (2.77b)$$

$$\frac{di}{dt} = 0 \quad (2.77c)$$

$$\frac{d\Omega}{dt} = -\frac{3}{2} J_2 n \left(\frac{r_{eq}}{p} \right)^2 \cos i \quad (2.77d)$$

$$\frac{d\omega}{dt} = -\frac{3}{4} J_2 n \left(\frac{r_{eq}}{p} \right)^2 (5 \cos^2 i - 1) \quad (2.77e)$$

$$\frac{dM_0}{dt} = -\frac{3}{4} J_2 n \left(\frac{r_{eq}}{p} \right)^2 \sqrt{1 - e^2} (3 \cos^2 i - 1) \quad (2.77f)$$

The J_2 perturbations affect spacecraft in GEO and below and should be accounted for when considering Δv budgets and performing orbit design trade studies.

Third Body Interactions

The Sun and the Moon are the two gravitational forces relevant for an Earth-referenced orbit. They cause periodic variations in all the orbit elements. In comparison, the effect is

similar to the J_2 perturbations caused by the Earth's equatorial bulge. However, the Sun and the Moon's effects are generally noticeable in orbits above GEO. The Sun and Moon apply external torques on orbits, causing a gyroscopic precession of the orbit about the ecliptic pole. There is little variation in the orbit elements a , e , i , and M_0 and therefore these elements are neglected. The perturbation caused by the Sun and Moon mainly affect the right ascension of the ascending node and the argument of perigee thus requiring the need for station keeping in GEO and beyond. The right ascension of the ascending node precesses at the following rate:

$$\dot{\Omega}_{Moon} = -0.00338(\cos i)/n \quad (2.78a)$$

$$\dot{\Omega}_{\odot} = -0.00154(\cos i)/n \quad (2.78b)$$

The argument of perigee precesses at the following rate:

$$\dot{\omega}_{Moon} = 0.00169(4 - 5 \sin^2 i)/n \quad (2.79)$$

$$\dot{\omega}_{\odot} = 0.00077(4 - 5 \sin^2 i)/n \quad (2.80)$$

where i is the orbital inclination, n is the number of orbit revolutions per day, and $\dot{\Omega}$ and $\dot{\omega}$ are in deg/day. These equations are only approximations, neglecting the variation caused by the changing orientation of the orbital plane with respect to both the Moon's orbital and elliptic planes.¹¹

Solar Radiation Pressure

Solar radiation pressure (SRP) exerts a force on the spacecraft causing periodic variations in all of the orbital elements. The effect is strongest for satellites with low mass and large cross-sectional areas. The magnitude of the acceleration (a_r) due to the SRP for satellites orbiting Earth is:

$$a_r \approx -4.5 \times 10^{-8} A/m \quad (2.81)$$

where A is the cross-sectional area of the satellite normal to the Sun and m is the mass of the satellite. Solar radiation pressure becomes increasingly important at higher altitudes and is the main perturbing force for interplanetary trajectories.¹¹

Atmospheric Drag and Satellite Decay

Atmospheric drag is the principal non-gravitational force acting on most satellites in LEO. Drag acts opposite the direction of the velocity vector. This slows the satellite and removes energy from the orbit. Consequently, this reduction of energy minimizes the orbit and leads to a further and continuous loss of energy until the satellite reenters the Earth's atmosphere.

Drag can vary by as much as an order of magnitude due to the attitude of the spacecraft and, particularly, the orientation of the solar arrays, with respect to the velocity vector. The atmospheric density at satellite altitudes varies by as much as two orders of magnitude depending upon the solar activity level. These variations result in overall difficulty for

predicting satellite lifetime, impact points, and location. The resulting equations of this section model approximate values due to the previously stated uncertainties

The acceleration due to drag, a_D is:

$$a_D = - \left(\frac{1}{2} \right) \left(\frac{C_D A}{m} \right) v^2 \quad (2.82)$$

where ρ is the atmospheric density, C_D is the dimensionless drag coefficient of the satellite, A is the cross-sectional area, m is the satellite mass, and v is the velocity. The quantity $m/C_D A$ is called the ballistic coefficient and ranges from 25 to 100 kg/m² for most satellites.¹⁷

The atmospheric density ρ , decreases approximately exponentially as altitude increases:

$$\rho = \rho_0 e^{-\Delta h/h_0} \quad (2.83)$$

where ρ and ρ_0 are the density at any two latitudes, Δh is the altitude difference, and h_0 is the atmospheric scale height, area which the atmospheric density drops by $1/e$. The scale height is typically between 50 and 100 km at satellite altitude.

As a result of drag removing energy from an orbit, the orbit begins to circularize from its original elliptical orbit. The drag creates changes in the semimajor axis and the eccentricity of the orbit. The following two equations govern these effects:

$$\Delta a/rev = -2\pi \left(\frac{C_D A}{m} \right) a^2 \rho_p e^{-c} (I_0 + 2eI_1) \quad (2.84a)$$

$$\Delta e_{rev} = -2\pi \left(\frac{C_D A}{m} \right) a \rho_p e^{-c} (I_1 + e/2(I_0 + I_2)) \quad (2.84b)$$

where ρ_p is the atmospheric density at perigee, $c \equiv ae/h$, and I_j is the modified Bessel functions of order j and argument c . Through the approximate equations from above and the interpolation of current data, predicting the future locations of spacecraft is attainable.

Various perturbations affect all orbits in one way or another all depending upon where the orbit is in reference to the perturbation. These orbital perturbations are the main cause for a need of orbit maintenance and station keeping which will be addressed in later sections.

2.1.7 Orbit Maintenance and Stationkeeping

As described in Section 2.1.6, orbital perturbations can change the orbital elements of an orbit. If mission objectives define that the satellite needs to remain in its original orbit, stationkeeping is required. Stationkeeping involves periodic propulsive maneuvers to maintain the mission's orbital elements within the desired accuracy. If low altitude orbits are not maintained, the spacecraft's orbit will naturally decay until the craft reenters the Earth's atmosphere. Deployed geostationary satellites are usually assigned a given longitude to prevent collisions. These longitudes are precessed by the J_2 resonance, and therefore stationkeeping must be employed to counteract the resulting transverse acceleration.

2.1.8 Guidance and Navigation Subsystem

The concepts discussed above are essential in designing a functional spacecraft. The most direct application of these concepts is with the spacecraft bus subsystem called Guidance and Navigation. The Guidance and Navigation Subsystem is responsible for maintaining and determining the actual satellite position and velocity.

Section 2.1.7 discusses Orbit Maintenance and Stationkeeping, which are two important subsets of the guidance component. The accuracy to which the orbit must be maintained to complete the mission will determine the accuracy constraints placed on the Guidance and Navigation Subsystem sensors.

Orbit determination, or navigation, is an essential part of operating a spacecraft. The navigation component uses actual position and velocity measurements to determine the orbit elements, and the resulting deviation from the desired elements. Section 2.1.3 contains a discussion regarding orbit determination.

The components used by the Guidance and Navigation subsystem are often the same components used by the ADCS. As a result, these subdivisions need to cooperate in the design and selection of the sensors and thrusters.

2.2 Attitude Determination and Control Systems

Designing the attitude determination and control system of a spacecraft first requires an understanding of the needs and constraints put on the system by the mission and the overall spacecraft configuration. Once those requirements are understood, various control modes can be defined, and external and internal torques can be quantified. The control approach can then be specified, and the chosen sensors and actuators appropriately sized. Following the selection and sizing phase, the control algorithm can be defined and established. This section details the considerations relevant to this process.

2.2.1 Requirements

As stated in the introduction, ADCS requirements are closely related to other subsystem requirements and the overall mission needs. The two main requirements, position and attitude control, and attitude determination may both be defined by the subsystems: accuracy and range.

For each mission, particular requirements are imposed on the design. Payload requirements, such as the attitude to be pointed or exclusion zones, and other requirements, such as pointing during thrusting or communications antenna pointing, will not be described in this report, as this report is more of a general understanding of the attitude determination and control subsystem. Such requirements are spacecraft dependant, and as such will be discussed in future design reports.

Determination

The accuracy in spacecraft determination is defined as how well a vehicle's orientation is known with respect to an absolute reference. Examples of this accuracy are having an error of 0.25% with 3σ amount of averaging or filtering allowed. Accuracy may be processed either at the time of measurement or may be processed later, depending on the information's importance to keeping the spacecraft in its proper orientation. Measurements may be processed later if the accuracy range is large enough or the craft's attitude change is small enough to not have an immediate impact on the orientation, or if the measurements are purely for data acquisition or experimental purposes.

The range of a spacecraft is best defined as the scope of angular motion in which accuracy must be met. For example, a slew requirement of 30° or less in the nadir direction must be met for some spacecraft.

Control

Control performance requirements are more extensive than typical attitude determination requirements, since control of a spacecraft is a harder task than determining the spacecraft's attitude. Accuracy and range are both major factors of control. Other minor requirements include jitter, drift, and settling time.

Jitter, defined as an angular rate limit on short-term, high frequency motion, have different requirements for each spacecraft. Some vehicles require movement less than 0.1° over 1 minute, or have a limitation of 1 to 20 Hz. These requirements are put in place to prevent sensor data from being blurry.

Drift is the limit on low frequency, slow spacecraft motion. A vehicle may drift off target unexpectedly, and would require a readjustment to stay on course. Expressed similarly to jitter, drift normally has a limit on movement of approximately 1° per hour, or a more general 5° maximum.

Settling time is the time a spacecraft has to recover from maneuvers or attitude disturbances. These limitations are slightly more complicated in describing; an example of limiting settling time also limits ringing or overshoot, such as a 2° maximum change in motion which decreases to less than 0.1° in a time span of one minute.

2.2.2 Control Modes

Performance requirements typically can be translated to control modes which may be used in different stages of the spacecraft's lifetime. Accuracy and range in both determination and control play vital parts in each control mode, helping to define the mode itself. Depending on the mode, a control method may be isolated for use, requiring that a spacecraft have multiple methods at its disposal.

Orbit Insertion

Orbit insertion is the phase directly after leaving the launch vehicle in orbit. The spacecraft's goal in this mode is to reach its final orbit. The spacecraft, prior to spinning, will be unstable. Spinning is usually achieved by thrusting at a given angular rate for the mission. Once these thrusters are burnt out, the spacecraft will be spinning about the maximum moment of inertia axis, with excessive nutation being damped out using a nutation damper.

Like all control modes, orbit insertion has certain requirements needing to be met by the attitude determination and control subsystem. Attitude determination may require a certain range of sensing, that any random attitude will be sensed. A spin rate range and its accuracy will also be given by a mission. A spin rate between 10 and 60 rotations per minute, and a spin rate accuracy of 0.01 radians per second are typical limitations. Attitude control requirements may have a spin rate range of 20 to 30 rotations per minute. Nutation can be listed under control requirements, and may have requirements such as a settling time of up to 3 hours, or a limitation on the angular nutation before damping will be implemented, such as 0.1° .

Normal Mode

Used for the majority of the mission, normal mode is the phase between thrusting maneuvers. The requirements for this mode drive the design of the system. The spacecraft spins without nutation, making attitude monitoring easier than other phases. Due to spinning, the attitude is inertially and randomly fixed in this stage. Orientation is not a major concern of normal mode since any orientation allows the mission to be performed. The attitude is monitored through orbit tracking by the ground station, which provides command uplink and data downlink that the spacecraft waits for. Since the spacecraft expects commands, the antennas provide plenty of coverage for communication.

Attitude determination needs to perform at a large range of attitudes, as orientation and spin rate makes all attitudes possible. The attitude must be monitored within a certain accuracy, of which 0.5° is not uncommon. As stated above, other determination requirements include orbit tracking from the ground station and having the attitude inertially fixed due to spin.

Slew Mode

Slew mode requires the spacecraft be reoriented as needed. The spacecraft will be turned around a fixed point, whether it be the center of rotation or an axis of inertia. The ground station will command the spacecraft to follow a slew or a sequence of slew maneuvers to reorient the craft to change orbit, examine a different attitude, and so on.

Slewing affects control actuator selection and the spacecraft in three different ways. With no slewing, the spacecraft is constrained to a highly-improbable singular attitude. Lighter or more efficient actuators, such as reaction wheels or magnetic torquers, may be used in this situation. Nominal rates of slewing would be the best combination of spacecraft effects

and actuator selection. Having typical rates of 0.05° to 0.5° per second, the effect on the spacecraft is minimal, and thrusters are likely although for a few particular cases reaction wheels may be adequate alone. Slewing at high rates of 0.5° per second may have high structural impacts on the appendages of the craft, as well as an increase in weight and cost. Thrusters may be used, but must have levels of force to satisfy station keeping and high rate maneuvers, though control moment gyros are typically used at high slewing rates.

Safe Mode

Safe mode is used in emergencies, when normal mode fails or when there is a major malfunction such as a thruster problem. Used as a backup, safe mode compromises the time constraints of the mission and minimizes power usage. The spacecraft waits for ground station commands while the telemetry system stays active and in full power to receive the commands and to send the previously stored attitude information.

Attitude determination requirements include measurement and storage of spin rate if the craft is spinning, tracking of the orbit from the ground station, and sensing and storage of attitude. There are no attitude control requirements, since the purpose of safe mode is to gather and send information.

Other Modes

Some less-used modes include acquisition, special, and thrusting modes. Acquisition mode is the initial determination of both the attitude and stabilization of the spacecraft. This mode is mainly used during safe mode recoveries. Special mode is used for special targets which require different requirements, or during special time periods such as eclipses or during blinding sunspots. Thrusting mode is fairly self explanatory, used during thrusting maneuvers, where the orientations of the spacecraft are precisely determined at the initial and final points.

2.2.3 Sensors

To determine the position and attitude of a spacecraft, its orientation and location relative to some frame of reference of a celestial body should be defined. Most commonly, unit vectors are directed towards the Earth, the Sun, a star, or Earth's magnetic field. Attitude sensors measure the orientation of the reference vectors in the body frame of reference of the spacecraft. Two or more determined reference vectors can determine the orientation of the craft, or similarly by triangulation of several reference vectors, such as using multiple stars as a frame of reference. The number and type of sensor depends on the purpose of the spacecraft, and is therefore mission dependant. Because of this, mathematic modelling and equations will not be included in this section. A table charting the accuracy range, weight, and power for each sensor is shown at the end of the section.

Sun Sensors

Sun sensors are the most commonly used attitude sensors because of their accuracy and reliability. They are visible light detectors that measure one or two angles between where they are mounted and the incident sunlight. The design of the sensor and its algorithms are simple and inexpensive due to the brightness of the Sun and the distance from the Earth making it appear as a point source. Sun sensors are vital for the majority of spacecraft since most missions require solar power, and due to the Sun-sensitive equipment the craft is equipped with that needs protection against the Sun's heat. There are two main types of Sun sensors: analog and digital sensors.

A common analog sensor has a continuous output signal that is a function of the sun incidence angle, making the output voltage a sinusoidal function. Analog sensors are based on photocells that have a current output proportional to the cosine of the angle between the sun's direction and perpendicular to the photocell:

$$I_\alpha = I_0 \cos \alpha \quad (2.85)$$

The direction of the sun is usually denoted by the vector:

$$\hat{\mathbf{s}} = \mathbf{s}_i^T \{\hat{\mathbf{i}}\} = \mathbf{s}_b^T \{\hat{\mathbf{b}}\} \quad (2.86)$$

And these two may be related by:

$$\hat{\mathbf{s}} \cdot \hat{\mathbf{n}} = \cos \alpha \quad (2.87)$$

where $\hat{\mathbf{n}}$ is the unit normal of the photocell. Sun sensors usually combine two photocells to provide the complete unit vector measurement, as the component of $\hat{\mathbf{n}}$ perpendicular to $\hat{\mathbf{s}}$ is unknown. The two cells are tilted at an angle of α_0 with respect to the normal $\hat{\mathbf{n}}$ of the sensor, creating currents in the photocells of:

$$I_{1\alpha} = I_0 \cos(\alpha_0 - \alpha) \quad (2.88)$$

$$I_{2\alpha} = I_0 \cos(\alpha_0 + \alpha) \quad (2.89)$$

Obtaining the difference of:

$$\Delta I = I_2 - I_1 \quad (2.90)$$

$$= I_0 [\cos(\alpha_0 + \alpha) - \cos(\alpha_0 - \alpha)] \quad (2.91)$$

$$= 2I_0 \sin \alpha_0 \sin \alpha \quad (2.92)$$

$$= C \sin \alpha \quad (2.93)$$

where $C = 2I_0 \sin \alpha_0$, depending on the photocell's electrical characteristics. If $\hat{\mathbf{n}}$ is allowed to be a unit vector, then the sun vector may reduce to:

$$\mathbf{s}_\odot^* = \left[1 \quad \frac{\tan \alpha_1}{\tan \alpha_2} \quad \tan \alpha_1 \right]^T \quad (2.94)$$

From this equation, the Sun vector components can be found by normalizing this vector:

$$\mathbf{s}_{\odot} = \frac{\begin{bmatrix} 1 & \frac{\tan \alpha_1}{\tan \alpha_2} & \tan \alpha_1 \end{bmatrix}^T}{\sqrt{\mathbf{s}_{\odot}^{*T} \mathbf{s}_{\odot}^*}} \quad (2.95)$$

Using four photocells allows the calculation of the sun sensor unit vector to be expressed in the frame of the sun sensor, normally denoted by \mathcal{F}_s .

Digital sensors are composed of a command unit and a measurement unit. The command unit acts as a Sun presence detector while the measurement unit puts out a digital output. When the Sun is in the field of view of the command unit, the output is a representation of the Sun's incidence angle, relative to the normal of the sensor face. After sunlight goes through the entrance slit, the Sun image is refracted and illuminates in a pattern of slits. The photocells below each row of slits generate a digital output. A bit pattern of an automatic threshold adjust, sign bit, encoded bits, and a fine bit, process an accuracy of 0.125 degrees in the Sun angle.

Horizon Sensors

Horizon sensors are the primary means for determining the attitude of the spacecraft with respect to the Earth. These sensors are fairly common, since the attitude relative to the Earth is an important aspect of ADCS, especially for communications and weather satellites. Horizon sensors are infrared devices that detect the difference between the heat of Earth's atmosphere and the cold in deep space. For most satellites in space, Earth covers 40% of the sky. Simply detecting the Earth is not sufficient enough to determine attitude; sensors therefore detect Earth's horizon only. The problems with these sensors include the difficulty in distinguishing between the true, or hard, horizon and the edge of the atmosphere. A horizon sensor has four basic components: an optical system, a scanning mechanism, a radiance detector, and signal processing electronics. The optical systems selects the observed spectral band through a filter and positions the target image on the radiance detector using a focusing system.

Scanning mechanisms require clear fields of view for their scan cones, which are typically either 45, 60, 90, or a half-angle. The sensors are typically classified by the scanning mechanism used to search the celestial sphere. One type utilizes the spin of the spacecraft, making them the simplest type. These include body-mounted horizon sensors, where the sensor is fixed to the body of the spinning spacecraft providing the scanning mechanism, and wheel-mounted horizon sensors, where the sensor is attached to a momentum wheel on the craft and the wheel's rotation provides the scanning mechanism. The momentum wheel consists of integrated systems all in one unit, including the wheel, the sensor, the scan wheels, and all other electronics.

Radiance detectors detect the horizon and are categorized by their light spectral sensitivity region. The scanned body radiates energy that is focused by the optical system on the detector, and then produces voltage. Photodiodes, thermistors, thermocouples, pyroelectric

crystals and bolometers are examples of some radiance detectors. If output voltage increases over the threshold, it is called an acquisition of signal (AOS) or in-crossing. A decrease in output voltage is referred to as a loss of signal (LOS), or an out-crossing.

Signal processing electronics include things such as reference to acquisition of signal time, reference to loss of signal time, reference to mid-scan time, and Earth width. These time signals are sent to the attitude determination software to acquire attitude data. The sensor mounting angle, the angle between the spin and optical axes, is important input data for the signal processing. Dual horizon sensor scanners are used to increase the accuracy and the reliability of the attitude, specifically about the roll axis. The accuracy of the roll axis is increased by determining the difference between the scanners observance of the two duty cycles, which are the percentages of scan period that the radiance is above the threshold given by the equation:

$$\text{duty cycle} = [(t_{LOS} - t_{AOS})/\text{scan period}] \times 100 \quad (2.96)$$

Magnetometers

Magnetometers are common in attitude determination for the reasons that they: are vector sensors (measuring both direction and magnitude of the magnetic field), require little power and are light weight, are reliable up to certain altitudes, can operate over a range of temperatures, and have no moving parts. Magnetometers are not precisely accurate since the magnetic field of Earth is not precisely known, and are therefore subject to position errors. Altitudes of 1000 km and above have small enough magnetic fields that they are particularly subject to error. A simple tilted dipole model of Earth's magnetic field is useful for writing the components of the magnetic field as:

$$\mathbf{m}_i^* = \frac{R_{\oplus}^3 H_0}{r^3} [3\mathbf{d}_i^T \hat{\mathbf{r}}_i \hat{\mathbf{r}}_i - \mathbf{d}_i] \quad (2.97)$$

$$\mathbf{m}_i^* = \frac{R_{\oplus}^3 H_0}{r^3} = \begin{bmatrix} 3(\mathbf{d}^T \hat{\mathbf{r}}) \hat{r}_1 - \sin \theta'_m \cos \alpha_m \\ 3(\mathbf{d}^T \hat{\mathbf{r}}) \hat{r}_2 - \sin \theta'_m \sin \alpha_m \\ 3(\mathbf{d}^T \hat{\mathbf{r}}) \hat{r}_3 - \cos \theta'_m \end{bmatrix} \quad (2.98)$$

The vector $\hat{\mathbf{r}}$ is a unit vector in the position vector of the spacecraft. The constant $R_{\oplus} = 6378$ km is the Earth's radius, and $H_0 = 30155$ nT is a constant characterizing the Earth's magnetic field. The vector $\hat{\mathbf{d}}$ is in the unit dipole direction:

$$\mathbf{d}_i = \begin{bmatrix} \sin \theta'_m \cos \alpha_m \\ \sin \theta'_m \sin \alpha_m \\ \cos \theta'_m \end{bmatrix} \quad (2.99)$$

In these equations, α_m is given by the equation:

$$\alpha_m = \theta_{g0} + \omega_{\oplus} t + \phi'_m \quad (2.100)$$

where θ_{g0} is the Greenwich sidereal time at epoch, ω_{\oplus} is Earth's average rotation rate, t is time since epoch, θ'_m is the coelevation of the dipole, and ϕ'_m is the East longitude of the dipole.

Magnetometers are composed of two primary categories: induction and quantum magnetometers. Induction magnetometers use a time varying magnetic flux in a coil, inducing an electric voltage in that coil. Search coil magnetometers generate accurate phase information in spin-stabilized spacecraft. Quantum magnetometers use quantum properties to measure the direction and magnitude of magnetic fields. Heavy and requiring more power, quantum magnetometers can not be used for small spacecraft and normally are not used as attitude sensors.

Magnetic field sensor signals are processed by the electronics unit, then the information is forwarded to attitude determination. The signals are compared with predicted values of the magnetic field data to determine a spacecraft's orientation.

Star Sensors

Star sensors represent the most common sensor for high-accuracy spacecraft missions. Star sensors may be divided into three major categories: scanners, fixed head star trackers, and gimbaled star trackers. Scanners use the spin of the spacecraft for the searching function, where stars pass through multiple slits in the scanner's field of view. The spinning motion results in the scanning of the celestial sphere. The spacecraft's attitude can be derived after several passings of the star.

Fixed-head star trackers electronically perform the search and track functions over a small field of view. Trackers are used on a three-axis attitude stabilized spacecraft to track one or more stars to derive attitude information. Trackers have no moving parts and are typically lighter and smaller than gimbaled star trackers. Using electronic means, the field of view is scanned in patterns, tracking a star until either it moves out of the field of view or another star needs to be monitored. The disadvantage of fixed head star trackers is stray electronic and magnetic fields make the image dissector subject to errors. Typical field of view size ranges from 16 arc-minute circles to 8×8 degree squares.

Gimbaled star scanners use a mechanical system to search and acquire stars. Using a very small field of view, the gimbal assembly maintains a centered star image. Gimbaled scanners are mostly used for missions that require operation in a variety of attitude positions. However, the mechanical motion of the assembly limits its usage to a short-term life span and limits its accuracy, ranging from one to sixty arcseconds.

All the star trackers have to be protected from bright objects by use of another sensor which closes a shutter until the object is outside the field of view. Equations of motion for star trackers can be seen in the algorithms section, using mainly the triad method, the QUEST method, and the q-method.

Gyroscopes

Gyroscopes are inertial sensors measuring the speed or angle of rotation from a reference point. They use rapidly spinning mass to sense and respond to changes in the inertial orientation of the spin axis. Three main types of attitude sensing gyros measure spacecraft orientation change: rate, rate integrating, and optical. The angular momentum of a gyro remains constant in magnitude and direction in space in the absence of external torques. Any rotation about the gyro's input axis results in a gimbal about the output axis, which in turn causes an output signal from the rate gyro or rate integrating gyro. If the axis is only supported by one gimbal, it is referred to as a single degree of freedom gyro since it is sensitive in only one direction. If the axis is supported by two gimbals, it is a two degree of freedom gyro. If three or more gyros or multiple two degree of freedom gyros are supported, attitude information is provided about all three axes.

Rate gyros (RG) measure the spacecraft rotation rate and are usually used in feedback control systems for attitude stabilization or spin rate control. Rotating about the RG input axis, gimbals rotate about the output axis, making the gyros generate an output signal. RGs are inexpensive, the simplest type of gyros, and have an accuracy good enough for spin rate control. However, they frequently have drift errors and must be calibrated using more accurate attitude measurements such as star tracker data. Rate gyros can also provide angular displacement data if integrated from some reference time or position.

Rate integrating gyros (RIG) are more frequently used in attitude determination because of their low drift and high accuracy characteristics. Rate integrating gyros output angular displacement instead of the angular rate that RGs output. Rate integrating gyros are subject to drift errors such as random drift, but may be modelled to predict output error. Star tracker data, like in RGs, can be used to calibrate and correct RIG output. Also as RG output can be integrated to find angular displacement, RIG output can be differentiated to obtain the average rotation rate during a certain time interval.

Optical gyroscopes utilize a light ring to determine rotational changes. All optical gyros operate on the principal called the Sagnac effect. The Sagnac effect works through two light beams travelling through circular paths around an optical coil in opposite directions. If the coil is rotating, the light beam will take a longer time to travel over the coil's circumference. This way, the gyroscopes' rotation can be measured. Great accuracy is achieved this way, with also a smaller chance of the gyroscope flipping over, which would cause problems with the mechanical gyroscopes. In a typical optical gyroscope, the ring laser gyroscope (RLG) passes a light beam through an amplifying gas of a laser in a ring, named the optical ring resonator. The frequency that resonates in the ring depends on the exact length of the light beam's path. If there is no rotation, there will be no change in the light path resonating frequency. Attitude is updated with the rate of rotation.

Sensors are important instruments used for determining the position and attitude at any point in the lifetime of a spacecraft. The different types of sensors discussed in this section are commercially available with a range of accuracy, field of view (FOV), mass, cost, and required power. Table B.6 shows a list of Earth, magnetic, star, and Sun sensors available from various companies with their respective model numbers.

Table 2.1: ADCS Sensors¹⁵

Sensor	Accuracy Range	Weight (kg)	Power (W)
Sun	0.01°	0.1 - 2.0	0 - 3
Horizon - Scanner	0.1° - 1°	1.0 - 4.0	5 - 10
Horizon - Fixed Head	<0.1°	0.5 - 3.5	0.3 - 5
Magnetometer	0.5 - 3°	0.3 - 1.2	<1
Star	0.0006°	2.0 - 5.0	5 - 20
Gyrometer	0.001°/hr	2.0 - 5.0	10 - 200

2.2.4 Disturbance Torques

While in orbit a spacecraft is affected by both external and internal torques. The four major types of external torques are solar radiation, gravity gradient, magnetic field, and aerodynamic. Internal torques include torques due to thruster misalignment, fuel sloshing and uncertainty in the center of gravity. The specific effects of the torques are presented below. Formulas for calculating the torques are provided wherever possible; however, some torques, particularly internal ones, are presented in purely qualitative terms.

Solar radiation torques depend on the solar radiation pressure distribution over the surface of the spacecraft. The materials used determine the transmissivity, absorptivity, and reflectivity of the spacecraft's surface.¹¹ The reflectivity of the surface affects the pressure applied to the surface; absorbent materials, such as a solar array, will have a lower pressure than reflective materials, such as the main spacecraft body. The pressure distribution is also affected by the orientation of the spacecraft and the location of the spacecraft's center of mass. Whenever there are uneven pressure distributions applied over the spacecraft's surface, torques are generated.

The worst case torque due to solar radiation, T_{srp} , is:

$$T_{srp} = F(C_{srp} - C_g) \quad (2.101)$$

where C_g is the center of gravity, C_{srp} is the center of solar pressure, and F is:

$$F = \frac{F_s}{c} A_s (1 + q) \cos i \quad (2.102)$$

where F_s is the solar constant (1,367 W/m²), c is the speed of light (3×10^8 m/s), A_s is the surface area of the spacecraft exposed to the radiation, i is angle of incidence from the Sun, and q is the reflection factor.¹¹ The reflection factor ranges from zero to one, with zero for pure absorption and one for pure reflection.⁵

The external torques due to solar radiation will vary depending on whether the Sun is experiencing a solar maximum or a solar minimum. During a solar maximum, the Sun experiences more events that eject solar particles into space, therefore increasing the solar radiation pressure on the spacecraft.⁴ In addition, as the spacecraft travels in orbit, the exposure to solar radiation will vary. For spacecraft that are Sun-orientated or for platforms

that are separated from a main vehicle, this variation in exposure to solar radiation pressure results in a constant torque, which requires active control. For spacecraft that are Earth-orientated, the solar radiation pressure causes a cyclical torque, which requires monitoring and either continual minor corrections or major occasional corrections.

Gravity gradient torque depends on the variations in the gravity field, as explained by Newton's Law of Universal Gravitation. The spacecraft experiences a larger gravitational attraction on the side closest to Earth, while the portion of the spacecraft further away from Earth experiences a smaller gravitational attraction. Torques are generated from the differences in gravitational pull along the spacecraft, and results in the spacecraft rotating until it is aligned along its minimum inertia axis. Irregularly shaped spacecraft are especially affected by gravity gradient torques, as gravity gradients will cause the spacecraft to rotate into a specific orientation.

The maximum gravity gradient torque, T_g , is

$$T_g = \frac{3\mu}{2r^3} |I_z - I_y| \sin 2\theta \quad (2.103)$$

where r is the orbit radius and θ is the maximum deviation of the z-axis from the local vertical, and I_z and I_y are the moments of inertia about the z and y axes, respectively. If the the moment of inertia about the x axis (I_x) is smaller than I_y , I_x should be used instead of I_y in Eq. 2.103.¹¹

Some satellites are designed to use gravity gradient torques to stabilize the spacecraft, as further explained in Section 2.2.5. If the spacecraft is not designed to use the gravity gradient torques for stabilization, the ability to adjust for the torques is necessary. For Earth-orientated spacecraft, the gravity gradient torque is constant and requires active control. For inertially orientated vehicles, the gravity gradient torque is cyclic and requires monitoring and occasional corrections.

Magnetic field torque results as the different magnetic fields produced by the spacecraft try to become aligned with the magnetic field produced by the Earth. The materials used on the spacecraft and the wiring for instrumentation within the spacecraft contribute to a magnetic field within and around the spacecraft, and may be considered as a residual dipole moment, or the magnetic moment inherent to the spacecraft.¹⁶ As the magnetic field from the spacecraft interacts with the Earth's magnetic field, a torque results from the tendency for the residual dipole moment to align with the Earth's magnetic field. The Earth's magnetic field, however, varies throughout the surrounding space environment, such that the orbit altitude and inclination determine the amount of influence the Earth's magnetic field has on any particular orbit.

The magnetic torque, T_m , is:

$$T_m = DB \quad (2.104)$$

where D is the residual dipole and B is the magnetic field. The magnetic field varies with inclination. For polar orbits, the magnetic field is approximated by

$$B \approx \frac{2M}{r^3} \quad (2.105)$$

For an equatorial orbit, the magnetic field is approximated by:

$$B \approx \frac{M}{r^3} \quad (2.106)$$

M is the magnetic moment of the orbited body. The magnetic torque is cyclic in nature, no matter what orientation the vehicle is in, and therefore requires minimal monitoring. The magnetic torque may also be used to minutely adjust for other torques.

Aerodynamic torques result from the interactions between the atmosphere and the vehicle. Similar to aerodynamic torques experienced by aircraft, a spacecraft responds to the medium it travels through; the amount of atmosphere rushing by the spacecraft will greatly affect the amount of aerodynamic torque experienced. The atmospheric density, however, not only changes with altitude, but also varies with the solar cycle. The effects of the solar cycle are especially influential at lower altitudes. In addition, the spacecraft shape and center of gravity affect the aerodynamic torque.

The aerodynamic torque, T_a , is:

$$T_a = F(c_{pa} - C_g) = FL \quad (2.107)$$

where c_{pa} is the center of the aerodynamic pressure, L is the distance between the center of gravity and the force F is:

$$F = 0.5[\rho C_d A_s v^2] \quad (2.108)$$

where ρ is the atmospheric density, v is the spacecraft velocity, and C_d is the drag coefficient. The C_d has nominal values between 2 and 2.5. For Earth-oriented vehicles, the aerodynamic torque remains constant; for inertially oriented vehicles, the aerodynamic torque is variable.¹¹

In addition to external torques, there are many internal torques that affect a spacecraft's stability. An uncertainty in the center of gravity, a thruster misalignment, and a mismatch of thruster outputs all result in internal torques that may be undesirable during firing of thrusters. For thruster misalignment, the torque \mathbf{T}_{thrust} is:

$$\mathbf{T}_{thrust} = \mathbf{s} \times \mathbf{T} \quad (2.109)$$

where \mathbf{s} is the vector distance from the center of mass to the thrust application point, and \mathbf{T} is the thrust vector applied. A typical range of thruster misalignment is from 0.1° to 0.5° . Typical uncertainties in the location of the center of gravity are 1-3 cm, and typical uncertainties in the thrust due to mismatch of thruster outputs is $\pm 5\%$. These three types of torques may be corrected within a closed-loop control system.¹¹

Two types of internal torques that cannot be corrected for within a closed-loop control system are torques that result from rotating machinery and liquid. Rotating machinery, such as tape recorders or pumps, result in torques that affect both the stability of the vehicle and the accuracy of the vehicle's attitude and control system. Typically in design, counter-rotating elements are added to the spacecraft to compensate for these torques. Torques caused by liquid sloshing are most often due to fuel motion in the tanks changing the spacecraft's center of mass. Again, these torques are largely dependent upon vehicle design, but items such as slosh baffles and bladders can be designed to suppress the amount of sloshing.¹¹

Other internal torques depend solely upon the spacecraft structure. For instance, torques may be generated due to the flexibility of the spacecraft. The dynamics of such flexibility results in oscillatory resonance at the bending frequencies, which in turn limits the control bandwidth that may be used. Torques may also result from thermal shocks interacting with flexible appendages, such as long inertia booms extending from the main vehicle. These torques result in attitude disturbances when the vehicle enters or leaves eclipse.¹¹ In addition, torques may also be generated by the deployment of a flexible appendage or by the movement of components such as antennas or solar panels.

Clearly, both external and internal torques must be considered during the design of a spacecraft. External torques such as those due to gravity gradients may become an integral part of the vehicle design. Other external torques require evaluation of the mission requirements, such as orbit altitude and inclination, to determine which torques must be actively controlled. Internal torques may often be taken into account in the design of a vehicle to minimize their effects. Occasionally, different torques may be useful in countering the effects of each other. Any torques that are not incorporated into the design of the spacecraft must then be controlled using hardware such as actuators and built-in angular momentum storage devices.

2.2.5 Control Approaches

As discussed in Chapter 1, multiple approaches to attitude control exist. Multiple design constraints and criteria must be considered and compared to each approach's performance characteristics in choosing a system or combination of systems to control the spacecraft. Once the selection has been made, the hardware must be sized to meet the mission requirements.

Mission Constraints

There are three major mission-specific constraints in control approach decision making. The first consideration is the payload pointing requirement, which could be either Earth-pointing or inertial pointing. Second, the slew requirements for the spacecraft must be defined and considered. Third, the required accuracy of the control system plays a large role in determining the make-up of the control system.

The mission payload defines the pointing requirement for a given spacecraft. For an Earth-pointing satellite, which generally points along the nadir axis, but must be able to slew off-nadir, a gravity-gradient control approach may be appropriate if the required accuracy is greater than 1° .¹¹ If gravity-gradient does not provide sufficient accuracy, then 3-axis stabilization would typically be used, although a dual-spin spacecraft may also be considered. On the other hand, in an inertial pointing system, gravity-gradient stabilization is not an option, whereas spin stabilization could provide the necessary accuracy. Again, 3-axis control provides accurate control with maximum flexibility in reorienting the spacecraft.¹¹

Slewing maneuvers and their required rates weigh heavily on the decision of control approach. For the unlikely event that a spacecraft requires no slewing, reaction wheels and magnetic torquers may supply sufficient stability to avoid the need for thrusters and other

pieces of more complicated control hardware. When nominal slew rates fall in the range of approximately 0.05° per second to 0.5° per second, reaction wheels may provide enough torque to effect such rates. Low-level thrusters could also be used in this case. For higher rate requirements, low-level thrusters and reaction wheels used to keep the spacecraft stabilized become incapable of delivering the necessary torques. When this occurs, control moment gyros or variable force thrusters must provide the torque needed.¹¹

The last major mission constraint is the payload pointing accuracy requirement. For payloads requiring an accuracy of greater than 5° , gravity-gradient stabilization may be used. When 1° to 5° accuracy is needed, spin stabilization and 3-axis control may both be considered. Between 0.1° and 1° accuracy, dual-spin, momentum-bias, and 3-axis stabilization all provide the necessary accuracy. Spacecraft requiring less than 0.1° accuracy require 3-axis stabilization.¹¹

Performance

Each different control approach exhibits different performance characteristics in terms of torque capability, weight, and power consumption. Torque capability may become the limiting constraint on systems subject to high external torques, whereas weight requirements may be more critical in other situations. Power consumption may be constrained by the total power available to the spacecraft.

Thrusters, reaction and momentum wheels, and control moment gyros all display varying levels of performance. Hot gas thrusters operate in the range between 0.5 and 9,000 N, whereas cold gas thrusters exert less than 5 N force. The torque available from the thrusters relies on the length of the moment arm about the center of gravity. Reaction and momentum wheels provide 0.4 to 400 N·m·s when rotating at speeds of 1,200 to 5,000 rpm. They also produce 0.01 to 1 N·m in maximum torque. The weight of reaction and momentum wheels typically range between 2 and 20 kg, and the required power falls between 10 and 110 W. Control moment gyros supply torques in the range of 25 to 500 N·m, but typically weigh in excess of 10 kg and require 90 to 150 W to operate.

Table 2.2 summarizes the respective capabilities of each control approach.¹⁵

Sizing

In sizing each control approach, the disturbance torque to be countered and the slew requirements both must be considered. In the equations in this section, disturbance torque is denoted by T_D , and the slew angle is denoted by θ .

Sizing of reaction wheels is governed by the magnitude of disturbance torques, the required slew maneuvers, and the amount of momentum it can store. To determine the torque required from a reaction wheel to counteract a given disturbance torque, the following equation is used:

$$T_{RW} = (T_D)(\text{Margin Factor}) \quad (2.110)$$

In this equation, the margin factor is simply a factor of safety to ensure that even slightly higher than predicted disturbance torques can be controlled by the reaction wheel. In order

Table 2.2: Attitude Control Methods and Their Capabilities (adapted from Ref. 11)

Type	Pointing Options	Attitude Maneuverability	Typical Accuracy	Lifetime Limits
<i>Gravity-gradient</i>	Earth local vertical only	Very limited	$\pm 5^\circ$ (2 axes)	None
<i>Gravity-gradient and Momentum Bias Wheel</i>	Earth local vertical only	Very limited	$\pm 5^\circ$ (2 axes)	Life of wheel bearings
<i>Passive Magnetic</i>	North/south only	Very limited	$\pm 5^\circ$ (2 axes)	None
<i>Pure Spin Stabilization</i>	Inertially fixed any direction Repoint with precession maneuvers	High propellant usage to move stiff momentum vector	$\pm 0.1^\circ$ to $\pm 1^\circ$ in 2 axes (proportional to spin rate)	Thruster propellant (if applies)*
<i>Dual-Spin Stabilization</i>	Limited only by articulation on despun platform	Momentum vector same as above Despun platform constrained by its own geometry	Same as above for spin section Despun dictated by payload reference and pointing	Thruster propellant (if applies)* Despin bearings
<i>Bias Momentum (1 wheel)</i>	Best suited for local vertical pointing	Momentum vector of the bias wheel prefers to stay normal to orbit plane, constraining yaw maneuver	$\pm 0.1^\circ$ to $\pm 1^\circ$	Propellant (if applies)* Life of sensor and wheel bearings
<i>Zero Momentum (thruster only)</i>	No constraints	No constraints High rates possible	$\pm 0.1^\circ$ to $\pm 5^\circ$	Propellant
<i>Zero Momentum (3 wheels)</i>	No constraints	No constraints	$\pm 0.001^\circ$ to $\pm 1^\circ$	Propellant (if applies)* Life of sensor wheel bearings
<i>Zero Momentum (CMG)</i>	No constraints	No constraints High rates possible	$\pm 0.001^\circ$ to $\pm 1^\circ$	Propellant (if applies)* Life of sensor wheel bearings

to size the reaction wheel for slew maneuvers, the following equation must be used:

$$T_{RW} = 4\theta \frac{I}{t^2} \quad (2.111)$$

In the above equation, I is the moment of inertia of the spacecraft, and t is the length of time of the slew maneuver. Because a reaction wheel eventually reaches a saturation speed, the amount of momentum it can store must be calculated to ensure that bleed-off maneuvers are not required too frequently. To calculate the required angular momentum of the reaction wheel, the disturbance torque is integrated over a single orbit of period P , and calculated using:

$$h = (T_D) \frac{P}{4} (0.707) \quad (2.112)$$

Momentum wheels also store momentum, and their size is defined by the allowable motion, θ_a , and the disturbance torque over a single orbit. This relationship is given in the equation:

$$h = \frac{T_D}{\theta_a} \cdot \frac{P}{4} \quad (2.113)$$

For spin-stabilized spacecraft the requisite angular momentum and the spin rate, ω_s are calculated in a manner similar to a momentum wheel, using Eq. 2.113 and the following: 2.114.

$$\omega_s = \frac{h}{I} \quad (2.114)$$

The torquing capability, or magnetic dipole (D), of a magnetic torquer is calculated using the disturbance torque, and the value of Earth's magnetic field (B).

$$D = \frac{T_D}{B} \quad (2.115)$$

When sizing thrusters for attitude control, many different considerations come into play. In order to counteract the external disturbance torques, the thruster force, F , must be calculated using the equation:

$$F = \frac{T_D}{L} \quad (2.116)$$

where L is the moment arm of the thruster. To meet required slew rates in a zero momentum system, the thruster force required can be calculated using:

$$F = \frac{I\ddot{\theta}}{L} \quad (2.117)$$

When slewing a momentum-bias spacecraft, the force required is dependent on the angular momentum of the wheel (h) as well as the thruster duty cycle (d) as seen in the following equation:

$$F = \frac{h\dot{\theta}}{Ld} \quad (2.118)$$

Another consideration in thruster force sizing is momentum dumping when using a momentum or reaction wheel. The force required for such a maneuver is given as:

$$F = \frac{h}{Lt} \quad (2.119)$$

where t is the length of the burn.

Lastly, once the force required has been calculated, the thruster propellant mass can be calculated based on the specific impulse (I_{sp}) of the thrusters and the total pulse length (t). The total pulse length is calculated by summing the number of impulses times their duration. The following equation shows how to calculate propellant mass:

$$M_P = \frac{Ft}{I_{sp}g} \quad (2.120)$$

The above equations can be used to size the control system for any control approach.

2.2.6 Algorithms

In order to determine and control the attitude of a spacecraft, there are many choices available in terms of attitude descriptions, feedback loops, and sensor accuracy. The following subsection will detail many of the algorithms used to determine, describe, and control the spacecraft's attitude. There are two main categories of attitude determination: static and dynamic. Static attitude determination only considers the orbit geometry at one specific point in time, whereas dynamic attitude determination looks at attitude measurements over the course of some specified amount of time. The majority of the algorithms presented in this section fall in the static attitude determination category.

Useful Mathematics

There are a few mathematical formulas that are useful for dealing with attitude determination and control algorithms. For instance, the transport theorem is useful for taking the derivative of a vector with respect to one coordinate system while being described in another coordinate system. For two reference frames, B and N , with a relative angular velocity of $\omega_{B/N}$, and a general vector \mathbf{r} , the transport theorem states:

$$\frac{{}^N d}{dt}(\mathbf{r}) = \frac{{}^B d}{dt}(\mathbf{r}) + \boldsymbol{\omega}_{B/N} \times \mathbf{r} \quad (2.121)$$

Another useful theorem is the parallel axis theorem, which transfers the moment of inertia about one point to another point. Given the moment of inertia about the center of mass (I_c) the moment of inertia about point O (I_O) is defined as:

$$[I_O] = [I_c] + m[\tilde{\mathbf{r}}_c][\tilde{\mathbf{r}}_c]^T \quad (2.122)$$

where \mathbf{r}_c is the position vector from the center of mass to point O and m is the mass of the object. Another useful formula to mention here is the direction cosine matrix, $[C]$. This

matrix is a method of mapping vectors in one reference frame to another. For instance, the formula:

$$\{\hat{\mathbf{b}}\} = [C]\{\hat{\mathbf{n}}\} \quad (2.123)$$

expresses the vectors in the B frame in terms of the N frame. The generalized form of the direction cosine matrix is:

$$[C] = \begin{bmatrix} \cos \alpha_{11} & \cos \alpha_{12} & \cos \alpha_{13} \\ \cos \alpha_{21} & \cos \alpha_{22} & \cos \alpha_{23} \\ \cos \alpha_{31} & \cos \alpha_{32} & \cos \alpha_{33} \end{bmatrix} \quad (2.124)$$

where α_{ij} is an angle between the unit vectors from one reference frame to the next.

Attitude Determination

The attitude of a spacecraft is determined using sensors, such as sun sensors, magnetometers, and star trackers. Each type of sensor has advantages and disadvantages, as described in Section 2.2.3.

A sun sensor provides an approximate unit vector that points towards the sun, $\hat{\mathbf{s}}$. This vector can be written in either inertial or body reference frames, as seen in Eq. 2.86. The use of photocells in sun sensors allows a normalized sun vector to be determined by Eq. 2.95. The components of the non-unit vector, \mathbf{s}_{\odot}^* are given by Eq. 2.94. The following algorithm is one way the inertial sun vector may be determined simply from knowing the Julian Date (JD):

$$T_{UT} = \frac{JD_{UT} - 2451545.0}{36525} \quad (2.125a)$$

$$\lambda_{M_{\odot}} = 280.4606184^{\circ} + 36000.77005361T_{UT} \quad (2.125b)$$

$$M_{\odot} = 357.52772333^{\circ} + 35999.05034T_{UT} \quad (2.125c)$$

$$\lambda_{ecliptic} = \lambda_{M_{\odot}} + 1.914666471^{\circ} \sin M_{\odot} + 0.918994643 \sin 2M_{\odot} \quad (2.125d)$$

$$s^* = 1.000140612 - 0.016708617 \cos M_{\odot} - 0.000139589 \cos 2M_{\odot} \quad (2.125e)$$

$$\varepsilon = 23.439291^{\circ} - 0.0130042T_{UT} \quad (2.125f)$$

$$\mathbf{s}_i = \begin{bmatrix} \cos \lambda_{ecliptic} \\ \cos \varepsilon \sin \lambda_{ecliptic} \\ \sin \varepsilon \sin \lambda_{ecliptic} \end{bmatrix} \quad (2.125g)$$

where T_{UT} is the period in universal time, $\lambda_{M_{\odot}}$ is the mean longitude of the Sun, M_{\odot} is the mean anomaly of the Sun, $\lambda_{ecliptic}$ is the ecliptic longitude of the Sun, s^* is given in AUs , and ε is the elevation angle.⁶

When two sensors are used, an algorithm known as the Vector Triad Method can be used to reconcile the measurements. This method constructs two triads of orthogonal unit vectors, one in the body frame and one in the inertial frame, and assumes that one of the two measurements is incorrect and the other is exact. The result of the Vector Triad Method is

an approximate rotation matrix used to relate the body and inertial reference frames.⁶ The two vector measurements must first be normalized in both reference frames. Assuming the first vector is accurate, the body reference matrix \mathbf{T}_b consists of the following t_i components:

$$\mathbf{t}_{1b} = \mathbf{v}_{1b} \quad (2.126a)$$

$$\mathbf{t}_{2b} = \frac{\mathbf{v}_{1b} \times \mathbf{v}_{2b}}{|\mathbf{v}_{1b} \times \mathbf{v}_{2b}|} \quad (2.126b)$$

$$\mathbf{t}_{3b} = \mathbf{t}_{1b} \times \mathbf{t}_{2b} \quad (2.126c)$$

where \mathbf{v}_{1b} is the normalized body vector of the first measurement, and \mathbf{v}_{2b} is the normalized body vector of the second measurement. The inertia reference matrix \mathbf{T}_i consists of the following components:

$$\mathbf{t}_{1i} = \mathbf{v}_{1i} \quad (2.127a)$$

$$\mathbf{t}_{2i} = \frac{\mathbf{v}_{1i} \times \mathbf{v}_{2i}}{|\mathbf{v}_{1i} \times \mathbf{v}_{2i}|} \quad (2.127b)$$

$$\mathbf{t}_{3i} = \mathbf{t}_{1i} \times \mathbf{t}_{2i} \quad (2.127c)$$

where \mathbf{v}_{1i} is the normalized inertial vector of the first measurement, and \mathbf{v}_{2i} is the normalized inertial vector of the second measurement. The final approximate rotation matrix, $[BI]$, from body to inertial coordinates is:

$$[BI] = \mathbf{T}_b \mathbf{T}_i^T = [\mathbf{t}_{1b} \ \mathbf{t}_{2b} \ \mathbf{t}_{3b}] [\mathbf{t}_{1i} \ \mathbf{t}_{2i} \ \mathbf{t}_{3i}]^T \quad (2.128)$$

The Vector Triad Method works well when there are only two measurements from the sensors to determine the spacecraft attitude from. Whenever there are multiple sensor measurements, statistical methods, such as the q-method and the QUEST method, are used to provide a better approximation of the rotation matrix. The q-method takes multiple sensor measurements, calculates the K matrix for these measurements, and determines the largest eigenvalue and corresponding eigenvector in the K matrix. The eigenvector is a set of Euler Parameters, which may be converted into a principal rotation vector and then into the inertial matrix that serves as the approximate rotation matrix. The principal rotation angle also serves as an indication of attitude error. The QUEST method is a slight variation of the q-method as it only estimates the maximum eigenvalue as a summation of the weights of each measurement. Using the estimated eigenvalue, the QUEST method then determines the Classical Rodrigues Parameters and converts the Classical Rodrigues Parameters into a rotation matrix. Again, the principal rotation angle, found in one of the intermediate steps, is an indication of the attitude error.⁶

The following equations present the q-method:

$$[B] = \sum_{k=1}^N w_k (\mathbf{v}_{kb} \mathbf{v}_{ki}^T) \quad (2.129a)$$

$$\mathbf{S} = \mathbf{B} + \mathbf{B}^T \quad (2.129b)$$

$$\mathbf{Z} = [B_{23} - B_{32} \quad B_{31} - B_{13} \quad B_{12} - B_{21}]^T \quad (2.129c)$$

$$\sigma = \text{trace}[B] \quad (2.129d)$$

$$\mathbf{K} = \begin{bmatrix} \mathbf{S} - \sigma \mathbf{I} & \mathbf{Z} \\ \mathbf{Z}^T & \sigma \end{bmatrix} \quad (2.129e)$$

$$\mathbf{K} \bar{\mathbf{q}} = \lambda \bar{\mathbf{q}} \quad (2.129f)$$

where \mathbf{B} , \mathbf{S} , \mathbf{Z} , and σ are the parameters that define the \mathbf{K} matrix, w_k is the weight of a measurement, \mathbf{v}_{kb} and \mathbf{v}_{ki} are the measurement vectors in the body and inertial frame, respectively, λ is the eigenvalue of the \mathbf{K} matrix, and \mathbf{q} is the vector of Euler parameters. There are actually four eigenvalues of the matrix \mathbf{K} , thus the optimal attitude description corresponds to the largest eigenvalue and its eigenvector. The eigenvector presents the attitude in terms of Euler parameters.

The following equations present the QUEST method:

$$\lambda_{opt} \approx \sum w_k \quad (2.130a)$$

$$[B] = \sum_{k=1}^N w_k (\mathbf{v}_{kb} \mathbf{v}_{ki}^T) \quad (2.130b)$$

$$\mathbf{S} = \mathbf{B} + \mathbf{B}^T \quad (2.130c)$$

$$\mathbf{Z} = [B_{23} - B_{32} \quad B_{31} - B_{13} \quad B_{12} - B_{21}]^T \quad (2.130d)$$

$$\sigma = \text{trace}[B] \quad (2.130e)$$

$$\mathbf{p} = [(\lambda_{opt} + \sigma) \mathbf{I} - \mathbf{S}]^{-1} \mathbf{Z} \quad (2.130f)$$

$$\bar{\mathbf{q}} = \frac{1}{\sqrt{1 + \mathbf{p}^T \mathbf{p}}} \begin{bmatrix} \mathbf{p} \\ 1 \end{bmatrix} \quad (2.130g)$$

where λ_{opt} is an approximation for the largest eigenvalue of the \mathbf{K} matrix discussed in the q-method, \mathbf{p} is the vector of classical Rodrigues parameters, and \mathbf{q} is the attitude presented as Euler parameters.

Attitude Description

There are multiple ways to describe the spacecraft's attitude once it has been determined by the sensors. For example, Euler angles, a principal rotation vector, Euler parameters, classical Rodrigues parameters, and modified Rodrigues parameters are all ways to describe

the attitude of a spacecraft. Each description has its own limitations and advantages; therefore control methods used to maintain an attitude rely on the method used to describe the attitude.

Euler angles are the most commonly used set of attitude parameters. Euler angles consist of three successive rotation angles that describe the orientation of a spacecraft. The rotations may occur about any of three orthogonal axes, but there cannot be two rotations about the same axis in a row. The order of the rotations is very important to the orientation, and there are twelve possible sets of Euler angles. The most common set is the (3-2-1) Euler angles, which correspond to the yaw-pitch-roll commonly used with aircraft. The (3-2-1) set is considered an asymmetric set since there are no repeated rotations, and it has singularities whenever the second angle has a value of $\pm 90^\circ$. The symmetric sets have a repeated rotation, such as the (3-1-3) set, and experience singularities whenever the second angle has a value of 0° or 180° . Clearly, these singularities limit the usefulness of Euler angle descriptions to small rotations. One of the main advantages of Euler angles is the ability to clearly visualize the orientation of the vehicle as it undergoes small rotations.

To determine the Euler angles, each single axis rotation is calculated in the matrices below:

$$[M_1(\theta)] = \begin{bmatrix} 1 & 0 & 0 \\ 0 & \cos \theta & \sin \theta \\ 0 & -\sin \theta & \cos \theta \end{bmatrix} \quad (2.131a)$$

$$[M_2(\theta)] = \begin{bmatrix} \cos \theta & 0 & -\sin \theta \\ 0 & 1 & 0 \\ \sin \theta & 0 & \cos \theta \end{bmatrix} \quad (2.131b)$$

$$[M_3(\theta)] = \begin{bmatrix} \cos \theta & \sin \theta & 0 \\ -\sin \theta & \cos \theta & 0 \\ 0 & 0 & 1 \end{bmatrix} \quad (2.131c)$$

The rotation matrix is created via rotation addition, which is simply multiplying the above single axis rotation matrices and arranging them in a specific order, with the last rotation first in the sequence and the first rotation last in the sequence. Thus, the direction cosine matrix for Euler angle set (α, β, γ) with angles $(\theta_1, \theta_2, \theta_3)$ produces:

$$[C(\theta_1, \theta_2, \theta_3)] = [M_\gamma(\theta_3)][M_\beta(\theta_2)][M_\alpha(\theta_1)] \quad (2.132)$$

The inverse transformation of the above direction cosine matrix can be used to determine the angles. For instance, for the (3-2-1) Euler angle set, with angles $(\theta_1, \theta_2, \theta_3)$, or (ψ, θ, ϕ) , has the direction cosine matrix:

$$[C] = \begin{bmatrix} \cos \theta_2 \cos \theta_1 & \cos \theta_2 \sin \theta_1 & -\sin \theta_2 \\ \sin \theta_3 \sin \theta_2 \cos \theta_1 - \cos \theta_3 \sin \theta_1 & \sin \theta_3 \sin \theta_2 \sin \theta_1 + \cos \theta_3 \cos \theta_1 & \sin \theta_3 \cos \theta_2 \\ \cos \theta_3 \sin \theta_2 \cos \theta_1 + \sin \theta_3 \sin \theta_1 & \cos \theta_3 \sin \theta_2 \sin \theta_1 - \sin \theta_3 \cos \theta_1 & \cos \theta_3 \cos \theta_2 \end{bmatrix} \quad (2.133)$$

The inverse transformations of this matrix result in:

$$\psi = \tan^{-1} \left(\frac{C_{12}}{C_{11}} \right) \quad (2.134a)$$

$$\theta = -\sin^{-1} (C_{13}) \quad (2.134b)$$

$$\phi = \tan^{-1} \left(\frac{C_{23}}{C_{33}} \right) \quad (2.134c)$$

The principal rotation vector is based upon the idea that any rigid body frame may be brought to another position through a single rotation about a principal axis. The principal axis unit vector (\hat{e}) is the eigenvector of the direction cosine matrix $[C]$ that corresponds to a eigenvalue of +1. Due to sign conventions, there are four possible ways to describe the same rotation: Φ and \hat{e} ; Φ and $-\hat{e}$; $\Phi - 2\pi$ and \hat{e} ; and $2\pi - \Phi$ and $-\hat{e}$. While these may appear to be similar, they are simply different routes to the same end position. The principal rotation vector experiences singularities at 0° and 180° and is undefined for zero rotation.¹⁵

The direction cosine matrix is used to determine the principal rotation vector and angle. The principal angle may be determined from:

$$\cos \Phi = \frac{1}{2}(C_{11} + C_{22} + C_{33} - 1) \quad (2.135)$$

The principal vector is then given by:

$$\hat{e} = \begin{pmatrix} e_1 \\ e_2 \\ e_3 \end{pmatrix} = \frac{1}{2 \sin \Phi} \begin{pmatrix} C_{23} - C_{32} \\ C_{31} - C_{13} \\ C_{12} - C_{21} \end{pmatrix} \quad (2.136)$$

Inversely, the direction cosine matrix may now also be defined in terms of the principal rotation angle and vector:

$$[C] = \begin{bmatrix} e_1^2 \Sigma + \cos \Phi & e_1 e_2 \Sigma + e_3 \sin \Phi & e_1 e_3 \Sigma - e_2 \sin \Phi \\ e_2 e_1 \Sigma - e_3 \sin \Phi & e_2^2 \Sigma + \cos \Phi & e_2 e_3 \Sigma + e_1 \sin \Phi \\ e_3 e_1 \Sigma + e_2 \sin \Phi & e_3 e_2 \Sigma - e_1 \sin \Phi & e_3^2 \Sigma + \cos \Phi \end{bmatrix} \quad (2.137)$$

where Σ is shorthand notation for the quantity $1 - \cos \Phi$.

The Euler parameters, or quaternions, are a redundant set of coordinates available and are completely non-singular due to the use of four coordinates. Due to the lack of singularities, Euler parameters are useful for both small and large rotations, yet the fourth parameter makes visualization of the rotation extremely difficult. There are two sets of coordinates to describe the same rotation; if on a four dimensional sphere (hence, the visualization difficulty), the antipole will describe the same rotation but as the longer way to get to the same end position. Euler parameters, however, have the constraint that the four parameters squared must equal 1, the condition for forming a hypersphere.

The Euler parameters are defined by the principal rotation vector and angle:

$$\beta_0 = \cos(\Phi/2) \quad (2.138a)$$

$$\beta_1 = e_1 \sin(\Phi/2) \quad (2.138b)$$

$$\beta_2 = e_2 \sin(\Phi/2) \quad (2.138c)$$

$$\beta_3 = e_3 \sin(\Phi/2) \quad (2.138d)$$

The first component of the Euler parameters relies only upon the principal rotation angle, and is thus only concerned with how far the rotation goes and not with the direction. The last three components are constrained by the principal rotation vector unit length constraint of $e_1^2 + e_2^2 + e_3^2 = 1$. The Euler parameters may also be calculated from the direction cosine matrix as:

$$\beta_0 = \pm \frac{1}{2} \sqrt{C_{11} + C_{22} + C_{33} + 1} \quad (2.139a)$$

$$\beta_1 = \frac{C_{23} - C_{32}}{4\beta_0} \quad (2.139b)$$

$$\beta_2 = \frac{C_{31} - C_{13}}{4\beta_0} \quad (2.139c)$$

$$\beta_3 = \frac{C_{12} - C_{21}}{4\beta_0} \quad (2.139d)$$

From the equations above, it is evident that a singularity will occur whenever the first component, β_0 , is zero. An alternative algorithm, known as Stanley's Method, may be used to find the Euler parameters without this singularity occurring and is described in Schaub.¹⁵ In addition, the direction cosine matrix may now be defined in terms of the Euler parameters:

$$[C] = \begin{bmatrix} \beta_0^2 + \beta_1^2 - \beta_2^2 - \beta_3^2 & 2(\beta_1\beta_2 + \beta_0\beta_3) & 2(\beta_1\beta_3 - \beta_0\beta_2) \\ 2(\beta_1\beta_2 - \beta_0\beta_3) & \beta_0^2 - \beta_1^2 + \beta_2^2 - \beta_3^2 & 2(\beta_2\beta_3 + \beta_0\beta_1) \\ 2(\beta_1\beta_3 + \beta_0\beta_2) & 2(\beta_2\beta_3 - \beta_0\beta_1) & \beta_0^2 - \beta_1^2 - \beta_2^2 + \beta_3^2 \end{bmatrix} \quad (2.140)$$

From the above definition of the direction cosine matrix, it is clear that the same direction cosine matrix will occur regardless of the sign of β .¹⁵

The classical Rodrigues parameters and the modified Rodrigues parameters are two more ways to describe the attitude of a spacecraft. Both may be defined either in terms of the principal rotation vector or in terms of the Euler parameters. The classical Rodrigues parameters are singular for rotations of 180° , whereas the modified Rodrigues parameters are singular for rotations of 360° and are therefore excellent choices for describing large rotations. The classical Rodrigues parameters reduces the redundant Euler parameters to three coordinates by:

$$q_i = \frac{\beta_i}{\beta_0} \quad \text{for } i = 1, 2, 3 \quad (2.141)$$

The classical Rodrigues parameters may also be described by the principal rotation vector:

$$\mathbf{q} = \tan \frac{\Phi}{2} \hat{\mathbf{e}} \quad (2.142)$$

The modified Rodrigues parameters are defined in terms of the Euler parameters by:

$$\sigma_i = \frac{\beta_i}{1 + \beta_0} \quad (2.143)$$

and in terms of the principal rotation vector by:

$$\boldsymbol{\sigma} = \tan \frac{\Phi}{4} \hat{\mathbf{e}} \quad (2.144)$$

Again, the direction cosine matrix may be rewritten in terms of either parameters; see Schaub for more details.¹⁵

There are additional methods to describing the attitude of a spacecraft. For instance, the classical and modified Rodrigues parameters are just two examples of stereographic orientation parameters that project the Euler parameter four dimensional sphere onto a three dimensional hyperplane. The (w, z) coordinates are a coordinate set useful in controlling under actuated axially symmetric spacecraft. The w coordinate describes the heading of one of the body axes, the z coordinate describes the relative rotation angle about this axis, and the stereographic projection occurs on the complex plane (w_1, w_2) . The Cayley-Klein parameters are a set of four complex parameters closely related to the Euler parameters, useful for their redundancy and non-singularity.¹⁵ The different attitude descriptions provide different methods to describe the rotations necessary to keep the spacecraft in the correct orientation. Each method has advantages and disadvantages, and it is the control method desired that will impact which description is utilized.

Attitude Control

Attitude control requires a knowledge of the spacecraft's current orientation and motion. Thus, knowledge of the kinetic energy, the angular momentum, and the equations of motion of the spacecraft are necessary to develop attitude control laws. Angular momentum in the simplest form is given by Euler's equation:

$$\dot{\mathbf{H}} = \mathbf{L} \quad (2.145)$$

where $\dot{\mathbf{H}}$ is the angular momentum and \mathbf{L} is the torque. The kinetic energy is given by:

$$T = \frac{1}{2} m \dot{\mathbf{r}}_c \cdot \dot{\mathbf{r}}_c + \frac{1}{2} \int \dot{\mathbf{r}} \cdot \dot{\mathbf{r}} dm = T_{trans} + T_{rot} \quad (2.146)$$

where \mathbf{r}_c is the center of mass position vector, \mathbf{r} is the radius of the body, and m is the mass. The Euler rotational equations of motion are derived from the angular momentum written in terms of the inertia matrix, and are given as:

$$[\mathbf{I}] \dot{\boldsymbol{\omega}} = -[\tilde{\boldsymbol{\omega}}][\mathbf{I}] \boldsymbol{\omega} + \mathbf{L}_c \quad (2.147)$$

where $\boldsymbol{\omega}$ is the body angular velocity vector.¹¹

Torque-free motion is useful for examining the energy state of a spacecraft. The basic assumption is that there are no external torques acting on the spacecraft, and therefore the total angular momentum and the total kinetic energy are both constant. Since the magnitude of angular momentum is constant, the angular velocities lie on the surface of the momentum sphere:

$$H^2 = I_1^2 \omega_1^2 + I_2^2 \omega_2^2 + I_3^2 \omega_3^2 = H_1^2 + H_2^2 + H_3^2 \quad (2.148)$$

where I_i is the i component of the diagonal, or principal, rigid body inertia matrix, ω_i is the i component of the angular velocity vector, and H_i is the i component of angular momentum. The angular velocities must also lie on the surface of the energy ellipsoid:

$$1 = \frac{H_1^2}{2I_1 T} + \frac{H_2^2}{2I_2 T} + \frac{H_3^2}{2I_3 T} \quad (2.149)$$

where T is the magnitude of kinetic energy. The intersection of the momentum sphere with the energy ellipsoid gives the possible angular velocities for that particular orbit. Inspection of the possible intersections also provides the minimum and maximum energy states. The minimum energy state occurs when the energy ellipsoid is small enough that it just barely intersects the momentum sphere. The maximum energy state occurs when the momentum sphere is so small that it barely intersects the energy ellipsoid. Both minimum and maximum energy states are considered stable states. Intermediate energy states occur in between these two extreme cases and are unstable energy states. The separatrix is a special intermediate energy case where the energy ellipsoid semi-axis is equal to H . Assuming the inertia matrix is such that $I_1 \geq I_2 \geq I_3$, the minimum energy state is:

$$T_{min} = \frac{H^2}{2I_1} \quad (2.150)$$

the separatrix energy state is:

$$T_{int} = \frac{H^2}{2I_2} \quad (2.151)$$

and the maximum energy state is:

$$T_{max} = \frac{H^2}{2I_3} \quad (2.152)$$

Torque-free motion is also useful for examining simplified rigid body motion. For example, for the (3-2-1) Euler angles of (ψ, θ, ϕ) , the body angular velocity vector is:

$$\begin{pmatrix} \omega_1 \\ \omega_2 \\ \omega_3 \end{pmatrix} = \begin{pmatrix} \frac{H}{I_1} \sin \theta \\ -\frac{H}{I_2} \sin \phi \cos \theta \\ -\frac{H}{I_3} \cos \phi \cos \theta \end{pmatrix} \quad (2.153)$$

The torque-free (3-2-1) Euler angles result in the following equations of motion:

$$\dot{\psi} = -H \left(\frac{\sin^2 \phi}{I_2} + \frac{\cos^2 \phi}{I_3} \right) \quad (2.154)$$

$$\dot{\theta} = \frac{H}{2} \left(\frac{1}{I_3} - \frac{1}{I_2} \right) \sin 2\phi \cos \theta \quad (2.155)$$

$$\dot{\phi} = H \left(\frac{1}{I_1} - \frac{\sin^2 \phi}{I_2} - \frac{\cos^2 \phi}{I_3} \right) \sin \theta \quad (2.156)$$

If the rigid body is axisymmetric, and assuming that $I_2 = I_3$, the equations of motion become:

$$\dot{\psi} = -\frac{H}{I_2} \quad (2.157)$$

$$\dot{\theta} = 0 \quad (2.158)$$

$$\dot{\phi} = H \left(\frac{I_1 - I_2}{I_1 I_2} \right) \sin \theta \quad (2.159)$$

Clearly, axisymmetric spacecraft bodies greatly simplify the equations of motion that are used to control the motion of the spacecraft.

Gravity gradient stabilized spacecraft have specific stability equations that may be used to determine whether a small disturbance from equilibrium results in a stable motion. If the motion is not stable, then more active control is required than the gravity gradient stabilization provides. Assuming small disturbances, there is one body axis that is not affected by the torque whereas the other two body axes are coupled and interdependent. For the (3-2-1) Euler angles, the pitch is independent and the roll-yaw are coupled. The equations of motion are expressed as:

$$\ddot{\theta} + 3\Omega^2 \left(\frac{I_{11} - I_{33}}{I_{22}} \right) \theta = 0 \quad (2.160)$$

$$\begin{pmatrix} \ddot{\phi} \\ \ddot{\psi} \end{pmatrix} + \begin{bmatrix} 0 & \Omega(1 - k_Y) \\ \Omega(k_R - 1) & 0 \end{bmatrix} \begin{pmatrix} \dot{\phi} \\ \dot{\psi} \end{pmatrix} + \begin{bmatrix} 4\Omega^2 k_Y & 0 \\ 0 & \Omega^2 k_R \end{bmatrix} \begin{pmatrix} \phi \\ \psi \end{pmatrix} = 0 \quad (2.161)$$

where the inertia ratios are:

$$k_R = \frac{I_{22} - I_{11}}{I_{33}} \quad (2.162)$$

$$k_Y = \frac{I_{22} - I_{33}}{I_{11}} \quad (2.163)$$

From Eq. 2.160, it is clear that the pitch stability condition is simply $I_{11} \geq I_{33}$. From Eq. 2.161, the characteristic equation is determined as:

$$\lambda^4 + \lambda^2 \Omega^2 (1 + 3k_Y + k_Y k_R) + 4\Omega^4 k_Y k_R = 0 \quad (2.164)$$

where λ_i are the roots of the characteristic equation. The roll-yaw motions are stable if none of these roots have real, positive parts. In order to ensure the roots are negative and real, the stability conditions become:

$$1 + 3k_R + k_Y k_R > 4\sqrt{k_Y k_R} \quad (2.165)$$

$$k_R k_Y > 0 \quad (2.166)$$

These stability conditions result in a small region of truly stable motion for gravity gradient spacecraft, which are summarized as the condition of principal inertias such that $I_{22} \geq I_{11} \geq I_{33}$.

Analytical dynamics are useful for alternative methods of examining the complex motions of spacecraft. Analytical dynamics are so fundamentally complex and variational in nature that variational calculus was developed at the same time. The most well known form of variational analytical dynamics occurs in Hamilton's variational principles, which are useful for addressing rigorous integrals of general motion and canonical forms of the equations of motion.

Two well-known forms of generalized analytical dynamics are d'Alembert's principle and Lagrangian dynamics. D'Alembert's principle develops the equations of motion while neglecting the internal forces and other constraint forces that are normally considered in the development of the equations of motion from Newton's second law. This disregard of such forces develops from the notion of virtual displacements and virtual work. The most general form of d'Alembert's principle for N number of particles is:

$$\delta W - \sum_{i=1}^N m_i \ddot{\mathbf{R}}_i \cdot \delta \mathbf{R}_i = 0 \quad (2.167)$$

where δW is the work, m_i is the mass of the particle, \mathbf{R}_i is the position vector of the particle, and $\ddot{\mathbf{R}}_i$ is the acceleration vector of the particle.¹⁵

Lagrangian dynamics only require velocity-level vector kinematics, unlike d'Alembert's or Newtonian methods which require acceleration-level vector kinematics.¹⁵ Lagrangian dynamics build upon d'Alembert's principle and are able to accommodate motion in both minimal coordinate and redundant coordinate systems. The Lagrangian function is defined as:

$$\mathcal{L} = \mathcal{L}(t, q_1, \dots, q_n; \dot{q}_1, \dots, \dot{q}_n) \equiv T - V \quad (2.168)$$

where T is the kinetic energy, V is the potential energy, and (q_i, \dot{q}_i) is a set of generalized coordinates. The most well known form of Lagrange's equations is:

$$\frac{d}{dt} \left(\frac{\partial \mathcal{L}}{\partial \dot{q}_j} \right) - \frac{\partial \mathcal{L}}{\partial q_j} = 0 \quad \text{for } j = 1, 2, \dots, n \quad (2.169)$$

All of the above equations regarding attitude position and spacecraft motion are necessary to develop control systems. Control systems allow a spacecraft to maintain the orbit necessary for its space mission, and often make use of feedback loops and key parameters to ensure the spacecraft does not deviate too far from its intended attitude. For example, a control system may utilize control loops to determine the difference between the current spacecraft attitude and the desired spacecraft attitude and to continually make adjustments based on the difference.

In three-axis stabilization systems, a linear control law is determined by decoupling control into three independent axes. Each axis is given a position gain, K_p , that provides attitude control accuracy even when disturbances are present. K_p is chosen such that:

$$K_p \geq \frac{T_D}{\theta_\varepsilon} \quad (2.170)$$

where T_D is the peak disturbance torque and θ_ε is the allowable attitude error. The position gain determines the frequency at which control authority begins to diminish. This frequency, known as the bandwidth ω_n , is calculated as:

$$\omega_n = \sqrt{K_p/I} \quad (2.171)$$

where I is the moment of inertia. A simple attitude control system for three-axis stabilization utilizes a proportional plus derivative (PD) controller, such as:

$$T_c \equiv K_p\theta_\varepsilon + K_r\dot{\theta}_\varepsilon \quad (2.172)$$

In this control law, K_p controls the system bandwidth, K_r , or rate gain, controls the damping, and T_c is the torque necessary to control the spacecraft.¹¹

Lyapunov's direct method is a common nonlinear approach to control laws. By studying the behavior of Lyapunov functions, the method bypasses the need to solve nonlinear differential equations. The method determines the stability characteristics of the spacecraft, yet the variety of Lyapunov functions available for study necessitates careful selection of the functions. Some Lyapunov functions describe velocity state errors whereas other Lyapunov functions describe position state errors. Combinations of these functions are used to model the system and derive an appropriate control law. The following formula is an example of a nonlinear control law derived for closed-loop dynamics:¹⁵

$$\mathbf{u} = [\tilde{\boldsymbol{\omega}}][\mathbf{I}]\boldsymbol{\omega} + [\mathbf{I}] \left(-P\boldsymbol{\omega} - 2 \left(K - \frac{\omega^2}{4} \right) \frac{\boldsymbol{\epsilon}}{\beta_0} \right) \quad (2.173)$$

The various methods available for creating control laws are useful in selecting the appropriate control system, complete with feedback loops, for the mission. While there are no incorrect methods, each way of determining, describing, and controlling the attitude has its own advantages and disadvantages. The interactions between accuracy requirements, feedback loops, and singularities in each method enable the design of an optimal control system.

2.3 Propulsion

The modelling and selection of the spacecraft propulsion system requires an understanding of several scientific fields, including thermodynamics, aerodynamics, and electromagnetics. By applying the principles of these disciplines, the performance characteristics of various propulsion systems can be determined. In this section, the fundamentals of propulsion system performance are outlined in detail. A discussion of chemical rockets, electric propulsion, and propellantless propulsion is also included, along with some examples of currently available propulsion systems.

2.3.1 Specific Impulse and the Rocket Equation

One of the most important performance characteristics of any space propulsion system is the specific impulse. The specific impulse (I_{sp}) is defined as the ratio of the thrust (F) created by the propulsion system to the weight flow rate of propellant through the system:¹¹

$$I_{sp} = \frac{F}{\dot{m}g} \quad (2.174)$$

Note that g in Eq. 2.174 is the acceleration due to gravity at the surface of the Earth and \dot{m} is the propellant mass flow rate. For most propulsion systems, the goal is to maximize I_{sp} ; however, for some propulsion systems there is an optimal I_{sp} that is not the maximum possible value.

The primary measure of performance for a space propulsion system is the change in velocity that the system can impart upon a spacecraft.¹¹ The Δv can be related to the I_{sp} and spacecraft masses through the *rocket equation*:

$$\Delta v = gI_{sp} \ln \left(\frac{m_0}{m_0 - m_p} \right) = gI_{sp} \ln \left(\frac{m_0}{m_f} \right) = gI_{sp} \ln(R) \quad (2.175)$$

In Eq. 2.175, m_0 is the initial (wet) mass of the spacecraft, m_p is the propellant mass consumed, m_f is the final mass of the spacecraft, and R is the mass ratio. Note that Eq. 2.175 ignores the effects of gravity and drag, meaning that it describes the theoretical maximum Δv capability. Accounting for gravity and drag, Eq. 2.175 becomes

$$\Delta v = \int_{t=0}^{t=t_b} \left(-gI_{sp} \frac{dm}{m} - \frac{D}{m} dt - g_L \cos \theta dt \right) \quad (2.176)$$

where t_b is the burn time, m is the spacecraft mass at any instant, D is the drag force acting on the spacecraft, g_L is the local gravitational constant, and θ is the angle between the spacecraft velocity vector and the direction of gravity.¹¹ One possible way to estimate D is:

$$D = \frac{1}{2} C_D \rho v^2 A_f \quad (2.177)$$

where C_D is the drag coefficient of the spacecraft, ρ is the local atmospheric density, v is the spacecraft velocity, and A_f is the cross-sectional area of the front of the spacecraft.⁷ Note that C_D depends on the spacecraft shape, speed, and inclination angle relative to the velocity vector.

Equations 2.174-2.177 can not only be used to calculate several vital propulsion system characteristics, but can also be used to illustrate the interactions between the propulsion system and other spacecraft subsystems. For example, a required thrust may be provided by the orbits subdivision and Eq. 2.174 may then be used to determine the I_{sp} . On the other hand, if the I_{sp} is constrained, Eq. 2.174 may be used to determine the maximum available thrust. This thrust value is then communicated to the orbits and ADCS subdivisions who alter their designs accordingly. Equations 2.174-2.177 also show how the propulsion system

interacts with the structures subdivision. Constrained spacecraft masses and dimensions may be used to determine performance characteristics, or the performance characteristics may be used to help size the spacecraft. In any case, the design or selection of the propulsion system will have an effect on the design of the spacecraft structure and visa versa.

2.3.2 Chemical Rockets

The most widely used in-space propulsion system is the chemical rocket. In general, a rocket is a propulsion system that carries all of its propellant with it and develops thrust by imparting energy and momentum to the propellant as it is expelled from the system (usually through a nozzle). In a chemical rocket, energy is supplied to the propellant through chemical combustion, while momentum is transferred to the propellant through pressure forces.⁷ There are three types of chemical rocket systems currently available: liquid, solid, and hybrid. The name of each system refers to the physical state in which the propellant is stored.¹¹ In general, liquid rockets are called engines or thrusters and solid rockets are called motors. The purpose of this section is to describe some basics of chemical rocket propulsion, as well as the operational details of the three types of chemical rockets. The interactions between the chemical rocket performance characteristics and other spacecraft performance characteristics are also discussed.

Thrust

Along with the specific impulse, the most important chemical rocket performance characteristic is thrust. The thrust is the amount of force applied to the rocket based upon the expulsion of gases,¹¹ and is given by:

$$F = \dot{m}v_{ex} + A_e(P_e - P_\infty) \quad (2.178)$$

where v_{ex} is the velocity of the propellant as it leaves the rocket (exit or exhaust velocity), A_e is the area of the rocket exit (usually the exit of a nozzle), P_e is the pressure at the rocket exit, and P_∞ is the ambient pressure. Equation 2.178 can be simplified by defining the effective exhaust velocity (v_{eq}) as:

$$v_{eq} = v_{ex} + \frac{A_e}{\dot{m}}(P_e - P_\infty) \quad (2.179)$$

Using Eq. 2.179, we can reduce Eq. 2.178 to:

$$F = \dot{m}v_{eq} \quad (2.180)$$

Two other useful chemical rocket performance parameters are the characteristic velocity (c^*) and the thrust coefficient (C_F). The characteristic velocity is a measure of the energy available during a rocket's combustion process and is given by:

$$c^* = \frac{P_c A_t}{\dot{m}} \quad (2.181)$$

where P_c is the combustion chamber pressure and A_t is the throat area of the rocket nozzle.¹¹ If the nozzle is a converging nozzle only, A_t is the nozzle exit area. Note that c^* is primarily a function of the properties of the rocket's combustion chamber and has units of velocity.⁷ The thrust coefficient of a rocket is a measure of how efficiently the rocket nozzle converts combustion energy to exhaust velocity and is a function of the rocket's nozzle geometry only:¹¹

$$C_F = \frac{F}{P_c A_t} \quad (2.182)$$

Combining Eqs. 2.181 and 2.182, the thrust and specific impulse can be related to c^* and C_F through

$$F = \dot{m} c^* C_F = \dot{m} g I_{sp} \quad (2.183)$$

Equations 2.181-2.183 provide a means of describing the performance of any chemical rocket based solely upon its combustion properties and physical dimensions. These equations allow for a quick and easy analysis of various rocket and propellant alternatives without information from other functional divisions. On the other hand, if the orbits subdivision provides the propulsion subdivision with a required thrust, Eqs. 2.181-2.183 may be used to size the rocket and select a propellant.

The Ideal Chemical Rocket

An easy and convenient way to determine the performance characteristics of a chemical rocket is to model it as an ideal chemical rocket. In such a rocket we assume that the working fluid (propellant) is a constant composition perfect gas, the chemical combustion reaction is equivalent to a constant-pressure heating process, and the expansion of the propellant through the nozzle is steady, one-dimensional, and isentropic. By making these assumptions we are limiting the accuracy of our analysis, so modelling a rocket as an ideal rocket should only be done in preliminary design to approximate performance characteristics. A more detailed analysis would need to account for pressure losses in the expansion process, the multi-dimensional nature of the flow, and changes in the composition of the propellant.⁷

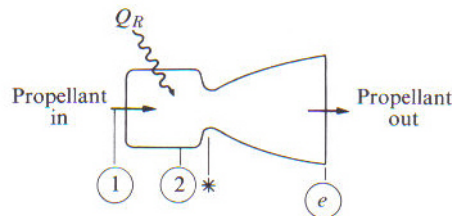


Figure 2.12: Schematic of an Ideal Rocket.⁷

Figure 2.12 shows a simple schematic of an ideal rocket. The propellant enters at state 1 and the combustion occurs between states 1 and 2. The heat added to the propellant during combustion is given the symbol Q_R . After combustion, the propellant is expanded

through the nozzle throat (*) and then out the exit (e), where the velocity is v_{ex} . Since the combustion is assumed to be a constant pressure heating process and the nozzle expansion is isentropic, we can express v_{ex} as:

$$v_{ex} = \sqrt{2Q_R \left[1 - \left(\frac{P_e}{P_{02}} \right)^{\frac{\gamma-1}{\gamma}} \right]} \quad (2.184)$$

In Eq. 2.184, P_{02} is the stagnation pressure after combustion and γ is the specific heat ratio of the propellant. We can also express the mass flow rate of propellant as

$$\dot{m} = A_t P_{02} \sqrt{\frac{\gamma}{R_g T_{02}} \left(\frac{2}{\gamma + 1} \right)^{\frac{\gamma+1}{\gamma-1}}} \quad (2.185)$$

where A_t is the nozzle throat area, R_g is the gas constant of the propellant, and T_{02} is the stagnation temperature after combustion. With the values of v_{ex} and \dot{m} known, Eqs. 2.174 and 2.178 can be used to determine the specific impulse and thrust of the rocket.⁷

Staging

For many space missions using chemical rockets, the propellant mass is minimized by breaking the thrusting into several stages, allowing for spent fuel tanks and structure, that no longer serve a purpose, to be discarded. By eliminating excess weight in this manner, the remaining available energy provides higher payload acceleration.⁷

Before we can describe the performance of a multistage rocket, we must first define a few terms. First, we define the payload ratio (λ) as the ratio of payload mass to initial mass. For the i th stage, the payload mass is the mass of all subsequent stages, and we have:

$$\lambda_i = \frac{m_{0(i+1)}}{m_{0i} - m_{0(i+1)}} \quad (2.186)$$

where m_{0i} is the initial mass of the i th stage. The structural coefficient (ϵ) is the ratio of structural mass to initial mass, and for stage i is defined as:

$$\epsilon_i = \frac{m_{si}}{m_{0i} - m_{0(i+1)}} \quad (2.187)$$

where m_{si} is the structural mass of the i th stage. We can now define the mass ratio of stage i as:

$$R_i = \frac{m_{0i}}{m_{bi}} = \frac{1 + \lambda_i}{\epsilon_i + \lambda_i} \quad (2.188)$$

where m_{bi} is the burnout mass of the i th stage. If all of the propellant for stage i is consumed during the burning period, then:

$$m_{bi} = m_{si} + m_{0(i+1)} \quad (2.189)$$

Using Eqs. 2.175 and 2.186-2.188, we can define the velocity increment, or change in velocity, for the i th stage as:

$$\Delta v_i = gI_{sp} \ln(R_i) \quad (2.190)$$

The total velocity increment for the vehicle is then the sum of all of the stage velocity increments:

$$\Delta v = \sum_{i=1}^n \Delta v_i = gI_{sp} \ln \left(\prod_{i=1}^n R_i \right) \quad (2.191)$$

where n is the number of stages. Note that the far right hand side of Eq. 2.191 is only valid if the I_{sp} of every stage is the same.

Another useful parameter is the overall mass ratio, or the ratio of the total initial mass of the vehicle to the payload mass, m_L . This ratio is related to the stage payload ratios through:

$$\frac{m_0}{m_L} = \prod_{i=1}^n \left(\frac{1 + \lambda_i}{\lambda_i} \right) \quad (2.192)$$

where the product is carried out over all of the stages. Note that the goal of any design is to minimize the overall mass ratio, as doing so maximizes the possible payload mass for a given initial vehicle mass.⁷

Liquid Chemical Rockets

In a liquid chemical rocket the propellants are stored in liquid form in tanks and are fed into the combustion chamber by means of pumps or gas pressurization. There are two types of liquid rockets currently in use: monopropellant and bipropellant. Monopropellant rockets create thrust through the catalytic decomposition of a single propellant, whereas bipropellant rockets create thrust from the the chemical reaction of a fuel and an oxidizer.¹¹

Monopropellant systems are typically chosen when small thrust levels, minimal impulse, and extended operational lifetime are required. Some of the benefits of monopropellant systems are that they have relatively low system complexity and cost and require only one set of tanks, components, and plumbing. On the other hand, monopropellant systems provide only moderate to poor performance, can be dangerous to handle, and contaminate the spacecraft with exhaust gases. There will also always be residual propellant in the tanks at the end of a mission that must be accounted for.

One of the most common monopropellant rockets currently in use is the hydrazine (N_2H_4) rocket, as shown in Fig. 2.13. Table B.2 shows a list of available monopropellant hydrazine rockets from Aerojet based on engine type and thrust produced. In monopropellant rockets, a valve opens allowing hydrazine to flow, and pressure in the propellant tank forces the hydrazine into an injector. This injector then sprays the hydrazine into a thrust chamber where it contacts multiple catalyst beds that consist of alumina pellets impregnated with iridium. Contact with the catalyst beds causes the hydrazine to heat to its vaporization temperature and then to a temperature at which its rate of decomposition becomes high enough to sustain chemical reactions. Lastly, the hydrazine decomposition products leave

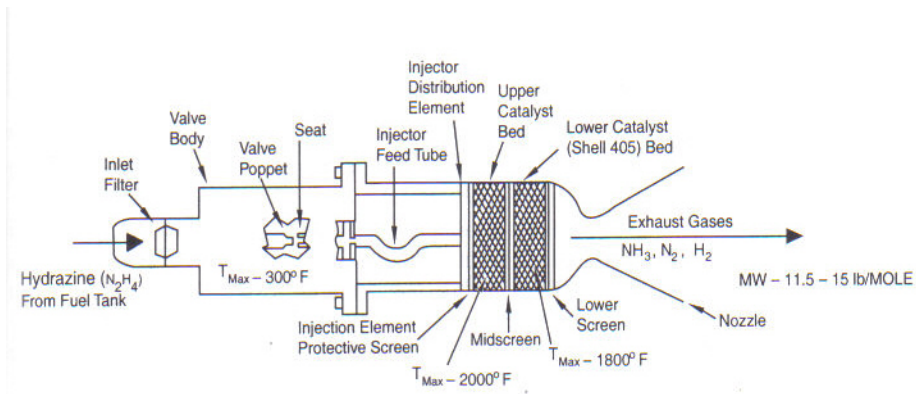


Figure 2.13: Schematic of a Typical Hydrazine Rocket.¹¹

the catalyst bed and are accelerated through a nozzle to generate thrust. The proportion of chemical products can be tailored to fit a specific application by controlling the flow variables and catalyst chamber geometry. For applications requiring a maximum I_{sp} , 30-40% ammonia dissociate must be provided. This range is about the lowest percent ammonia dissociate that can be reliably maintained.¹¹

Most liquid chemical rockets are bipropellants, which have the benefit of providing a higher specific impulses than monopropellants. Like monopropellants, bipropellants can be used for missions requiring a long operational life. The tradeoff for improved performance, however, is increased system complexity and cost as more tanks, components, and plumbing are needed. Bipropellants are also often dangerous from a system safety and handling standpoint and require tight control on the mixture of the fuel and oxidizer.

Table B.3 lists some available bipropellant rockets and their performance characteristics. Most of the rockets in Table B.3 use nitrogen tetroxide (N_2O_4) as the oxidizer and monomethyl hydrazine (MMH) as the fuel. Nitrogen tetroxide has a relatively high vapor pressure (1 atm at 294 K), meaning that its storage tanks must have thick walls for use in space. This fact must be considered when selecting a propellant as the increased wall thickness may drive up the spacecraft mass to an unacceptable level. Another fact to consider is that N_2O_4 has a freezing point of 261 K. If nitrogen tetroxide is to be used on a spacecraft, attention must be paid to insulating its storage tanks to prevent freezing. This task would fall to the thermal subdivision but would also impact the structures subdivision, as increased insulation will increase the overall mass and alter the structure. The fuel MMH is a good alternative to hydrazine because it is safer and easier to handle.¹¹

Solid Chemical Rockets

In a solid chemical rocket the fuel and oxidizer are stored in a solid form called a grain. Typically, the propellant is powdered aluminum and the oxidizer is ammonium perchlorate, with the two held together by a synthetic rubber such as polybutadiene. Solid rockets are usually used when high thrust extended operational lifetime is required. Despite the fact

that they provide lower performance than liquid rockets, solid rockets are often the rockets of choice due to their relative simplicity and high reliability. The major drawback to solid rockets, however, is that they can only be fired once, and once they are ignited they are difficult to shut down if the need to do so arises.¹¹

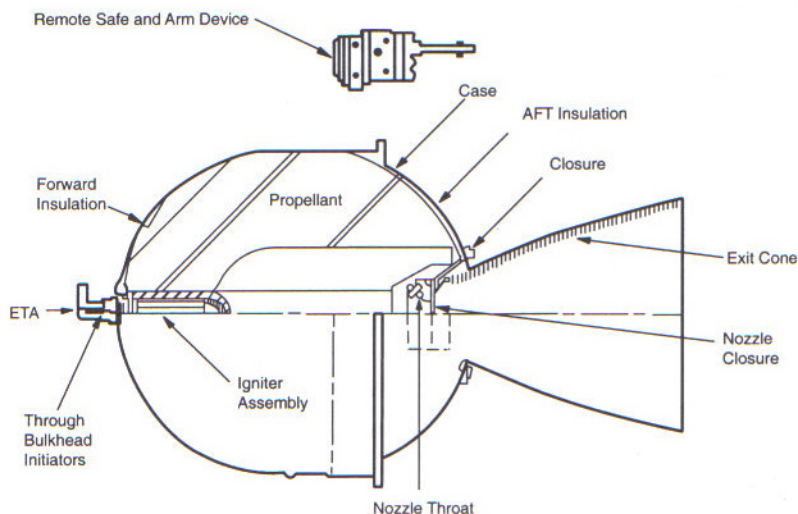


Figure 2.14: Schematic of a Typical Solid Rocket¹¹

Figure 2.14 shows a schematic of a typical solid rocket. An igniter in the forward end of the rocket starts the burn by sending burning particles into the grain. These burning particles completely ignite the grain which typically burns until it is gone. The combustion gases of the burning grain are then accelerated through a nozzle to create thrust. Table B.4 gives a list of some available solid rockets.¹¹

The rate of generation of combustion gases, and thus the thrust, is directly proportional to the rate at which the surface area of the grain changes. This surface area is known as the burning area. For constant thrust (neutral burning), the burning area must remain constant. An increase in the burning area causes an increase in thrust (progressive burning), and a decrease in burning area causes a decrease in thrust (regressive burning). Figure 2.15 shows examples of several solid rocket grain cross sections with their burning profiles and thrust time histories. As Fig. 2.15 shows, the thrust generated by a solid rocket may be tailored to a given mission profile by simply choosing the appropriate grain shape.⁷

Hybrid Chemical Rockets

A hybrid chemical rocket is a rocket in which the fuel and oxidizer are stored in different forms. In most cases the fuel is a solid and the oxidizer is a liquid or gas. The development and use of hybrid rockets has increased gradually since the 1960's, mainly because hybrid rockets have a number of attractive features. First, hybrid rockets are safe because it is impossible to create an explosive mixture of fuel and oxidizer in them. Throttling can also

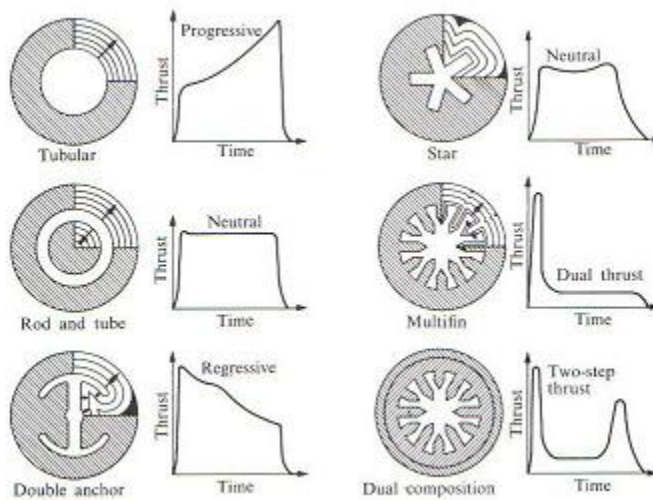


Figure 2.15: Solid Rocket Grain Designs with Their Thrust Time Histories.⁷

be easily controlled on a hybrid rocket by controlling oxidizer flow rate, and the engine can be idled to ensure system operation prior to launch. Hybrid rockets can also be stopped and restarted, which gives them an advantage over solid rockets. Lastly, hybrid rockets are environmentally clean since they can be made so that their exhaust contains no hydrochloric acid or aluminum oxide. Figure 2.16 shows a schematic of a hybrid rocket, and Table B.5 lists some hybrid rockets that are currently available or in development.

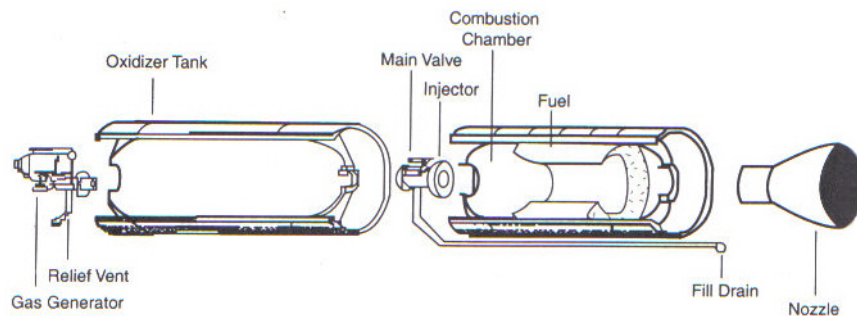


Figure 2.16: Schematic of a Typical Hybrid Rocket.¹¹

2.3.3 Cold Gas Propulsion

Cold gas propulsion systems represent the simplest form of rocket, consisting of nothing more than a controlled, pressurized gas source and a nozzle. They are typically used when small thrust levels and minimum impulse are required and when the operational lifetime of the system is short. Since they involve no combustion, cold gas systems are safe and have

low system complexity. They are also highly reliable and cause little or no contamination from exhaust gases. Cold gas systems do have some drawbacks, however, most notably poor performance (low I_{sp}), poor storability, and leakage. A good example of a cold gas system is the Manned Maneuvering Unit used by astronauts.¹¹

A cold gas system can be modelled simply as a rocket with no combustion, so Eq. 2.178 may be used to calculate thrust. In addition, Eqs. 2.181 and 2.182 are used to determine the characteristic velocity and thrust coefficient, with the combustion chamber pressure taken to be the pressure in the gas storage tank.

2.3.4 Electric Propulsion

Electric propulsion (EP) systems are fundamentally different from chemical propulsion systems with respect to what limits their performance. Electric rockets convert electrical energy directly to propellant kinetic energy. Thus, the rockets are power limited, not energy limited, meaning the thrust is limited by the rate at which the rockets are supplied energy. The energy transformation also does not necessarily raise the temperature of the working fluid or solid and eliminates the temperature constraint common to chemical propulsion. The most fundamental limit on EP is that the speed of light cannot be breached. For electrically powered rockets, efficiency is defined as the ratio of output kinetic energy to the input energy. The efficiency (η) is defined by the power ratio:

$$\eta = \frac{\dot{m}v_{ex}^2}{2P_i} \quad (2.193)$$

where η is the overall efficiency, \dot{m} is the mass flow rate, v_{ex} is exhaust velocity, and P_i is the input power. Electric powered rockets fall under two main categories: electrostatic and electromagnetic. All types of electric propulsion are operated at low thrust levels, but some can be used for long periods of time.

Electrostatic Propulsion

Electrostatic propulsion accelerates ions between charged plates and expels them. The highest performance EP characteristics and options are represented within the electrostatic propulsion category. For ion rockets, neutral propellant is pumped into an ion production chamber which separates ions and electrons into different streams. The ion stream is then passed through a strong electric field and accelerated to high speeds. The thrust from the ion rockets comes solely from the reaction to ion accelerated forces. The ionization chamber is composed of many sets of electrodes maintained at a positive acceleration potential. The last electrode is grounded at the spacecraft's potential while other electrodes can be held at other potentials to help with ion extraction and the creation of a suitable exhaust beam. In order to prevent the ions from returning to the ship by electromagnetic attraction to the electrons, the electrons are grounded to the spacecraft's potential by a generator and

discharged inside a hot filament. The I_{sp} of an ion rocket beam is as follows:

$$I_{sp} = \frac{1}{g} \sqrt{2V_a \frac{q}{m}} \quad (2.194)$$

where q is the electric charge, m is the particle mass, and V_a is the potential difference between electrodes. The beam power is then defined as:

$$\frac{P_b}{T} = \frac{gI_{sp}}{2} \quad (2.195)$$

where P_b is the beam power and T is the thrust. Propellant atoms are ionized by electron bombardment to produce the most successful electrostatic thrusters. In this process, electrons are emitted from a cathode surface and gain energy from the potential difference between the cathode and anode. The most thruster efficient propellant is mercury, but due to its toxic nature, xenon and argon are more commonly used. Energy loss comes from many factors. The gas density is so low that most radiation emitted by the ions is not absorbed before it reaches the chamber wall. Other losses occur when ions collide with the wall and recombine with electrons. These atoms then require re-ionization. The most common and mature electrostatic propulsion systems are Hall effect thrusters (HETs) and ion thrusters (ITs). Figure 2.17 shows a possible look of a nuclear electric ion propulsion vehicle. These

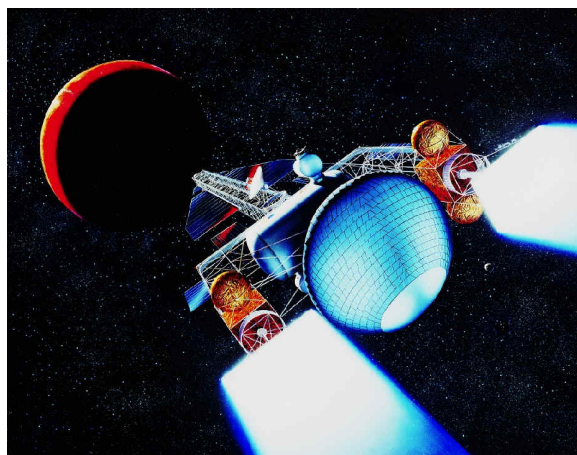


Figure 2.17: Nuclear Electric Propulsion Vehicle Concept.¹³

concepts have the highest I_{sp} of EP rockets, but each pose their own design challenges. Ion thrusters are constrained to I_{sp} s of 2500+ seconds due to the ion optics systems of which they are composed. Hall effect thrusters, on the other hand, have a greater thrust to power ratio but have lifetime issues at I_{sp} s above 2500 seconds.

Electromagnetic Propulsion

Electromagnetic propulsion accelerates a plasma with an induced current through the use of magnetic fields. The term *plasma* refers to an electrically neutral mixture of ions, electrons,

and neutral particles flowing at a high temperature in a fluid stream. The plasma acceleration is achieved by placing a thin wire across two long parallel electrodes and discharging a high voltage. This vaporizes and ionizes the wire material and the high current within the loop or an electric coil produces a magnetic field to interact with the current creating a body force:

$$\mathbf{F}_b = \mathbf{j} \times \mathbf{B} \quad (2.196)$$

where \mathbf{F}_b is the body force, \mathbf{j} is the current, and \mathbf{B} is the magnetic field strength. This body force then accelerates the plasma through the electrodes into an exhaust. Problems with the designs for electromagnetic rockets occur with losses and material erosion due to arc impingements. Pulsed plasma thrusters (PPTs) have a small impulse bit capability, use solid propellant, and have an ability to operate near a constant performance level over large power ranges. Pulsed plasma thrusters are anticipated to be used in attitude control system processes and moderate Δv applications for smaller spacecrafts.

2.3.5 Thermal Propulsion

Thermal propulsion involves the heating of a gas, typically hydrogen, increasing its temperature and pressure. The gas is then released, generating thrust. The distinctions between the different forms of thermal propulsion are driven by the source of the energy used to heat the gas, with the two types of thermal propulsion being nuclear and solar.

Nuclear Thermal Propulsion

Nuclear thermal rockets operate by transferring heat from a reactor core to a fluid propellant. Performance increases with higher operating temperatures and working with the lowest molecular weight propellants. Reactor core configurations are split into three categories: solid-core, liquid-core, and gas-core reactors. Solid-core designs are currently the only versions in operation and transmit heat to the propellant as it flows past the outside of the core. In both liquid-core and gas-core reactor, the core material is rotated, producing a toroid which entraps the fuel to produce the fission reaction. The fluid propellant then flows through the core and receives heat. Liquid- and gas-core reactors allow for higher temperature operation, and therefore a higher I_{sp} , but are more complex in their design. Figure 2.18 shows an artist's rendition of an nuclear thermal propulsion (NTP) vehicle concept.

Although NTP systems provide a higher I_{sp} , they can only be used for upper stages due to their low thrust to weight ratio. Nuclear thermal propulsion can provide spacecraft with a longer burn time than chemical propulsion, enabling outer-planetary research.

Solar Thermal Propulsion

Solar thermal propulsion (STP) uses solar radiation to heat the fuel before it is released. Deployed mirrors are used to reflect solar radiation onto a block made of a material with a high melting temperature, such as graphite. The fuel, usually hydrogen gas, is then passed



Figure 2.18: Nuclear Thermal Propulsion Vehicle Concept.¹³

through this block, absorbing the heat before being released. Therefore, the I_{sp} of the system is proportional to the temperature of the block:

$$I_{sp} = I_{sp,max} \sqrt{\frac{T}{T_{max}}} \quad (2.197)$$

where T is the temperature of the block and T_{max} is the maximum temperature of the block at which the maximum specific impulse, $I_{sp,max}$, was calculated. The maximum specific impulse can be calculated using the following relation:

$$I_{sp,max} = K \sqrt{\frac{T_{max}}{M_w}} \quad (2.198)$$

where K is a constant based on the ratio of specific heats and M_w is the molecular weight of the propellant. This relationship shows that I_{sp} increases as M_w decreases, making hydrogen the ideal fuel.

Unless extremely large mirrors are used, it is difficult to keep the block's temperature high enough to maintain a steady thrust because the energy absorbed by the block will be less than the energy being transmitted to the fuel. This imbalance results in a loss of temperature and can be further compounded in planetary orbits by eclipses. As a result, the engine is typically operated by starting to thrust once a certain temperature has been



Figure 2.19: Solar Orbit Transfer Vehicle.¹⁰

reached, and stopping once the temperature of the block has dropped below the acceptable temperature. The length of the burn is given by:

$$t_b = \frac{C_{p,b}(T_{max} - T_{min})m_{block}}{\dot{m}T_{max}C_{p,p}} \quad (2.199)$$

where t_b is the burn time, $C_{p,b}$ is the specific heat of the block's material, $C_{p,p}$ is the specific heat of the propellant, T_{max} is the maximum temperature, T_{min} is the stop temperature, m_{block} is the mass of the block, and \dot{m} is the mass flow rate of the propellant.²

2.3.6 Propellant-less Propulsion

The two principal propellant-less propulsion types are tethers and solar sails, which interact with the spacecraft environment to exert forces, and thus impart Δv 's, on the spacecraft. Tethers interact with the magnetic field, whereas solar sails interact with the solar wind and solar radiation pressure (SRP) to generate forces on the spacecraft.

Solar Sails

Solar sails are a type of propellant-less propulsion that interact with the solar wind and SRP to generate thrust for the spacecraft. There are two different types of solar sails: physical and magnetic. Physical solar sails use a thin sheet of material to reflect solar radiation, with the resulting momentum transfer creating a Δv . The thinnest sail materials are on the order 0.9 to 2 microns thick. Magnetic solar sails, on the other hand, use a thin, super-conducting filament to generate a magnetic field that redirects the solar wind to generate a Δv .

The primary advantage of solar sails is the lack of propellant required, allowing the spacecraft to perform its mission as long as its components continue to function. This advantage makes solar sails ideal for a number of missions: high-energy transfers, artificial orbits, and multiple object surveys. Missions requiring high-energy transfers, such as interplanetary or sample return missions, make use of the solar sail to reduce the total wet mass at the expense

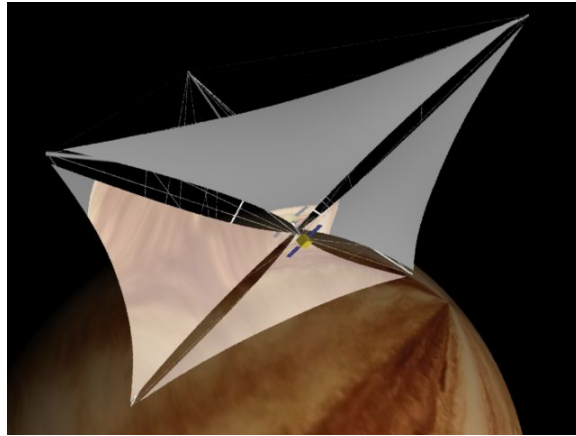


Figure 2.20: Physical Solar Sail.³



Figure 2.21: Magnetic Solar Sail.¹⁸

of increased transfer time. Solar sails can also be used to place satellites in exotic Keplerian orbits, such as creating artificial Lagrange Points or synchronous orbits by countering the gravitational force with the thrust generated by the pressure. Solar sails operate most efficiently in regions near the Sun, where the solar radiation pressure and solar wind are greater.

Unlike the various types of rocket propulsion, I_{sp} is a poor measure of performance for solar sails, since no propellant is required. Instead, the principal figure of merit for used solar sails is the sail lightness factor, β , given by:

$$\beta = \frac{\sigma_{crit}}{\sigma_{sc}} \quad (2.200)$$

where σ_{crit} is the critical solar sail loading factor and σ_{sc} is the solar sail loading factor. The critical solar sail loading factor is the ratio of spacecraft mass to solar sail area at one astronomical unit (AU) such that the solar radiation pressure on the sail is equal to solar acceleration due to gravity, and is equal to 1.53 g/m^2 . The spacecraft sail loading factor is given by:

$$\sigma_{sc} = \frac{m_{sc}}{A_{sail}} \quad (2.201)$$

where m_{sc} is the mass of the spacecraft and A_{sc} is the solar sail area. To optimize the system, the Propulsion Subdivision needs to cooperate with the Structures Subdivision to maximize the sail lightness factor and minimize the sail loading factor by minimizing the spacecraft mass and maximizing the sail area.

2.3.7 Conclusion

The propulsion section provides a detailed outline on the fundamentals of various propulsion systems. Table B.1 provides a list of thrusters available from various companies, which can be used in the selection of a propulsion system.

2.4 Analysis Tools

Commercially available analysis tools, such as Satellite Toolkit (STK), WinOrbit, and Spacecraft Control Toolbox, greatly enhance the modelling of spacecraft and their subsystems. These analysis tools have several advantages over tools developed in-house: require no development time, have user-friendly graphical user interfaces, and need no debugging. In addition, they often perform several different types of analyses, maximizing the amount of analyses performed for the quantity of data inputted. Their primary disadvantage is that the user often lacks the ability to modify the code to perform case specific analyses for unique missions, since the programs' source codes are not usually provided.

2.4.1 Satellite Tool Kit

Satellite Tool Kit is the leading commercial spacecraft analysis and visualization tool. The program is structured around a base module whose core capabilities include generation of position and attitude data, analysis of spacecraft fields-of-view, acquisition time, and sensor coverage. From the perspective of the D&C Functional Division, the base module is useful in that it allows orbits to be modelled examining a number of critical factors that affect a number of the spacecraft subsystems. These factors include sensor coverage areas, frequency and length of ground station acquisition periods, and duration and frequency of eclipses. In addition, the module allows the attitude configuration and the orbit path to be visually examined, providing the systems engineer with an additional perspective through which a better grasp of the situation can be obtained. In addition to the core module, the program also has the capability to add other modules which enhance the capabilities of the core module. Analytical Graphics, Inc.(AGI), the manufacturers of STK, provide additional modules to increase the capabilities of the base module. Some of the modules that are useful, from the perspective of the D&C Functional Division include Astrogator, Attitude, and Coverage.

2.4.2 WinOrbit

WinOrbit is a free software package that is used to model satellite positions in real-time, simulation, or manual modes. The results are presented in graphical and tabular forms, with the program having the capability of providing current tracking information to client programs. WinOrbit is particularly useful to the Astrodynamics Subdivision as a tool through which a visual representation of the orbit can be obtained. Furthermore, the tool can be used to examine the location of current satellites that might be important to the mission design.

2.4.3 Spacecraft Control Toolbox

Spacecraft Control Toolbox is a software package designed to work with MATLAB and is used to simulate and analyze spacecraft control systems. The program models the spacecraft using a CAD model and a software block diagram, with the ability to simulate the system. During these simulations, commands can be issued to the spacecraft, as in real mission operations.

2.5 Interactions with Other Functional Divisions

Communication between functional divisions is crucial in the spacecraft design process. Each functional division impacts the others, and therefore the final design depends on the interactions between the functional divisions. By mapping these interactions the communication

processes can be streamlined. This section outlines the interactions between the D&C subdivisions and the three functional divisions.

2.5.1 Astrodynamics and S&LV

The interactions between the Astrodynamics Subdivision and the S&LV Functional Division encompass two main considerations: the mass and the cross-sectional area. The mass is the main constraint when selecting a launch vehicle, since the launch vehicle must be capable of supporting the mass of the spacecraft. The task of the launch vehicle is to get the spacecraft to its initial parking orbit. Once in its initial parking orbit, the spacecraft's cross-sectional area to mass ratio then becomes the critical constraint. In most cases, the initial parking orbit is in LEO, where the main perturbation affected by structure is drag. Therefore, Eq. 2.82 indicates that the A/m ratio determines the impact of drag on the spacecraft. This perturbation contributes to the need for orbit maintenance and affects the satellite lifetime. If the mission requires an orbit above LEO, the main perturbation affected by structure is due to solar radiation pressure. Equation 2.81 depicts how the A/m ratio governs the effect of acceleration due to the pressure. When considering the cross-section and mass of spacecraft, a middle ground must be reached that keeps costs down and allows the craft to operate at maximum efficiency.

2.5.2 Astrodynamics and PT&E

The Astrodynamics Subdivision interacts with the PT&E Functional Division generally in two ways. The power requirements of the Guidance and Navigation Subsystem must be communicated to the Power Subdivision, and the type of orbit for the mission must be established. Orbit type determines the power source needed to meet the power required. If a mission requires an orbit close to the Sun, then all the power needed can be drawn from the Sun and nuclear power is not necessary. However, when considering an interplanetary mission, the available power source is no longer the sun and nuclear power is a possible alternative to power the navigation and guidance subsystem.

2.5.3 Astrodynamics and CC&DH

Many of the CC&DH mission requirements are derived from the requirements provided by the Astrodynamics Subdivision. The type of orbit a spacecraft is in determines the visibility of the spacecraft from the ground stations, as discussed in Section 2.1.3. A positive elevation angle, as defined in Eq. 2.47, corresponds to a spacecraft which is above the horizon and therefore visible. Conversely, a negative elevation angle corresponds to a spacecraft which is not visible because it is below the horizon. A spacecraft can only communicate with a ground station when the spacecraft is visible from that ground station. Another consideration is the amount of time which the spacecraft is visible from the ground station. The speed of the ground track, given in Eq. 2.39, is the main contributor to the amount of time where

communication between the spacecraft and the ground station is possible. A fast moving ground track will spend shorter amounts of time over the ground station during a single pass, but it will also make more passes.

2.5.4 ADCS and S&LV

The ADCS Subdivision directly interacts with the S&LV Functional Division. The structure of the spacecraft affects the location of the center of mass for the spacecraft, which is integral to the stability of the spacecraft. Similarly, the structure determines the different inertias of the spacecraft, which are factors in attitude determination and control. Further, the structure must be able to withstand the torques placed on the spacecraft by the control system. The torque requirements are different depending on the type of control system used. For example, an active control system using thrusters generally places larger torques on the spacecraft compared to a gravity gradient stabilization system. A final interaction between the ADCS Subdivision and the S&LV Functional Division lies in the location of components such as thrusters and sensors.

2.5.5 ADCS and PT&E

The ADCS Subdivision and the PT&E Functional Division place certain requirements on one another. The power budget of the spacecraft must take into account the requirements of the ADCS sensors and actuators. For spacecraft using solar panels, there are additional pointing requirements placed on the ADCS, because solar panels must be kept aligned with the Sun for optimal performance.

2.5.6 ADCS and CC&DH

The CC&DH Functional Division places pointing requirements on the ADCS Subdivision. If the spacecraft antenna is not pointed within a given accuracy, communication to and from the spacecraft is not possible. The requirements placed on the communication system are affected by whether the ADCS system is an autonomous on-board system or an off-board system. Further, the quality of the data control algorithm places additional requirements on the communications system. The combined CC&DH and ADCS pointing requirements are necessary to determine the safe mode of operation for the control system.

2.5.7 Propulsion and S&LV

The Propulsion Subdivision interacts with the S&LV Functional Division on a number of levels. First, the size and type of propulsion system used impacts the spacecraft's structural ability to accommodate the desired propulsion system. The propulsion method, along with mission objectives, determines the amount and type of fuel used, which dictates fuel tank size. However, these tank sizes may be too large for the spacecraft structure to accommodate, and

the Structures Subdivision will require further fuel considerations. This process continues until the requirements of both subdivisions are met. Propulsion systems that have deployable elements impact the spacecraft structure as well. For example, if solar sails are used, the Structures Subdivision requires the sizing of the sails in order to design deployment and storage mechanisms. Finally, the forces created by the propulsion system also impact the spacecraft structure. If the propulsion system causes stresses that will lead to structural failure, the propulsion system or the structure must be altered to eliminate such stresses.

2.5.8 Propulsion and PT&E

The most important interaction between the Propulsion Subdivision and PT&E Functional Division concerns power requirements. If not enough power can be supplied to the propulsion system, a system that consumes less power needs to be used, or more power must become available. The Thermal Subdivision must also know what temperatures are going to be present in the propulsion system. For example, a great deal of heat is generated in a rocket's combustion chamber and heat shielding should be implemented to protect other areas of the spacecraft. Determining the type and location of such shielding is the responsibility of the Thermal Subdivision. In addition, fuels used in propulsion systems are generally stored and maintained at low temperatures, and the Thermal Subdivision must design a system to meet these temperature requirements. The Environmental Subdivision determines the effects of the propulsion system exhaust gases on the spacecraft. If the exhaust gases are corrosive, the spacecraft may be damaged, in which case either an alternative propellant or a form of shielding should be considered. The environment the spacecraft is operating in may also have an impact on the performance of the propulsion system. For instance, magnetic fields and gas clouds could possibly reduce the efficiency of the propulsion system.

2.5.9 Propulsion and CC&DH

For any propulsion system, communication with the ground station is vital in determining whether or not the system is operating properly. Diagnostic checks must be completed on a regular basis, with sufficient time during communication windows to perform these checks. If a vehicle is unmanned, communication is essential in monitoring the effectiveness and efficiency of the propulsion system.

2.6 Interactions Among D&C Subdivisions

While mapping interactions outside of a functional division is important, mapping internal interactions is equally important. The following section contains the interactions occurring among the subdivisions within the D&C Functional Division.

2.6.1 Astrodynamics and ADCS

The Astrodynamics and ADCS Subdivisions are closely related. The orbit type determines the perturbations that the control system is required to counter. In LEO the main considerations are atmospheric drag and J_2 perturbations. For GEO and other high altitude orbits, the effects of atmospheric drag and J_2 perturbation are negligible. At these altitudes solar radiation pressure and third body interactions are the dominant effects. The effect of third body perturbation is dependent on the third body being considered. For example, in GEO, possible third bodies would be the Moon or the Sun. The spacecraft attitude is affected by these perturbations and corrections must be made.

The inclination of the orbit also places restrictions on the types of sensors that can be used by the control system. For example, there would be restrictions on the inclination of an Earth orbiting spacecraft using a magnetometer for attitude determination. Attitude determination is critical when changing orbits. In order to meet the highest efficiencies during a Δv burn, the spacecraft must be pointed accurately. If the burn is performed slightly off course, fuel is wasted and a second correctional burn will have to be made. The orbit of the spacecraft affects which sensor types can be used. For instance, the use of a magnetometer sensor requires the presence of a known magnetic field. A second attitude determination system would be needed if this requirement cannot be met.

2.6.2 Astrodynamics and Propulsion

The Astrodynamics Subdivision is responsible for providing the Propulsion Subdivision with a Δv budget. There are two main contributors to the Δv budget: orbit maintenance and orbit transfer. Orbit maintenance encompasses the correction of perturbation effects and end of life Δv burns. One type of orbit maintenance required in GEO is caused by third body interactions.

The summation of all the Δv 's calculated for various orbit maneuvers provide a large part of the Δv budget for the Propulsion Subdivision. From this Δv budget and the use of Eq. 2.175, the required propellant mass can be determined. If the determined propellant mass does not meet mission constraints, the Astrodynamics Subdivision must modify the techniques used for orbit maintenance and orbit transfers.

Another possibility for interactions between Astrodynamics and Propulsion Subdivisions is the use of low, constant thrust burns in order to change orbits. The Propulsion Subdivision would need to place an adequate propulsion system on the spacecraft, such as a solar sail. These low thrust orbit transfers can be more energy efficient, and desirable, than higher thrust alternatives.

2.6.3 ADCS and Propulsion

The ADCS Subdivision is directly coupled with the Propulsion Subdivision. The torques exerted on the spacecraft due to external forces are provided to propulsion by ADCS. From these torques, the Propulsion Subdivision can determine thruster placement and size so that

spacecraft attitude can be maintained. With the thruster placement determined, Eq. 2.178 can be used to determine thruster size. Further, a separate Δv budget must be established accounting for all the attitude corrections expected for the mission lifetime. Using Eq. 2.175 and the ADCS Δv budget, the required propellant mass can be determined. If the determined propellant mass does not meet mission constraints, the ADCS Subdivision must incorporate usage of other types of control mechanisms that do not require propellant. Control moment gyros and momentum wheels are examples of control mechanisms that do not require any propellant.

2.7 Conclusion

Chapter 2 gives an in-depth analysis of the modelling of the ADCS, the propulsion subsystem, and the trajectory of a spacecraft. The interactions between each subdivision and the other functional divisions is established and discussed. The next chapter of the report includes example applications of the models and equations found in Chapter 2.

Chapter 3

Examples

Modelling and analysis is a necessary part of spacecraft design. Chapter 3 applies the models presented in Chapter 2 to specific applications and shows the necessary calculations and considerations required by each subdivision. A discussion of interplanetary transfers, determination and control, and propulsion trade studies is provided.

3.1 Orbit Examples

This section presents illustrations of Hohmann transfers, plane changes, and hyperbolic trajectories. An interplanetary spacecraft travelling from Earth to Mars utilizes each of these cases. Two possible options upon reaching Mars are a hyperbolic fly-by or an orbital insertion. Examples of Hohmann and Type I direct transfers to Mars from Earth are presented in the following sections.

3.1.1 Hohmann Transfer from Earth to Mars

A spacecraft is orbiting Earth in a circular orbit with a radius of 6700 km. The patched conics method of orbit analysis, discussed in Section 2.1.4, is used to determine the Hohmann transfer of the spacecraft from Earth to Mars. A number of constants are needed to determine the transfer including: the gravitational coefficients for the Sun, Earth, and Mars, as found in Appendix A; the average orbit radii for both Earth and Mars; and the average equatorial radius of Mars. The radii constants are as follows:

Earth orbit radius	r_{\oplus}	149.6	$\times 10^6$	km
Mars orbit radius	r_m	227.94	$\times 10^6$	km
Mars equatorial radius	R_m	3.4	$\times 10^3$	km

The patched conic analysis has three main components: a departure from Earth's sphere of influence, a Hohmann transfer from Earth to Mars, and an entrance into Mars' sphere of

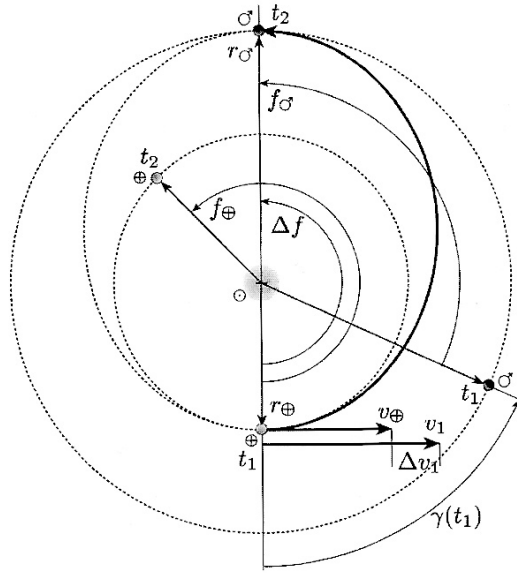


Figure 3.1: Hohmann transfer from Earth to Mars¹⁵

influence. The following subscripts are used to differentiate between the various velocities associated with the Hohmann transfer: c for the orbital velocity around Earth; 0 for immediately after the initial burn; 1 for exiting Earth's sphere of influence; 2 for arriving Mars' sphere of influence; 3 for the insertion orbit around Mars; and 4 for exiting Mars' sphere of influence. The heliocentric velocity (v_1) necessary to perform the Hohmann transfer is obtained using Eq. 2.8, which is re-written as:

$$\frac{v_1^2}{2} - \frac{\mu}{r_\oplus} = \frac{-\mu}{\frac{2(r_\oplus + r_m)}{2}} \quad (3.1)$$

and solving for v_1 yields:

$$v_1 = \sqrt{2\mu_\oplus \left(\frac{1}{r_\oplus - \left(\frac{1}{r_\oplus} + \frac{1}{r_m} \right)} \right)} = 33.02 \text{ km/s} \quad (3.2)$$

The heliocentric velocity of Earth (v_\oplus) is calculated using Eq. 2.25 with $r = r_\oplus$ and $\mu = \mu_\odot$. The Earth relative velocity (ν_1) is the difference between the heliocentric velocities of the spacecraft and Earth:

$$\nu_1 = v_1 - v_\oplus = 3.05 \text{ km/s} \quad (3.3)$$

The Earth relative velocity (ν_0) necessary to exit Earth's sphere of influence with heliocentric velocity (v_1) is found by:

$$\nu_0 = \sqrt{2\nu_c^2 + \nu_1^2} = 11.30 \text{ km/s} \quad (3.4)$$

where ν_c is the Earth relative velocity of the spacecraft calculated using Eq. 2.25 with $r = 6700$ km and $\mu = \mu_{\oplus}$. The Δv necessary to enter the hyperbolic departure orbit ($\Delta\nu_0$) has magnitude given by:

$$\Delta\nu_0 = \nu_0 - \nu_c = 3.61 \text{ km/s} \quad (3.5)$$

Once the $\Delta\nu_0$ is applied, the spacecraft exits Earth's sphere of influence in a hyperbolic orbit path and enters into a Hohmann heliocentric trajectory. The specifics of a Hohmann transfer are discussed in Section 2.1.4. The next component of the Hohmann transfer involves the insertion of the spacecraft into Mars' sphere of influence. Upon arrival at Mars, the spacecraft has a slower heliocentric velocity than Mars. This difference in velocity means the spacecraft must enter the sphere of influence in front of Mars, and allow the planet to catch up to the spacecraft. The spacecraft must not be aimed directly at Mars in order to prevent the gravitational attraction of Mars from pulling the spacecraft directly into the planet. Insertion into a circular orbit around Mars and performing a planetary fly-by are two maneuvers developed below.

Orbit Insertion

The hyperbolic orbit is circularized at periapsis with a radius equal to 1.25 times the equatorial radius of Mars. The periapsis radius is dependent on the miss distance (d_m) measured along Mars' orbit path, as well as the heliocentric velocity (v_2) with which the spacecraft enters Mars' sphere of influence. The heliocentric velocity of the spacecraft is found by rearranging Eq. 2.8:

$$v_2 = \sqrt{v_1^2 + \left(2\mu_{\odot} \left(\frac{1}{r_m} - \frac{1}{r_{\oplus}}\right)\right)} = 21.39 \text{ km/s} \quad (3.6)$$

An error of 4% is added to account for an imperfect burn:

$$v_2 = 1.04v_2 = 22.24 \text{ km/s} \quad (3.7)$$

The angle between the heliocentric arrival velocity and Mars' heliocentric velocity (v_m) is defined as:

$$\sigma_2 = \arccos\left(\frac{h}{r_m v_2}\right) = 15.94^\circ \quad (3.8)$$

where h is the heliocentric angular momentum of the spacecraft calculated using Eq. 2.9. The heliocentric angular momentum is calculated when the spacecraft exits the Earth's sphere of influence. The angle between the heliocentric position and velocity vectors is 90° at this point, so the angular momentum expression is simplified to:

$$h = r_{\oplus} v_1 = 4.87 \times 10^9 \text{ m}^2/\text{s} \quad (3.9)$$

The Mars relative velocity (ν_2) is found using the law of cosines:

$$\nu_2 = \sqrt{v_2^2 + v_m^2 - 2v_2 v_m \cos \sigma_2} = 6.69 \text{ km/s} \quad (3.10)$$

The angle between the heliocentric and Mars relative velocity vectors (ϕ_2) is:

$$\phi_2 = \arcsin\left(\frac{v_m}{\nu_2} \sin \sigma_2\right) = 98.17^\circ \quad (3.11)$$

The eccentricity of the hyperbolic entry orbit is found using the radius of periapsis (r_p) as:

$$e = 1 + \frac{r_p \nu_2^2}{\mu_m} = 5.45 \quad (3.12)$$

The eccentricity is greater than 1 because the orbit is hyperbolic. The eccentricity is used to find the closest approach of the hyperbolic asymptote to Mars (d_a):

$$d_a = \sqrt{(e^2 - 1) \frac{\mu_m^2}{\nu_2^4}} = 5.12 \times 10^3 \text{ km} \quad (3.13)$$

The miss distance needed is then calculated as:

$$d_m = \frac{d_a}{\sin(\phi_2 + \sigma_2)} = 5.61 \times 10^3 \text{ km} \quad (3.14)$$

This value of d_m ensures that the radius of periapsis for the hyperbolic entry orbit is twice the equatorial radius of Mars. To circularize the orbit around Mars at the radius of periapsis, the Mars relative velocity of the spacecraft is calculated as:

$$\nu_3 = \sqrt{2 \frac{\mu_m}{r_p} + \nu_2^2} = 8.06 \text{ km/s} \quad (3.15)$$

Using Eq. 2.25 to calculate the circular velocity of an orbit with radius equal to the periapsis radius (ν_{cm}) the burn necessary to circularize the orbit is calculated as:

$$\Delta \nu_3 = \nu_{cm} - \nu_3 = -4.89 \text{ km/s} \quad (3.16)$$

The inclination difference between the transfer orbit and Mars orbit must also be accounted for. A separate burn is performed to change the inclination of the orbit plane. Such a burn has components in only two directions and keeps the energy of the orbit constant. The components are as follows:

$$\Delta v_y = -v_y(1 - \cos \Delta i) \quad (3.17)$$

$$\Delta v_z = v_y \sin \Delta i \quad (3.18)$$

The magnitude of the complete burn, Δv_i is determined by:

$$\Delta v_i^2 = \Delta v_y^2 + \Delta v_z^2 \quad (3.19)$$

Substituting the expressions for Δv_y and Δv_z yields:

$$\Delta v_i^2 = v_y^2[(1 - \cos \Delta i)^2 + \sin^2 \Delta i] \quad (3.20)$$

The calculation is simplified using trigonometric identities to:

$$\Delta v_i = v_y \sqrt{2(1 - \cos \Delta i)} \quad (3.21)$$

Equation 3.21 indicates that the burn should be made when the spacecraft is moving at its slowest velocity in order to minimize the magnitude of the burn required. Assuming a difference of 1.85° between the orbit planes of Earth and Mars, the magnitude of the plane change burn is:

$$\Delta v_i = v_2 \sqrt{2(1 - \cos \Delta i)} = 0.72 \text{ km/s} \quad (3.22)$$

The total Δv budget for the transfer is determined by summing the requirements for each burn:

$$\Delta v = |\Delta \nu_0| + |\Delta \nu_3| + |\Delta v_i| = 9.21 \text{ km/s} \quad (3.23)$$

Planetary Fly-by

A spacecraft can also perform a fly-by upon arrival at Mars. Planetary fly-bys are used to increase or decrease the heliocentric velocity of a spacecraft. The spacecraft enters and exits Mars' sphere of influence with the same relative velocity magnitude:

$$\nu_4 = \nu_2 = 6.69 \text{ km/s} \quad (3.24)$$

The angle between the Mars relative velocity vector and the Mars orbit path (θ_i) is expressed as $\theta_i = \phi_i + \sigma_i$. Examining the geometry yields:

$$\theta_4 = 180^\circ + 2\Phi - \theta_2 = 224.73^\circ \quad (3.25)$$

where Φ is half of the turn angle and determined by:

$$\Phi = \arccos \frac{1}{e} = 79.42^\circ \quad (3.26)$$

The magnitude of the heliocentric velocity as the spacecraft exits the sphere of influence is then determined using the law of cosines:

$$v_4 = \sqrt{\nu_4^2 + v_m^2 + 2\nu_4 v_m \cos \theta_4} = 19.93 \text{ km/s} \quad (3.27)$$

The angle between the heliocentric and Mars relative velocity vectors is determined from the geometry as:

$$\phi_4 = \arcsin \left(\sin \theta_4 \frac{v_m}{v_4} \right) = -58.40^\circ \quad (3.28)$$

The angle between the heliocentric exit velocity and Mars' orbital path is determined by:

$$\sigma_4 = \theta_4 - \phi_4 = 283.13^\circ \quad (3.29)$$

The magnitude of the heliocentric velocity when the spacecraft exits the sphere of influence (v_4) is less than the heliocentric velocity when the spacecraft entered the sphere of influence (v_2). The fly-by decreases the heliocentric velocity of the spacecraft by transferring heliocentric angular momentum from the spacecraft to Mars.

3.1.2 Type I Direct Earth-Mars Transfer

While the Hohmann transfer uses the smallest Δv budget, sometimes the spacecraft is required to reach the planet quickly despite additional propellant cost. An example of such an orbit, seen in Figure 3.2, uses an initial Δv twice the Δv required for the Hohmann transfer. For this trade study, we assume the same initial conditions as in the Hohmann example to arrive at Mars from Earth.

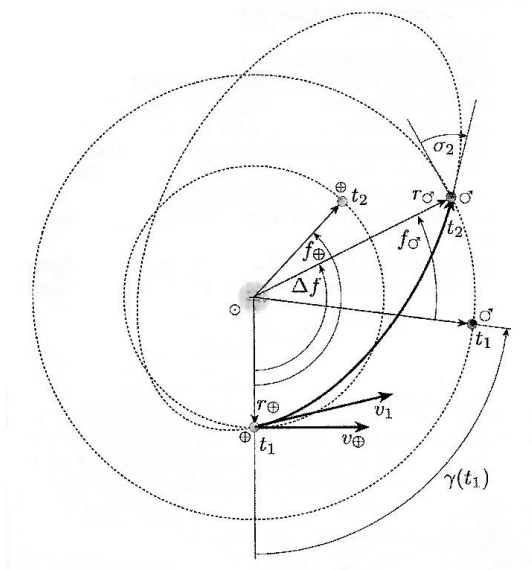


Figure 3.2: Nonminimum energy transfer orbit from Earth to Mars¹⁵

From the Hohmann example:

$$\Delta\nu_{0\text{Hohmann}} = 3.61 \text{ km/s}$$

For this example, the initial burn is twice the Hohmann burn:

$$\Delta\nu_0 = 2\Delta\nu_{0\text{Hohmann}} = 7.21 \text{ km/s} \quad (3.30)$$

This $\Delta\nu_0$ and the current radius r_p determine the hyperbolic exit orbit. Rearranging Eq. 3.4 for ν_1 yields:

$$\nu_1 = \sqrt{\nu_0^2 - \frac{2\mu_{\oplus}}{r_p}} = 10.19 \text{ km/s} \quad (3.31)$$

Once the satellite leaves Earth's sphere of influence, it has a velocity relative to the sun of:

$$v_1 = \nu_1 + v_{\oplus} = 40.16 \text{ km/s} \quad (3.32)$$

Since the satellite is at periapsis, the velocity at this point in the transfer orbit relative to the sun is purely tangential, and the semi-major axis of the orbit is determined through the

energy equation as:

$$a = \frac{1}{\frac{2}{r_{\oplus}} - \frac{v_1^2}{\mu_{\odot}}} = 7.22 \times 10^8 \text{ km} \quad (3.33)$$

Due to conservation of energy, the velocity at the point where the satellite reaches the Mars orbit radius is determined as:

$$v_2 = \sqrt{\mu_{\odot} \left(\frac{2}{r_m} - \frac{1}{a} \right)} = 31.31 \text{ km/s} \quad (3.34)$$

From this point, the analysis to determine the total Δv budget is exactly like that performed for the Hohmann transfer. The angle between the heliocentric arrival velocity, v_2 , and Mars' heliocentric velocity, v_m , is determined using Eq. 3.8:

$$\sigma_2 = \arccos \left(\frac{h}{r_m v_2} \right) = 46.91^\circ \quad (3.35)$$

where h is calculated with Eq. 3.9:

$$h = r_{\oplus} v_1 = 4.87 \times 10^9 \text{ m}^2/\text{s} \quad (3.36)$$

The Mars relative velocity, ν_2 , is found using the law of cosines shown in Eq. 3.10:

$$\nu_2 = \sqrt{v_2^2 + v_m^2 - 2v_2 v_m \cos \sigma_2} = 23.02 \text{ km/s} \quad (3.37)$$

The angle between the heliocentric and Mars relative velocity vectors, ϕ_2 , is found through Eq. 3.11:

$$\phi_2 = \arcsin \left(\frac{v_m}{\nu_2} \sin \sigma_2 \right) = 130.09^\circ \quad (3.38)$$

Using the periapses radius and Eq. 3.12, the eccentricity of the hyperbolic orbit is determined as:

$$e = 1 + \frac{r_p \nu_2^2}{\mu_m} = 53.61 \quad (3.39)$$

The closest approach of the hyperbolic asymptote to Mars is found using the eccentricity and Eq. 3.13:

$$d_a = \sqrt{(e^2 - 1) \frac{\mu_m^2}{\nu_2^4}} = 4.33 \times 10^3 \text{ km} \quad (3.40)$$

Continuing to follow the previous Hohmann example, the miss distance needed is then calculated using Eq 3.14:

$$d_m = \frac{d_a}{\sin(\phi_2 + \sigma_2)} = 8.26 \times 10^4 \text{ km} \quad (3.41)$$

The velocity of the spacecraft relative to Mars at periapses is found using Eq. 3.15:

$$\nu_3 = \sqrt{2 \frac{\mu_m}{r_p} + \nu_2^2} = 23.46 \text{ km/s} \quad (3.42)$$

Using Eq. 2.25 to calculate the circular velocity and then using Eq. 3.16, $\Delta\nu_3$ is calculated as:

$$\Delta\nu_3 = \nu_{cm} - \nu_3 = -20.28 \text{ km/s} \quad (3.43)$$

Using Eq. 3.22 and assuming a difference of 1.85° between the orbit planes of Earth and Mars, the magnitude of the plane change burn from Eq. 3.22 is:

$$\Delta v_i = v_2 \sqrt{2(1 - \cos \Delta i)} = 1.01 \text{ km/s} \quad (3.44)$$

The total Δv budget for the transfer is the sum of the absolute values of each of the individual burn requirements:

$$\Delta v = |\Delta\nu_0| + |\Delta\nu_3| + |\Delta v_i| = 28.51 \text{ km/s} \quad (3.45)$$

The Δv for the type I direct Earth-Mars transfer is approximately three times larger than the Δv for the Hohmann transfer. The type I transfer consumes more fuel due to the larger Δv requirement. The propulsion examples in Section 3.3 show an example calculation for fuel mass required for a given Δv .

3.2 ADCS Examples

An example of how ADCS subsystems are designed is presented in the Terribly Inaccurate Space System Utilization Experiment (TISSUE) spacecraft. The spacecraft is in a circular orbit at an altitude of 400 km, with an inclination of 10° . The payload monitors Earth, and therefore the spacecraft is nadir pointing with an accuracy of 0.01° . The spacecraft slew is $\pm 15^\circ$, with a slew rate of 0.25° per second. The residual dipole moment of the spacecraft is 1.0 amp m².

The TISSUE spacecraft is shown in Fig. 3.3. The spacecraft is a rectangular parallelepiped, with dimensions of 0.5 m along the x and z axes and 1.0 m along the y axis. The coordinate system utilized is such that the z axis is aligned with the nadir direction and the x axis is the forward velocity direction. The TISSUE spacecraft has a mass of 50 kg, and the moments of inertia are:

$$\begin{aligned} I_{xx} &= 5.2083 \text{ kg m}^2 \\ I_{yy} &= 2.0833 \text{ kg m}^2 \\ I_{zz} &= 5.2083 \text{ kg m}^2 \end{aligned}$$

The pointing accuracy requirements of 0.01° limit the available sensors that may be used on the spacecraft. Possible sensors that fall within the accuracy requirements are shown in Table B.6 in Appendix B. This table indicates that the DDS sun sensor manufactured by Sodern is capable of meeting the accuracy requirements at a low monetary cost, although at a high mass cost. If the spacecraft mass exceeds limits set by the S&L Functional Division, then a trade study may be necessary to determine the best combination of weight and accuracy for the spacecraft's mission.

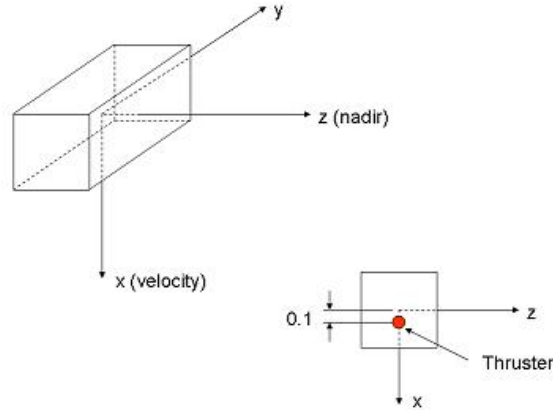


Figure 3.3: TISSUE Spacecraft

3.2.1 Torques

The external and internal torques experienced by a spacecraft influence the control systems selected for the spacecraft. Factors such as spacecraft geometry and orbit altitude influence the types of torques acting on the spacecraft. Many of these factors are interrelated with the various subdivisions within both the D&C Functional Division and the other functional divisions. However, for demonstration purposes, several assumptions are made about these interrelations in order to simplify the ADCS example problem.

First, it is assumed that only the spacecraft's zenith pointing face is exposed to SRP, and that the resulting force acts 0.05 m forward of the center of gravity. Similarly, it is assumed that the aerodynamic drag mainly affects the spacecraft's forward face and acts 0.05 m above the center of gravity. The reflectance factor is assumed to be 0.75; this number indicates that the majority of the spacecraft is a reflective material. Typical drag coefficient values range from 2 to 2.5; since the spacecraft is rectangular in shape, with no protrusions, the drag is assumed to be slightly above the lower end of the range and is taken as 2.2. Thrusters are assumed to be placed along the starboard and port faces of the spacecraft, at mid height, and slightly aft, such that the vector from the center of mass to the thruster is $(0,0.5,0.1)^B$ m. The thrust applied is assumed to be acting only along the nadir and forward axes, and is taken as $(0.2,0,0.05)^B$ N.

All of the above assumptions are crude estimations and over simplify the factors that enter into the ADCS design. For example, the cross-sectional area exposed to solar radiation

is constantly changing and cannot be accurately expressed as the area of the zenith pointing face. In addition, without knowing the actual materials used for the spacecraft, it is difficult to estimate the reflectance factor. However, these assumptions enable an initial analysis of the torques acting on the spacecraft, from which the appropriate control methods may be selected. As the design process progresses, the torque calculations will become more precise.

Equations 2.101 through 2.109 are used to determine the torques acting on the spacecraft. The four main external torques are calculated as:

$$\begin{aligned} T_{srp} &= 1.9633 \times 10^{-7} \text{ N-m} \\ T_g &= 2.0941 \times 10^{-7} \text{ N-m} \\ T_m &= 2.5563 \times 10^{-5} \text{ N-m} \\ T_a &= 4.3988 \times 10^{-6} \text{ N-m} \end{aligned}$$

These results indicate that the magnetic field has the largest impact on the spacecraft, followed by the aerodynamic drag. The internal torques are difficult to model, but also must be considered. Equation 2.109 is used to determine the thruster misalignment torque as 0.105 N-m. Other internal torques, such as fuel sloshing, are heavily dependent on other functional divisions, and are not easily modelled.

3.2.2 Algorithms

A few simple examples of the algorithms in Chapter 2 are provided below; however, the following examples are not meant to be a comprehensive review of the various algorithms available to the ADCS designer.

Measurements from several sensors are often combined to accurately determine the orientation of the spacecraft relative to a common reference point. Sensors such as star trackers make use of the q-method described in Eq. 2.129 to provide a statistically determined orientation. The q-method describes the attitude in terms of Euler parameters. Using the inverse transformation of Eq. 2.138a and the transformation in Eq. 2.137, the attitude description changes from Euler parameters to the inertial rotation matrix for easier visualization of the rotations necessary to keep the spacecraft correctly orientated. Control laws, such as the one described in Eq. 2.172, are used to determine the rotation necessary to maintain a specified attitude.

For the spacecraft in this example, the sensors are assumed to acquire three different measurements in both \mathbf{v}_b and \mathbf{v}_i :

$$\mathbf{v}_b = \begin{bmatrix} 0.837 & 0.621 & 0.243 \\ -0.834 & 0.619 & -0.104 \\ 0.839 & 0.627 & 0.187 \end{bmatrix}$$

$$\mathbf{v}_i = \begin{bmatrix} -0.152 & -0.932 & 0.093 \\ 0.825 & 0.538 & 0.315 \\ 0.882 & -0.587 & 0.217 \end{bmatrix}$$

Using the q-method, the attitude described in Euler parameters is $\beta = [0.2024 \ -0.0375 \ -0.7667 \ 0.6081]$. Using attitude transformations, the attitude is described in terms of the inertial rotation matrix:

$$[BN] = \begin{bmatrix} -0.1786 & -0.9477 & -0.2647 \\ 0.9173 & -0.2576 & 0.3036 \\ -0.3560 & -0.1886 & 0.9153 \end{bmatrix}$$

A control law is now necessary to determine the torque required to maintain the above attitude. First, the position gain is defined by Eq. 2.170, using the previously determined magnetic torque of 2.5563×10^{-5} N-m as the peak external torque. Assuming an allowable attitude error of 0.01° , K_p is 0.1465 N-m/rad. If the rate of allowable attitude error is assumed to be 0.005° per second and the rate gain is assumed to be 0.001 N-m-s/rad, then the torque required to maintain the spacecraft orientation is 2.5656×10^{-5} N-m from Eq. 2.172. This required torque influences the control method selected, as the spacecraft must provide at least 2.5656×10^{-5} N-m to control the expected external torques.

3.2.3 Control Approaches

Since the spacecraft is nadir-pointing and requires a pointing accuracy of $\pm 0.01^\circ$, the available control approaches are limited. Section 3.2.1 describes the disturbance torques on the spacecraft as it orbits Earth. Sizing of the various control components is completed using the control torque ($T_D = 2.5656 \times 10^{-5}$ N-m) and assuming that slews are done about the largest moment of inertia axis. The spacecraft must be able to slew $\pm 15^\circ$ at a rate of 0.25° per second. At an altitude of 400 km, the spacecraft has an orbital period of 92.3938 min.

If the spacecraft uses reaction wheels, the size is governed by either the magnitude of the disturbance torque or the slew requirement. Equation 2.110 can be used to determine the reaction wheel sizes based on the disturbance torque and assuming a margin factor of 2:

$$\begin{aligned} T_{RW} &= T_D(\text{Margin Factor}) \\ &= (2.5656 \times 10^{-5} \text{ N-m})(2) \\ &= 5.1312 \times 10^{-5} \text{ N-m} \end{aligned}$$

Alternatively, Eq. 2.111 can be used to size the reaction wheels based on slew requirements:

$$\begin{aligned} T_{RW} &= 4\theta \frac{I}{t^2} \\ &= \frac{4(15^\circ \times \pi/180^\circ)(5.2083 \text{ kg-m}^2)}{(60 \text{ sec})^2} \\ &= 1.5150 \times 10^{-3} \text{ N-m} \end{aligned}$$

Equation 2.112 can be used to size the reaction wheels based on its momentum storage

capabilities:

$$\begin{aligned}
 h &= (T_D) \frac{P}{4} (0.707) \\
 &= (2.5656 \times 10^{-5} \text{ N-m}) \left(\frac{92.3938 \text{ min}}{4} \right) \left(\frac{60 \text{ sec}}{1 \text{ min}} \right) (0.707) \\
 &= 2.5139 \times 10^{-2} \text{ N-m-s}
 \end{aligned}$$

Based on these results, one possible control actuator for the spacecraft is Honeywell's Miniature Reaction Wheel HR04, which has a nominal momentum storage of 0.2 to 1 N-m-s and a nominal torque capability of more than 0.028 N-m, and weighs only 1.5 kg.⁸

A momentum wheel is sized for the spacecraft using Eq. 2.113 as follows:

$$\begin{aligned}
 h &= \frac{T_D}{\theta_a} \cdot \frac{P}{4} \\
 &= \frac{2.5656 \times 10^{-5} \text{ N-m}}{0.01^\circ \times \pi/180^\circ} \cdot \frac{5543.628 \text{ sec}}{4} \\
 &= 203.7256 \text{ N-m-s}
 \end{aligned}$$

where θ_a is the allowable pointing error. A momentum wheel of this size would be so massive that other approaches would be more feasible because they require less mass. If the spacecraft is spin-stabilized, the above momentum could be achieved through the spacecraft rotating at the speed:

$$\begin{aligned}
 \omega_s &= \frac{h}{I} \\
 &= \frac{203.7256 \text{ N-m-s}}{5.2083 \text{ kg-m}^2} \\
 &= 39.1156 \text{ rad/sec} = 373.5264 \text{ rpm}
 \end{aligned}$$

This speed is prohibitive, and since the spacecraft is a nadir-pointing spacecraft, a spin-stabilized system is not possible.

Although the TISSUE Box can be controlled both in normal and slew modes by a relatively small reaction wheel, thrusters may still be required to bleed off excess momentum from the RWs once the saturation speed has been reached. With a 0.3 N-m-s size reaction wheel, and thrusters mounted at the edge of the box, the thruster force can be calculated using Eq. 2.119 as:

$$\begin{aligned}
 F &= \frac{h}{Lt} \\
 &= \frac{0.3 \text{ N-m-s}}{(0.5 \text{ m})(0.5 \text{ sec})} \\
 &= 1.2 \text{ N}
 \end{aligned}$$

assuming a burn time of 0.5 sec. As cold thrusters can provide forces up to 5 N, this is an entirely feasible design.

3.3 Propulsion Examples

The work performed by the Astrodynamics and Propulsion Subdivisions are directly inter-related. The Astrodynamics Subdivision determines the Δv and the Propulsion Subdivision uses that Δv to determine the propellant mass or solar sail area. Three examples are presented: a transfer from Earth to Mars, a transfer from LEO to GEO, and a transfer from Earth to Venus. The transfer from Earth to Mars examines the selection of an upper-stage rocket, and illustrates the sizing of the propellant tanks. The LEO to GEO transfer compares the propellant's mass ratios resulting from the use of high-thrust and low-thrust propulsion. The transfer from Earth to Venus determines the solar sail area required to make the transfer in less than three years. All three examples are preliminary analyses used in design to assist in the initial sizing of the spacecraft.

3.3.1 Selection of an Upper-Stage Rocket and Sizing of Propellant Tanks for a Mission to Mars

The National Aeronautics and Space Administration has proposed a mission to Mars, for which an upper-stage rocket must be selected to place the spacecraft on an Earth-to-Mars transfer orbit. The transfer orbit requires a total Δv of 6.5 km/s. The mass of the spacecraft, excluding the propulsion system and propellant, is 200 kg, and the propellant mass cannot be more than 85% of the initial vehicle mass. Funding for the mission is low, therefore cost is a driving factor in the design.

Rocket Selection

The first step in selecting an upper-stage rocket for the proposed mission is to determine what range of I_{sp} values can be used. Figure 3.4 shows a plot of the propellant mass ratio, m_p/m_0 , versus I_{sp} for the proposed mission. Note that this plot is created using Eq. 2.175 and the given Δv . Figure 3.4 indicates that a rocket with an I_{sp} of 350 sec or greater must be used to ensure the propellant mass ratio is less than 0.85. Because of this constraint on I_{sp} , the rockets considered are limited almost exclusively to liquid bipropellant rockets. For this example, the Pratt and Whitney RL10 and the Rocketdyne MB-60 upper-stage rockets are considered. The RL10 has an I_{sp} of approximately 448 sec and uses liquid hydrogen as the fuel and liquid oxygen as the oxidizer. It has a mass of 155 kg and provides thrust in the range of 16,500 - 22,300 lb. The MB-60 has a slightly higher I_{sp} of 467 sec and also uses liquid hydrogen and liquid oxygen as the fuel and the oxidizer. The MB-60, at 595 kg, has almost four times the mass of the RL10 but provides a higher thrust of approximately 60,000 lb.

Using Eq. 2.175, the propellant mass ratio required is 0.772 for the RL10 and 0.758 for the MB-60. The total mass of the spacecraft, excluding the rocket and the propellant is 200 kg. The mass is defined by the following equation:

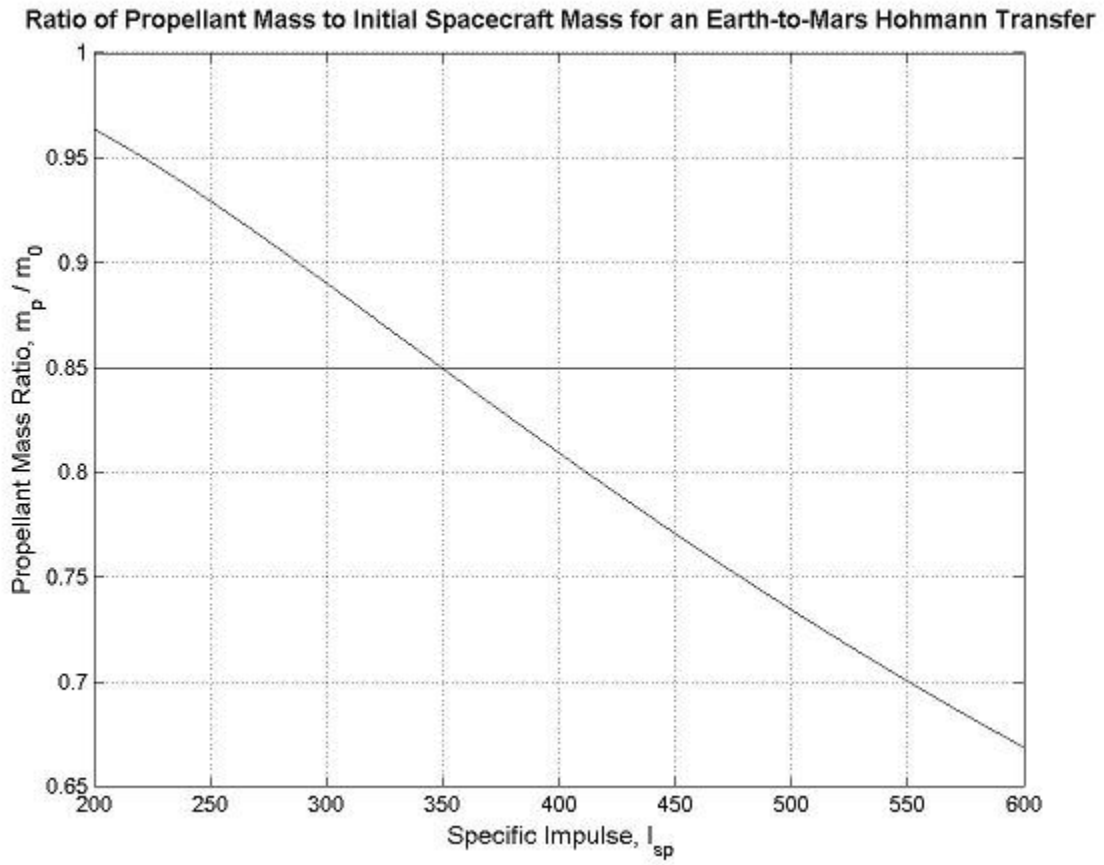


Figure 3.4: Propellant mass ratio versus specific impulse for a Mars mission with a Δv of 6.5 km/s.

$$m_0 - m_p - m_r = 200 \text{ kg} \quad (3.49)$$

where m_r is the mass of the rocket. Solving Eq. 3.49 for m_0 , we have:

$$m_0 = \frac{(200 \text{ kg}) + m_r}{1 - (m_p/m_0)} \quad (3.50)$$

and:

$$\begin{aligned} m_o &= 1560 \text{ kg for the RL10} \\ m_o &= 3285 \text{ kg for the MB-60} \end{aligned}$$

Lower mass means that the mission will cost less, so the RL10 is optimum. Using the MB-60 would allow for a heavier payload, but its high mass could drive the cost of the mission to an unacceptable level.

The propellant mass needed for the RL10 can be determined by:

$$m_p = 1.1m_0 \left(\frac{m_p}{m_0} \right) = 1325 \text{ kg} \quad (3.51)$$

where the coefficient of 1.1 accounts for any reserve fuel that may be needed and for the propellant necessarily left in the tanks at the end of the mission.

Sizing of Propellant Tanks

The RL10 is a bipropellant rocket, therefore two propellant tanks must be designed: a fuel tank and an oxidizer tank. The total mass of the propellant is:

$$m_p = m_H + m_{OX} = (1 + R)m_H \quad (3.52)$$

where m_H is the fuel mass, m_{OX} is the oxidizer mass, and R is the mixture ratio, defined as $R = m_{OX}/m_H$. Note that for the RL10, the fuel is liquid hydrogen, the oxidizer is liquid oxygen, and the mixture ratio is 5.1. Using Eq. 3.52, the mass of hydrogen required for the mission is 210 kg and the mass of oxygen required is 1115 kg. The volume of each tank is determined by:

$$V = \frac{m}{\rho} \quad (3.53)$$

where m and ρ are the mass and density, respectively, of the hydrogen or oxygen. Liquid hydrogen has a density of 76 kg/m³ and liquid oxygen has a density of 1130 kg/m³. These densities dictate that a 2.8 m³ hydrogen tank and a 0.91 m³ oxygen tank are needed for the RL10. Two options for the shape of the tank are cylindrical and spherical. The stress in a walls of a pressurized cylindrical tank is:

$$\sigma_{cyl} = \frac{pr}{t} \quad (3.54)$$

and the stress in the walls of a spherical tank is:

$$\sigma_{sph} = \frac{pr}{2t} \quad (3.55)$$

In Eqs. 3.54 and 3.55, σ_{cyl} and σ_{sph} are the allowable stresses in the tank walls, p is the pressure in the tank, r is the inner radius of the tank, and t is the tank wall thickness.¹¹ As these equations show, for equal tank pressures and inner radii, a spherical tank can have a wall thickness that is half that of a cylindrical tank. A smaller wall thickness means that less material is needed to construct the tanks, and the spacecraft is less massive. As stated before, less mass means lower cost, so spherical tanks are desirable. The volume of each spherical tank is:

$$V = \frac{4}{3}\pi r^3 \quad (3.56)$$

Rearranging Eq. 3.56, the radius of the each tank is:

$$r = \left(\frac{3V}{4\pi}\right)^{1/3} \quad (3.57)$$

Using the volumes calculated earlier, the radius of the hydrogen tank, r_H , and the radius of the oxygen tank, r_O , are:

$$\begin{aligned} r_H &= 0.87 \text{ m} \\ r_O &= 0.6 \text{ m} \end{aligned}$$

The placement of the fuel tanks affects the spacecraft's center of mass. As fuel is expended, the center of mass can move, and the tanks must be placed so that this center of mass movement is minimized. Accounting for and minimizing this movement is the job of the S&LV Functional Division, and is therefore not discussed in this example. Nevertheless, the movement of the spacecraft center of mass as fuel is expended is an important aspect of spacecraft design that cannot be ignored.

3.3.2 Low Earth Orbit to Geosynchronous Orbit Transfer

A good example of modelling a mission using electric propulsion is a simple transfer from LEO to GEO. In this subsection, the transfer considered uses a spiral orbit, which assumes constant thrust throughout the entire transfer.

Modelling

For this example, the LEO is assumed to have an elevation of 300 km and the GEO has an altitude of 35,787 km. Using Eq. 2.68, the Δv for the spiral transfer orbit is 4651 m/s. Once the change in velocity required for orbit transfer is known, the propellant mass ratios are determined for various thrusters using Eq. 2.175 and the mean I_{sp} for each thruster's range.

Using the rockets outlined in Sections 2.3.5 and 2.3.4, a table comparing the different types of thrusters is displayed below. The data within Table 3.1 indicates that a high specific impulse allows for a smaller propellant mass ratio. By having a lower propellant mass, the spacecraft can handle a larger payload mass and a larger structure.

Table 3.1: Mass Ratios for Different Thrusters.

Thruster	I_{sp} (s)	Mass Ratio
MITEE	1000	0.37766
NEXT	3155	0.13957
T-40	1300	0.30568
T-140/T-220	2000	0.21112

3.3.3 Earth to Venus Transfer

A mission is proposed to send a 100 kg satellite to Venus using solar sails. The project manager (PM) has requested that the Astrodynamics and Propulsion Subdivisions determine the area of the solar sail if the mission is to make the transit in under three years. The solar sail area information is then provided to the Structures Subdivision for determining the fraction of spacecraft mass the sail requires.

Modelling

As the example only requires preliminary analyses, certain assumptions are made to simplify the required calculations. First, the solar sail is assumed to be in a logarithmic trajectory at a fixed spiral angle corresponding to the optimum pitch angle. This assumption neglects the fact that a rather large Δv results from placing the spacecraft in and taking the spacecraft out of such an orbit. More in-depth analyses may be performed later using numerical optimization techniques to create an optimum transfer orbit that is constrained by initial and final spiral angles of zero degrees. Although the typical value for reflective efficiency is 90%, the solar sail is assumed to be purely reflective. Finally, the entire sail is assumed to be oriented at a fixed pitch angle. Some solar sail configurations, such as helio-gyros, have the ability to twist and bend parts of the solar sail to control their attitude. While this reduces the propulsive efficiency of the sail, it eliminates the need for an ADCS.

The mass of the spacecraft is fixed at 100 kg, with a variable solar sail. At each different area, the optimum pitch angle is calculated using Eq. 2.73. The optimum pitch angle, spacecraft mass, and solar sail area are then used to calculate the time of flight for a given area using Eq. 2.72. The resulting time of flights are plotted as a function of the solar sail areas in Fig. 3.5. The figure also shows the three year constraint required for the mission. The results show that the solar sail area needs to exceed 1,100 m² for the mission to make the transfer in less than three years.

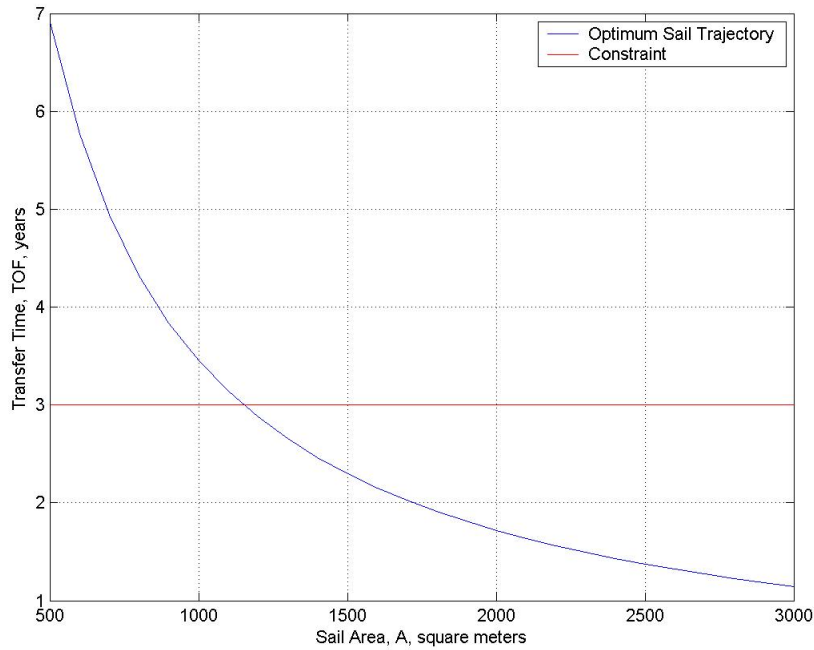


Figure 3.5: Solar Sail Time of Flight from Earth to Venus.

Further Analyses

This model of an Earth-to-Venus transfer is a best-case scenario, and is used to get an initial value that the other subsystems can be sized to. As the design process progresses the model will need to be refined. Some of the initial work involves determining preliminary launch windows and possible transfer opportunities. Once the Structures Subdivision has chosen a material, the reduced reflection of the material needs to be taken into account. A model that optimizes trajectory needs to be created, which should incorporate the ability to use the sail to maintain and control the spacecraft's attitude.

3.4 Conclusion

Chapter 3 defines examples using the analysis laid out in Chapter 2. These examples are intended to cover a wide range of topics, but do not cover all subjects detailed previously. The examples present trade studies on interplanetary transfers, attitude determination and control component sizing, and propulsion system comparisons. The next chapter will summarize this report and provide recommendations of topics to be researched further.

Chapter 4

Summary and Conclusions

The Dynamics and Control Function Division consists of the Astrodynamics, Attitude Determination and Control, and Propulsion Subdivisions. These subdivisions are responsible for determining and controlling the location and orientation of the spacecraft throughout the mission. Therefore, the subdivisions must design the spacecraft's orbit, insert the spacecraft into that orbit, and control the spacecraft's orientation in that orbit. Within this chapter, summaries of these responsibilities are given along with recommendations for further work that would contribute to the overall design effort.

4.1 Astrodynamics

The astrodynamics sections of this report model the following items:

- Equations of motion
- Orbit geometry
- Mission analysis
- Orbit maneuvers
- Launch windows
- Orbit perturbations

The equations of motion in Section 2.1.1 describe the n-body and two-body problems beginning with Newton's and Kepler's laws. Newton's laws of gravity govern the forces between the attracting bodies and lead to the general equation of motion for the two-body problem. Kepler showed that in the two-body problem all orbits are conic sections and can be described by the same set of variables. These conic sections are classified based on the orbit shape: elliptic, parabolic, and hyperbolic. Six variables are required to describe an orbit, with the most common set of variables being the orbital elements. Two of these orbital elements, the

semimajor axis and eccentricity, describe the size and shape of the conic section. Three more variables, the inclination, ascending node, and argument of periapsis, are used to describe the three dimensional orientation of the conic section with respect to the reference plane. The last element, the mean anomaly, describes the orbiting body's location within the orbit.

In mission analyses, the relationship between the orbit and other relevant elements of the mission is quantified. Some mission analyses described in this report are satellite ground tracks, coverage, and instantaneous access areas. These relationships are often used to measure the effectiveness of a given orbit.

Orbit maneuvers described in this paper include plane changes, transfers, and station-keeping. Orbit plane changes are necessary for transfers between orbits with different inclinations, as shown in the example problems in Chapter 3. Transfers are often necessary to achieve mission requirements, and achieve the spacecraft's orbits. An example of Hohmann and direct transfers from Earth to Mars are outlined in Chapter 3. Stationkeeping is often necessary to correct for orbit perturbations.

The most common orbit perturbations are: J_2 , third body, solar radiation, and atmospheric drag. The oblateness of the central body causes the J_2 perturbations. Often the attraction of a third body is significant enough to cause small deviations from the two-body model, with the Sun and Jupiter being significant for interplanetary transfers, and local moons for planetary orbits. Solar radiation pressure also causes periodic variations in all of the orbital elements in planetary orbits. Satellites in low orbits around planets with atmospheres encounter atmospheric drag that cause their orbits to decay.

The Guidance and Navigation Subsystem ascertains the spacecraft's location and determines the error between that true position and the desired position. The sensors used by the Guidance and Navigation Subsystem determine the spacecraft position. Using the data from the sensors, the Guidance and Navigation Subsystem determines the inertial position and velocity. Thrusters are then used to perform orbital maneuvers to correct for the effects of orbital perturbations.

4.1.1 Conclusions

Based on the topics covered in the scope of this report, the following items must be addressed when selecting an orbit for a mission:

- Desired orbit elements
- Desired coverage area
- Desired area access rate
- Station keeping requirements
- Time restrictions
- Debris and other satellites

The desired instantaneous access area, coverage area, and area access rate are defined by the mission requirements. Missions requiring specific periods or altitudes greatly influence the possible orbit. In selecting an orbit, the total station keeping requirements must be minimized. The limits of current propulsion systems must be considered during the orbit selection process. The time restriction influence the type of orbit chosen for transfers, since some orbits, such as Hohmann and direct transfers, take less time than low-thrust transfers. A final consideration for the orbit selection process is the location of known debris and other satellites. The orbit needs to be selected to minimize the affect debris and other satellites on the mission.

4.1.2 Recommendations

Several topics could be further studied and discussed in this paper, including:

- Transfers
- Orbit types
- Launch windows
- Guidance and navigation

Only a general discussion of low-thrust transfers is provided, so prior to implementing such a trajectory a more detailed analysis would be required. Furthermore, there are types of transfers useful when considering the three-body problem, some of which require less energy than a Hohmann transfer. Lagrange points are another result of three-body models that provide new orbital possibilities.

Further knowledge of launch windows and synodic periods is required to design interplanetary trajectories. The alignment of planets for these transfers is vital to the success of the missions, with the required alignments being available for defined periods of time. The periods of alignment set the time constraints for missions' launch windows.

Research into the hardware, software and sensors available for guidance and navigation is necessary to designing the subsystem. Determining the equipment's flight heritage and in-space performance also provides insight on possible design options.

A variety of potential difficulties listed below may arise during the design process.

- Modelling low thrust trajectories
- Perturbations
- Modelling atmospheres
- Avoiding debris and other satellites

Low thrust trajectories are difficult to model due to the long time durations over which the transfer occurs and the non-Keplerian nature of the orbits. Determining precisely the satellite's trajectory requires intensive computation. Similar to low-thrust trajectories, modelling perturbations in a given orbit requires intensive computational models to determine their affect on the spacecraft position and orientation. Particularly, the affect of the atmosphere, which vary significantly over time, will be hard to model. Another potential difficulty is debris and satellite avoidance, with the orbit being designed to minimize possible collisions with other bodies.

To reduce the potential difficulties and ensure success, the following items must be addressed.

- Use proven off-the-shelf software
- Include factors of safety
- Incorporate satellite and debris data
- Know celestial data

Off-the-shelf software can simulate a variety of trajectories, accounting for known perturbations. Some computer programs are designed to work with low-thrust trajectories, and other non-Keplerian orbits, to accurately determine required burn times and launch windows. Factors of safety ensure enough propellant and time are available to mitigate the affect of unforeseen perturbations or events. Obtaining data concerning the orbits of known debris and satellites helps in designing an orbit that minimizes the threat of collisions. Similarly, celestial data, to include the orbital elements of the planets and their moons, would assist in determining the periods of planetary alignments, which are used to calculate the launch windows for interplanetary missions.

4.2 ADCS

The Attitude Determination and Control System is essential to a spacecraft's ability to accomplish any mission with specified pointing requirements. Conceptually, the ADCS deals with the following issues: where the spacecraft is looking; where the spacecraft needs to look; the methods the spacecraft utilizes to correct for differences between the two; and the accuracy with which the spacecraft resolves the above issues. The spacecraft ADCS is broken into three main sections: sensors for determination; actuators for control; and algorithms for quantitative relationships between the sensors and actuators.

During the mission the spacecraft uses various control modes. The definition of these modes is not significant during the initial design phase, since normal mode is used for the majority of the mission. Other modes are used more infrequently, such as after the failure of mission critical hardware or during the firing of thrusters.

The primary drivers for ADCS are the pointing requirements, both accuracy and stability, which must be achieved to successfully accomplish the mission. When selecting sensors

that will be used on the spacecraft, they must meet these minimum accuracy requirements, after which certain other characteristics must be considered, such as mass, power, and cost. Typically high accuracy sensors, such as sun and star sensors, are more massive and consume more power than lower accuracy sensors.

Knowing the disturbance torques a spacecraft experiences is necessary for understanding the spacecraft's motion in absence of control. External torques such as those due to solar radiation pressure, gravity gradients, magnetic fields, and aerodynamic drag are highly dependent on the spacecraft attitude, altitude, and geometry. Different spacecraft attitudes, altitudes and geometries can result in a different external torque dominating. Internal torques are difficult to model, yet also have a significant impact upon on the spacecraft's inherent movement. Some internal torques are due to the spacecraft's geometry, such as torques due to fuel sloshing, while others are due to the spacecraft's materials and structure, such as those torques due to structural flexibility. Once the internal and external torques are correctly modelled, the ADCS can be designed to control those torques and keep the spacecraft in the correct attitude.

Multiple control approaches exist and must be chosen on the basis of the mission pointing requirements and the performance characteristics of the various approaches. These approaches can be categorized into passive stabilization, spin-stabilization, and 3-axis control. Passive stabilization, which includes gravity gradient stabilization, is typically neither as accurate, nor as maneuverable as the other approaches. Spin-stabilization systems apply the law of conservation of momentum to maintain a given attitude, making them more accurate, but only slightly more maneuverable than passive techniques. Three-axis control techniques use control moment gyros, reaction or momentum wheels, magnetic torquers, and thrusters to control the spacecraft with greater precision and maneuverability than the other methods. However, three-axis control techniques are also typically more complex, expensive, and massive. These systems, and the methods used to size them, are described in detail in Section 2.2.5.

Various algorithms may be used to determine and describe the spacecraft's attitude, and to determine the control torques required to maintain a specified attitude. Algorithms are first employed to reduce data from sensors into a description of the spacecraft's attitude and to obtain the error between the current attitude and the desired attitude. This description may be transformed into another attitude description to avoid mathematical singularities. Other algorithms are used to ascertain the spacecraft's current rotation. Control laws then use these descriptions of the spacecraft's rotation and attitude to calculate the torques required to correct and maintain the spacecraft's attitude. Often, the control laws consist of feedback loops that continually control the spacecraft's attitude.

4.2.1 Conclusions

In the Attitude, Determination, and Control Subdivision, there are five steps used to analyze the mission. First, the pointing and maneuverability requirements of the spacecraft need to be defined. These two constraints determine the control approaches used throughout the

mission and provide requirements that limit the options for sensors and control actuators. These options will later be further reduced by other system requirements.

Once this preliminary selection occurs, the alternatives are compared to the mass, volume, power, and other constraints placed on the ADCS by the mission and specified spacecraft parameters. These constraints will determine the sensors and control actuators used, although this step may identify mutually exclusive constraints that must be resolved before the design continues.

The third step consists of estimating the torques, both internal and external, present on the spacecraft while in normal mode, with the ADCS components being sized using these values. The algorithms and control actuators are modelled for a better understanding of the spacecraft's movement and pointing. Next, the constraints are re-examined to ensure the design does not violate them.

Finally, minor adjustments are made. Control torques and algorithms are optimized. The control modes are taken into consideration and are developed more in-depth with respect to the mission's constraints.

4.2.2 Recommendations

While this paper provides a comprehensive overview of the topics necessary to design an ADCS, there are several topics that warrant further investigation:

- Variable speed CMGs, tethers, and other emerging technologies
- Control modes
- Sensor algorithms
- Non-linear control algorithms
- Internal torque estimation

Variable speed CMGs and tethers represent new technologies currently in development that may offer improved control performance over the control approaches that this paper discusses and research into their capabilities and readiness levels would be beneficial. Further, the discussion of control modes and sensor algorithms provides a top-level understanding of these topics, but more detailed information may be required to implement an appropriate system design. Lastly, both non-linear control algorithms and internal torques require additional research as they both require more in-depth analysis than that presented here to be of much use.

Several recommendations can be made regarding best practices of engineers wishing to design an ADCS, including:

- Work with knowledgeable engineers to address potential problem areas, such as:
 - Internal torque estimation

– Non-linear control algorithm determination

- Purchase components off-the-shelf, if available
- Include a significant factor of safety to compensate for peak disturbance torques

As mentioned before, non-linear control algorithms and internal torque estimations may present the most difficult challenges in designing and analyzing the ADCS of a spacecraft. Calculating internal torques requires many assumptions and approximations to be made, and the factors contributing to these assumptions and approximations must be fully understood to complete an accurate analysis. Many spacecraft utilize non-linear control algorithms; however, these algorithms are complex and difficult to understand. Both of these issues may be resolved through discussions with engineers with extensive experience in attitude determination and control systems. Off-the-shelf components typically provide more reliable results than components internally designed and fabricated, and so should be used as much as possible. Lastly, the ADCS should be designed to counteract the average disturbance torques encountered over the course of the mission. A significant factor of safety should be included for instances where the spacecraft encounters peak disturbance torques much greater than the average disturbance torque.

4.3 Propulsion

The propulsion systems examined in this report were chemical, thermal, electric, and propellantless. Descriptions of the operational principles and the performance characteristics of these propulsion systems are provided in Chapter 2. Examples detailing some of these calculations and solutions to specific design problems are provided in Chapter 3. Information on specific propulsion systems are also provided in Appendix B.

The chemical, thermal, and electric propulsion systems described in this report are rockets, whose performance can be defined in terms of their specific impulse and thrust. Based on their thrusts, these rockets are divided into two categories: high- and low-thrust. High-thrust propulsion systems consist primarily of chemical rockets, which are classified by their type of propellant: liquid, solid, and hybrid. Liquid propulsion systems typically have I_{sp} s of 200-500s, can be throttled, and have more complex propellant feed systems. Solid propulsion systems have I_{sp} s of 200-300s, cannot be throttled, and are simpler than liquid propulsion. Hybrid propulsion systems combine the advantages of solid and liquid propulsion, with I_{sp} s of 280-305s and having the ability to be throttled.

Low-thrust propulsion consists of thermal and electric propulsion. Low-thrust propulsion systems have lower thrust than chemical propulsion, but have significantly higher I_{sp} s and require less propellant. Low-thrust propulsion systems are typically classified according to the source of the power. Therefore thermal propulsion is classified into nuclear and solar, whereas electric propulsion is classified into electrostatic, electromagnetic, and electrothermal. The thermal and electric propulsion types with a constant energy source, which includes nuclear thermal, have the advantage of high I_{sp} s and the disadvantage of highly

complex systems. Solar thermal propulsion has the further disadvantage of a non-constant power source, which makes it difficult to operate in orbits that have eclipses.

Non-rocket propulsion, or propellantless propulsion, consists of both tethers and solar sails, with only solar sails being discussed in this report. Solar sails are classified into two categories based on their sail material: physical and magnetic. Their performance is characterized by their sail lightness factor, which is a function of spacecraft mass and sail area. Solar sail propulsion systems are useful for exotic Keplerian orbits, inner solar system transfers, and asteroid surveys. Solar sails also use their sails to make attitude corrections, eliminating the need for an ADCS.

4.3.1 Conclusions

The propulsion subdivision's responsibility is to select and design the subsystem to accomplish the mission design profile selected by the Astrodynamics subdivision. In the selection process, the following considerations must be addressed:

- Minimization of propulsion subsystem mass.
- Maximization of payload mass.
- Power requirements.
- Transfer time.
- Thrust levels.
- Adjustability of performance.
- System complexity.
- System redundancy.
- System environmental effects.
- System cost.
- System safety.
- EOL disposal procedures.

The primary consideration of the propulsion subdivision is to minimize the subsystem mass, while maximizing the payload mass. If a propulsion subsystem is required to meet the objectives, accomplishing this objective would typically result in the minimization of propellant mass for rockets, and minimization of subsystem mass for propellantless propulsion types. Certain types of a propulsion systems, such as thermal and electric require significant quantities of power and these high power levels must be taken into account in the design.

The mission requirements, such as the transfer time, thrust levels, and performance adjustability, must to be considered. Shorter transfer times might require the use of high-thrust propulsion, and orbits requiring throttling eliminate the use of certain propulsion types, such as solid rockets. Minimization of complexity is also important, as complex systems are more apt to fail. To prevent the loss of a mission due to a failure in the propulsion subsystem, the redundancy of the system must be considered. Environmental effects must be considered, as certain propulsion types and propellants have adverse effects on spacecraft performance. In subsystem component selection, the cost of the subsystem must be minimized.

4.3.2 Recommendations

Certain topics should be researched and discussed further in-depth. These topics include:

- Propellant types and combinations.
- Analyses of specific rocket components.
- Definition and capabilities of nuclear reactors.
- Principles of electric propulsion operation.
- Definition of different solar sail configurations.
- Tethers

Different propellant types and combinations provide different performance levels, and have different effects on system safety. These different performance levels and safety effects should be studied more in-depth to determine the best possible propellant types and combinations. While analyses of overall rocket performance is provided, quantifying the performance of specific rocket components would allow design of propulsion systems in instances when commercial propulsion systems either do not exist or do not meet the needs of the mission. One such propulsion system that is still in the design phase is nuclear thermal propulsion, which also requires further research into the performance characteristics of available nuclear reactors. The principles of electric propulsion were only generally described in this report, as significant developmental work is still required in this field. Therefore, to implement such a system, further research would be required. In addition, another system described in the report that is still under development is solar sails. While not discussed, different solar sail configurations provide different performance characteristics, particularly in relation to the ADCS system, which need to be quantified. Furthermore, the other propellantless propulsion system, tethers, is only briefly mentioned.

4.4 Conclusion

This report provides a comprehensive overview of the Astrodynamics, Attitude Determination and Control, and Propulsion Subdivisions. Chapter 1 provides a brief overview of the three subdivisions, defining the scope of their responsibilities. Chapter 2 provides in-depth analyses of the subsystems and defines in details the interactions between these subdivisions and the other spacecraft design team subdivisions. In Chapter 3, examples of these analyses are performed. Chapter 4 summarizes these descriptions of the subdivisions and provides recommendations of topics for future research.

Bibliography

- [1] Roger R. Bate, Donald D. Mueller, and Jerry E. White. *Fundamentals of Astrodynamics*. Dover Publicatinos, Inc., Mineola, N.Y., 1971.
- [2] N. Cummings and et al. Solar orbit transfer vehicle. *Virginia Tech*, 1 June 2001. Available internet <<http://www.aoe.vt.edu/~cdhall/courses/aoe4065/OldReports/sotv.pdf>>.
- [3] B. Diedrich. Solar sails. Available internet <<http://www.solarsails.info>>, 10 November 2004.
- [4] European Space Agency. *Space Weather Workshop: Looking Towards a European Space Weather Programme*, 2001. Available internet <http://www.estec.esa.nl/wmwww/wma/spweather/workshops/SPW_W3/PROCEEDINGS_W3>.
- [5] E. Frazolli. Solar radiation pressure. *University of Illinois at Urbana-Champaign*, 2004. Available internet <<http://brunello.aae.uiuc.edu/aae206/lnotes/aae206-Space8.pdf>>.
- [6] C. D. Hall. Chapter 4: Attitude Determination. *Virginia Tech*, 18 March 2003. Available internet <<http://www.aoe.vt.edu/~cdhall/courses/aoe4140/attde.pdf>>.
- [7] P. G. Hill and C. R. Peterson. *Mechanics and Thermodynamics of Propulsion*. Addison-Wesley, Reading, MA, 1992.
- [8] Honeywell. Constellation series reaction wheels. *Honeywell International, Inc.*, December 2003. Available internet <http://content.honeywell.com/dses/assets/datasheets/constellation_series_reaction_wheels.pdf>.
- [9] T. S. Kelso. Celestrak. Available internet <<http://www.celestrak.com>>, Accessed 17 November 2004.
- [10] T. Kessler. Solar orbit transfer vehicle. *Boeing*, Accessed 17 November 2004. Available internet <<http://www.boeing.com/defense-space/space/propul/SOTV.html>>.

- [11] W. J. Larson and J. R. Wertz, editors. *Space Mission Analysis and Design*. Microcosm Press, El Segundo, California, third edition, 1999.
- [12] C. P. McInnes. *Solar Sailing*. Springer-Verlag, LLC, New York, April 2004.
- [13] A. Sanchez. Propulsion systems. *NASA Johnson Space Center*, 3 May 2004. Available internet <<http://aerospacescholars.jsc.nasa.gov/HAS/cirrr/em/11/29.cfm>>.
- [14] H. Schaub. Satellite motion with respect to the topological frame. *Virginia Tech*, 1 October 2003. AOE 4134 class notes.
- [15] H. Schaub and J. L. Junkins. *Analytical Mechanics of Space Systems*. AIAA Education Series, Reston, VA, 2003.
- [16] A. J. Turner. An open-source, extensible spacecraft simulation and modeling environment framework. Master's thesis, Virginia Tech, 2003.
- [17] J. R. Wertz. *Mission Geometry: Orbit and Constellation Design and Management*. Microcosm Press, El Segundo, California, 2001.
- [18] R. M. Winglee and et al. Advanced electric propulsion. *University of Washington*, 1 June 2001. Available internet <<http://www.ess.washington.edu/Space/propulsion.html>>.

Appendix A

Astronomical Data

Table A.1: Astronomical Data¹⁵

Body	μ (km ³ /s ²)	a (km)
Sun	1.326×10^{11}	
Mercury	2.208×10^4	5.791×10^7
Venus	3.248×10^5	1.082×10^8
Earth	3.986×10^5	1.476×10^8
Moon	4.902×10^3	3.815×10^5
Mars	4.282×10^4	2.279×10^8
Jupiter	1.267×10^8	7.786×10^8
Saturn	3.795×10^7	1.429×10^9
Uranus	5.796×10^6	2.871×10^9
Neptune	6.87×10^6	4.504×10^9
Pluto	4.402×10^4	5.914×10^9

☉ The Sun	♃ Jupiter
☾ The Moon	♄ Saturn
☿ Mercury	♅ Uranus
♀ Venus	♆ Neptune
♁ The Earth	♇ Pluto
♂ Mars	

Figure A.1: Planetary Symbols

Appendix B

Useful Tables

Table B.1: Various Companies's Thrusters

Company	Thruster Type	Mass (kg)	Pressure Range/Thrust
Marotta	2 Way 2 Position Direct Acting 3,000 psig	0.363	0 - 3,000 psig
	No Oscillation HP Relief Valve 10,000 psig		0 - 10,000 psig
	Variable High Pressure Regulator 1/4" Port	0.47	30 - 6,000 psig
	Thruster Multi-Function Valve	< 0.4	50 - 2,175 psig
Rafael	Hydrazine Mono-propellant	1.25	180 N
TRW	Hydrazine Mono-propellant MRE15-OMV	1.13	44.5 - 89 N
Marquardt	R-1E Hypergolic	3.7	67 - 155.7 N
	R-40A Thruster	10.25	3,114 - 5,338 N
Aerojet	Orbital Maneuvering Systems	118	26,700 N

Table B.2: Examples of Available Monopropellant Hydrazine Rockets.¹¹

Engine	Developer	Thrust (lbf)
MR-80	Aerojet	600
MR-103G	Aerojet	0.2
MR-104B	Aerojet	100
MR-106E	Aerojet	5.0
MR-107B	Aerojet	30
MR-111C	Aerojet	1.0

Table B.3: Examples of Available Bipropellant Rockets.¹¹

Engine	Developer	Nominal Thrust (N)	Spec. Impulse (sec)	Propellants	Oper. Life (sec)	Engine Mass (kg)
HiPAT	Aerojet	4.44×10^2				
R-1E	Aerojet	1.11×10^2				
R4D	Aerojet	4.89×10^2				
hlineR40 B	Aerojet	4.00×10^3				
R42	Aerojet	8.89×10^2				
Transtar	Aerojet	1.67×10^4	330-338	N_2O_4/MMH	5,400	57.15
Transtage	Aerojet	3.56×10^4	315	$N_2O_4/A - 50$	1,000	107.95
Delta-II	Aerojet	4.36×10^4	320	N_2O_4/MMH	1,200	99.79
OME/UR	Aerojet	2.67×10^4	340	N_2O_4/MMH	1,200	90.72
HS 601	ARC/LPG	4.89×10^2	312	N_2O_4/MMH	10,000	4.08
AKE						
R4-D	Marquardt	4.00×10^3	309	N_2O_4/MMH	25,000	7.26
R4-D	Marquardt	4.89×10^2	310	N_2O_4/MMH	20,000	3.76
R42	Marquardt	8.90×10^2	305	$MON3/MMH$	15,000	4.54
R-40A	Marquardt	4.00×10^3	309	N_2O_4/MMH	25,000	7.26
TR-308	Norhrop	4.71×10^2	322	N_2O_4/N_2H_2	24,190	4.76
	Grumman					
TR-312-100MN	Northrop	5.03×10^2	325	N_2O_4/MMH	25,000	6.03
	Grumman					
TR-312-100YN	Northrop	5.56×10^2	330	N_2O_4/N_2H_2	25,000	6.03
	Grumman					
RL10-A	Pratt and Whitney	7.34×10^4	446	LO_2/LH_2	400	138.35
RD-0146	Pratt and Whitney	9.79×10^4	451	LO_2/LH_2		243
RL10B-2	Pratt and Whitney	1.10×10^5	465.5	LO_2/LH_2		302
RL-60	Pratt and Whitney	2.56×10^5	465	LO_2/LH_2		500
MB-60	Rocketdyne	2.67×10^5	467	LO_2/LH_2		591
RS-41	Rocketdyne	1.11×10^4	312	N_2O_4/MMH	2,000	113.40
RS-72	Rocketdyne	5.54×10^4	338	MMH/NTO		155
XLR-132	Rocketdyne	1.67×10^4	340	N_2O_4/MMH	5,000	51.26
DM/LAE	TRW	4.45×10^2	315	N_2O_4/N_4H_4	15,000	4.54
MMBPS	TRW	4.45×10^2	302	N_2O_4/MMH	20,000	5.22
ADLAE	TRW	4.45×10^2	330	N_2O_4/N_4H_4	28,000	4.50
HPLAM	TRW	4.45×10^2	325	N_2O_4/MMH	30,000	4.60

Table B.4: Examples of Available Solid Rockets.¹¹

Motor	Loaded Weight (kg)	Propellant Mass Fraction	Average Thrust (N)	Max. Thrust (N)	Effective I_{sp}
LEASAT PKM	3,658	0.91	157,356	193,200	285.4
IUS SRM-1 (ORBUS-21)	10,374	0.94	198,435	260,488	295.5
IUS SRM-2 (ORBUS-6)	2,995	0.91	80,157	111,072	303.8
STAR 13B	47	0.88	7,015	9,608	285.7
STAR 30BP	543	0.94	26,511	32,027	292.0
STAR 30C	626	0.95	31,760	37,031	284.6
STAR 30E	667	0.94	35,185	40,990	289.2
STAR 37F	1,149	0.94	44,086	49,153	291.0
STAR 48A	2,559	0.95	79,623	100,085	283.9
STAR 48B(L)	2,141	0.95	67,435	72,017	292.2
STAR 48B(S)	2,135	0.95	66,034	70,504	286.2
STAR 75	8,066	0.93	198,426	242,846	288.0

Table B.5: Examples of Hybrid Rockets Currently Available or in Development.¹¹

Motor	Company	Average Thrust (kN)	Fuel	Oxidizer	Comments
H-500	American Rocket Company	333	HTPB	LOx	Qualified for flight
H-250	American Rocket Company	142	HTPB	LOx	In development
H-50	American Rocket Company	44	HTPB	LOx	In development
U-50	American Rocket Company	29	HTPB	LOx	In development
U-1	American Rocket Company	0.44	HTPB	LOx	In development
	United Technologies	178	HTPB	IRFNA	Flown on Firebolt target drone, 1968
	Stars Truck	178	CTBN	LOx	Flown on Dolphin sounding rocket, 1984

Table B.6: Available Earth, Magnetic, Star, and Sun Sensors

Type	Company	Model	Accuracy	FOV	Mass	Cost	Power Req	Comment
Earth	Sodern	STD 15	0.105°		3.4kg		7.5 W	
	Sodern	STD 16	0.18		2.5		7.5 W	
	OETI		1° optimum		< 100g	\$16,000	< 50mW	
	Goodrich	13-410						
	Goodrich	13-470-RH	0.2°	20x14.8°	38.7 oz		1-5 W	3 telescopes
Mag	SSTL	3-axis fluxgate magnetometer		±10 nT	295g		5mA @ -10.5 V	100+ orbit years
	SSTI	3-axis fluxgate magnetometer Mk II		±10 nT	94g		5mA @ -10.5 V	TopSat
Billingsley		TFM100G2	0.50%	±100μT	100g		15-34V @25mA	
		TFM100-S	0.50%	100,000nT	200g		20 mA @ 28V	SCATHA, Iridium
Star	Aeroastro		100"					
	Ball Aero	CT-631	6"	20x20°	2.4kg		9W	
	Ball Aero	CT-632	11" @72°/s spin	20x20°	2.4kg		9W	
	Ball Aero	CT-633	< 6"	20x20°	2.4kg		9W	
	Ball Aero	ACA	0.07"					Chandra
	Goodrich	HD-1003						
Sun	SSTL	ALTAIR-HB	1 σ	15.74x10.53°	1695g		3 W	Po and UoSat-12
	Aeroastro	Coarse	5.0°	120°	20 grams		none	Pegasas XL
	Aeroastro	Medium	1.0°	134°	36 grams		none	ALEXIS
	Sodern	DDS	0.01	120x120°	0.3 kg	Low	1 W	Digital
	OETI	0.5	0.5°	100°	< 40g	\$16,000	< 50mW	
	OETI	0.05	0.5°	100°	< 40g	\$40,000	for ±1° albedo < 50mW	
	TNO	SAS	0.5°		.155kg		none	
	TNO	DSS	.04~0.02°	128x128°	< 250g		< 1W	
	Goodrich	13-517	<0.3°	128x168°	< 15 oz		0.3 W	Usually 2 pairs
	SSTL	2-axis Sun Sensor	0.5°	±50°	300g		Dark- 100mW	UoSat-12